

8-1-2018

Dissolution Rates of Allophane, Fe-Allophane, and Hisingerite and Implications for Aqueous Alteration on Mars and in Potential Returned Martian Samples

S. J. Ralston
sjralston6@gmail.com

Follow this and additional works at: <https://digitalscholarship.unlv.edu/thesesdissertations>



Part of the [Geochemistry Commons](#), and the [Soil Science Commons](#)

Repository Citation

Ralston, S. J., "Dissolution Rates of Allophane, Fe-Allophane, and Hisingerite and Implications for Aqueous Alteration on Mars and in Potential Returned Martian Samples" (2018). *UNLV Theses, Dissertations, Professional Papers, and Capstones*. 3377.
<https://digitalscholarship.unlv.edu/thesesdissertations/3377>

This Thesis is protected by copyright and/or related rights. It has been brought to you by Digital Scholarship@UNLV with permission from the rights-holder(s). You are free to use this Thesis in any way that is permitted by the copyright and related rights legislation that applies to your use. For other uses you need to obtain permission from the rights-holder(s) directly, unless additional rights are indicated by a Creative Commons license in the record and/or on the work itself.

This Thesis has been accepted for inclusion in UNLV Theses, Dissertations, Professional Papers, and Capstones by an authorized administrator of Digital Scholarship@UNLV. For more information, please contact digitalscholarship@unlv.edu.

DISSOLUTION RATES OF ALLOPHANE, FE-ALLOPHANE, AND HISINGERITE AND
IMPLICATIONS FOR AQUEOUS ALTERATION ON MARS AND IN POTENTIAL RETURNED
MARTIAN SAMPLES

By

S. J. Ralston

Bachelor of Science – Earth and Atmospheric Sciences
Georgia Institute of Technology
2014

A thesis submitted in partial fulfillment
of the requirements for the

Master of Science – Geoscience

Department of Geoscience
College of Sciences
The Graduate College

University of Nevada, Las Vegas
August 2018



Thesis Approval

The Graduate College
The University of Nevada, Las Vegas

May 18, 2018

This thesis prepared by

S.J. Ralston

entitled

Dissolution Rates of Allophane, Fe-Allophane, and Hisingerite and Implications for
Aqueous Alteration on Mars and in Potential Returned Martian Samples

is approved in partial fulfillment of the requirements for the degree of

Master of Science – Geoscience
Department of Geoscience

Elisabeth Hausrath, Ph.D.
Examination Committee Chair

Kathryn Hausbeck Korgan, Ph.D.
Graduate College Interim Dean

Oliver Tschauner, Ph.D.
Examination Committee Member

Arya Udry, Ph.D.
Examination Committee Member

Jacimara Batista, Ph.D.
Graduate College Faculty Representative

ABSTRACT

Recent measurements from Mars document X-ray amorphous/nano-crystalline materials in multiple locations across the planet. However, despite their prevalence, little is known about these materials or what their presence implies for the history of Mars. The amorphous component of the martian soil in Gale Crater has an X-ray diffraction pattern that can be partially fit with allophane (approximately $\text{Al}_2\text{O}_3 \cdot (\text{SiO}_2)_{1.3-2} \cdot (\text{H}_2\text{O})_{2.5-3}$), as well as low-temperature water release consistent with allophane. The chemical data from Gale Crater suggest that other silicate phases similar to allophane, such as Fe-substituted allophane (here, approximately $(\text{Fe}_2\text{O}_3)_{0.01}(\text{Al}_2\text{O}_3)_{0.99}(\text{SiO}_2)_2 \cdot 3\text{H}_2\text{O}$) and hisingerite (approximately $\text{Fe}^{3+}_2\text{Si}_2\text{O}_5(\text{OH})_4 \cdot (\text{H}_2\text{O})$), may also be present. In order to investigate the properties of these poorly crystalline components of the martian soil, we synthesized allophane, Fe-substituted allophane, and hisingerite; characterized the synthetic materials by infrared spectroscopy, electron microscopy, X-ray diffraction, and evolved gas analysis; and performed dissolution experiments at acidic, near-neutral, and alkaline conditions in order to determine dissolution kinetics and alteration phases for these poorly crystalline materials. Our analyses demonstrate that allophane, Fe-allophane, and hisingerite are appropriate analogs for silicate phases in the martian amorphous soil component. These poorly crystalline materials dissolve rapidly at all experimental pH conditions, indicating that similar materials on Mars must have had limited interaction with liquid water since their formation. For allophane, $\log r_{\text{diss}} = -11.05 - 0.088 \times \text{pH}$; for Fe-allophane, $\log r_{\text{diss}} = -11.09 - 0.091 \times \text{pH}$; and for hisingerite, $\log r_{\text{diss}} = -11.49 - 0.032 \times \text{pH}$. Additionally, incipient phyllosilicate phases form in hisingerite and allophane under high pH conditions, but are much more sparse at low pH, which, combined with the enrichment of Fe expected from weathering, may be a useful tool for examining returned samples of martian soils for evidence of past aqueous alteration.

ACKNOWLEDGEMENTS

We would like to acknowledge the following people for their contributions to this research: Liz Rampe, Brad Sutter, Lisa Danielson, Roy Christoffersen, Joanna Hogancamp, Toluwalope Bamisile, Dave Hatchett, Minghua Ren, and Michael Strange. Additionally, we acknowledge the Faculty Opportunity Award, the UNLV Doctoral Award, NASA Mars Data Analysis Program Grant 80NSSC17K0581, the Geological Society of America Graduate Research Grant, the UNLV Graduate and Professional Student Association research and travel grants, and the Southwest Travel Award for funding this research.

TABLE OF CONTENTS

Abstract	iii
Acknowledgements	iv
Table of Contents	v
List of Tables	vi
List of Figures	viii
1. Introduction	1
2. Materials and methods	4
3. Results	10
4. Discussion	23
5. Conclusions	30
Appendix	32
References	82
Curriculum Vitae	91

LIST OF TABLES

Table 1. Measured pH, dissolution rates, and standard error of dissolution experiments.	21
Table 2. Comparison of synthetic material compositions with martian materials.	24
Table S1. Table of experiments examined by TEM for alteration products.	49
Table S2. EDS results from selected unaltered grains.	49
Table S3. EDS results from selected altered and unaltered hisingerite grains.	49
Table S4. Particle size analysis and BET specific surface area of synthetic materials.	49
Table S5. Dissolved silica analysis for experiment Al+Si-p3-1.	50
Table S6. Dissolved silica analysis for experiment Al+Si-p3-2.	51
Table S7. Dissolved silica analysis for experiment 1:99-p3-1.	52
Table S8. Dissolved silica analysis for experiment 1:99-p3-2.	53
Table S9. Dissolved silica analysis for experiment 50:50-p3-1.	54
Table S10. Dissolved silica analysis for experiment 50:50-p3-2.	55
Table S11. Dissolved silica analysis for experiment Al+Si-p5-1.	56
Table S12. Dissolved silica analysis for experiment Al+Si-p5-2.	57
Table S13. Dissolved silica analysis for experiment 1:99-p5-1.	58
Table S14. Dissolved silica analysis for experiment 1:99-p5-2.	59
Table S15. Dissolved silica analysis for experiment 50:50-p5-1.	60
Table S16. Dissolved silica analysis for experiment 50:50-p5-2.	61
Table S17. Dissolved silica analysis for experiment Al+Si-p8-1.	62
Table S18. Dissolved silica analysis for experiment Al+Si-p8-2.	63
Table S19. Dissolved silica analysis for experiment 1:99-p8-1.	64
Table S20. Dissolved silica analysis for experiment 1:99-p8-2.	65
Table S21. Dissolved silica analysis for experiment 50:50-p8-1.	66

Table S22. Dissolved silica analysis for experiment 50:50-p8-2	67
Table S23. Dissolved silica analysis for experiment Al+Si-p10.3-1.	68
Table S24. Dissolved silica analysis for experiment Al+Si-p10.3-2.	69
Table S25. Dissolved silica analysis for experiment 1:99-p10.3-1.	70
Table S26. Dissolved silica analysis for experiment 1:99-p10.3-2.	71
Table S27. Dissolved silica analysis for experiment 50:50-p10.3-1.	72
Table S28. Dissolved silica analysis for experiment 50:50-p10.3-2.	73
Table S29. Dissolved Al analysis for experiment Al+Si-p3-1.	74
Table S30. Dissolved Al analysis for experiment Al+Si-p3-2.	75
Table S31. Dissolved Al analysis for experiment 1:99-p3-1.	76
Table S32. Dissolved Al analysis for experiment 1:99-p3-2.	77
Table S33. Dissolved Al analysis for experiment 50:50-p3-1.	78
Table S34. Dissolved Al analysis for experiment 50:50-p3-2.	79
Table S35. Dissolved Fe analysis for experiment 50:50-p3-1.	80
Table S36. Dissolved Fe analysis for experiment 50:50-p3-2.	81

LIST OF FIGURES

Figure 1. FTIR spectra of allophane, Fe-substituted allophane, and hisingerite.	11
Figure 2. Synthetic Fe-allophane imaged by FE-SEM.	12
Figure 3. TEM images of synthetic unaltered hisingerite and allophane.	14
Figure 4. Change of pH with time for dissolution experiments at pH 3 and 10.	16
Figure 5. Al/Si and Fe/Si ratios from allophane, Fe-allophane, and hisingerite at pH 3.	17
Figure 6. Si, Al, and Fe release from allophane, Fe-allophane, and hisingerite at pH 3.	19
Figure 7. Dissolution rates of allophane, Fe-allophane, and hisingerite.	20
Figure 8. TEM image of altered synthetic hisingerite and allophane.	22
Figure 9. Comparison of obtained dissolution rates with those of other phases.	26
Figure S1. Diffraction pattern of unaltered synthetic hisingerite.	32
Figure S2. Incipient phyllosilicate structure in hisingerite reacted at pH 3.	33
Figure S3. Incipient phyllosilicate structure in hisingerite reacted at pH 10.	34
Figure S4. Incipient phyllosilicate structure in allophane reacted at pH 10.	35
Figure S5. Beam-sensitivity of allophane reacted at pH 10.	36
Figure S6. SEM images of unaltered synthetic materials.	36
Figure S7. SEM image of unaltered hisingerite.	37
Figure S8. SEM image of hisingerite reacted at pH ~4 for two days.	37
Figure S9. SEM image of hisingerite reacted at pH ~4 for one month.	37
Figure S10. FE-SEM image of synthetic allophane.	38
Figure S11. FE-SEM image of synthetic Fe-allophane.	38
Figure S12. FE-SEM image of synthetic hisingerite.	39
Figure S13. Mass-18 H ₂ O release from synthetic allophane and hisingerite.	39
Figure S14. Mass-32 O ₂ release from synthetic allophane and hisingerite.	40

Figure S15. Mass-44 CO ₂ release from synthetic allophane and hisingerite.	40
Figure S16. Mass-64 SO ₂ release from synthetic allophane and hisingerite.	40
Figure S17. XRD patterns of synthetic allophane, Fe-allophane, and hisingerite.	41
Figure S18. Dissolution rates and rate laws for synthetic materials.	42
Figure S19. Silica release from allophane, Fe-allophane, and hisingerite at pH 3.	43
Figure S20. Silica release from allophane, Fe-allophane, and hisingerite at pH 5.	44
Figure S21. Silica release from allophane, Fe-allophane, and hisingerite at pH 8.	45
Figure S22. Silica release from allophane, Fe-allophane, and hisingerite at pH 10.	46
Figure S23. Fe release and Al release from dissolution experiments at pH 3.	47

1. Introduction

Recent observations have shown that Mars likely once had abundant water (e.g. Carr, 1996; Bibring et al., 2006; Vaniman et al., 2014; Grotzinger et al., 2015), widely considered to be a critical prerequisite for life. However, it is not yet clear how much water was present on Mars or for how long. Clues to the characteristics and longevity of Mars's ancient aquatic environments may lie in the aqueous alteration products, including the martian amorphous soil component that has been detected widely on Mars both from orbit (e.g. Singer, 1985; Milliken et al., 2008; Rampe et al., 2014; Weitz et al., 2014) and *in situ* by the Pathfinder, Spirit, and Curiosity rovers (e.g. Morris et al., 2000; Squyres et al., 2008; Bish et al., 2013). Remote and *in situ* measurements have identified globally distributed hydrogen associated with hydrated phases. It has been hypothesized that the source of the observed global hydration is an amorphous material that contains structural or adsorbed water (Meslin et al., 2013). One such material, allophane, has been detected from orbit across many regions of Mars (Rampe et al., 2011; Rampe et al., 2012; Bishop and Rampe, 2016), as well as proposed at Gale Crater, the landing site of the Mars Science Laboratory rover Curiosity (Bish et al., 2013; Dehouck et al., 2014).

Measurements from the Chemistry and Mineralogy (CheMin) instrument aboard Curiosity indicate ~15-70 wt% X-ray amorphous material is present in all samples measured to date (e.g. Bish et al., 2013; Dehouck et al., 2014; Vaniman et al., 2014; Rampe et al., 2017). The X-ray amorphous material occurs in both scoops of unconsolidated, modern aeolian sediment and in drill tailings from ancient sandstones and mudstones along the rover traverse (e.g. Blake et al., 2013; Bish et al., 2013; Dehouck et al., 2014; Sutter et al., 2017). The broad hump in the CheMin X-ray diffraction (XRD) patterns, which was assigned to amorphous material, has been fit by a combination of allophane, ferrihydrite, and/or rhyolitic and basaltic glass for samples of modern aeolian sediment (Bish et al., 2013; Achilles et al., 2017). Plausible chemical composition of the amorphous component for inactive aeolian sediment (i.e., soil) was estimated by subtracting the composition of the crystalline component (determined from

CheMin data) from the bulk sample composition, obtained from Curiosity's Alpha Particle X-Ray Spectrometer (APXS) (Bish et al., 2013; Dehouck et al., 2014). Based on the Fe-rich nature of the material, hisingerite may be present instead of or in addition to allophane (Bish et al., 2013; Dehouck et al., 2014).

Allophane (approximately $\text{Al}_2\text{O}_3 \cdot (\text{SiO}_2)_{1.3-2} \cdot (\text{H}_2\text{O})_{2.5-3}$) is a poorly ordered aluminosilicate that forms on Earth from the weathering of volcanic rocks and ash (Wada, 1989). It has short-range atomic order and forms nano-scale spherules approximately 50 Å in diameter, which then aggregate into clumps (Abidin et al., 2004). These nano-spherules consist of a rolled gibbsite sheet surrounding a silica sheet (Wada, 1989; Iyoda et al., 2012) and are hollow and porous, giving allophane a large adsorption capacity and a high surface area (Ohashi et al., 2002; Iyoda et al., 2012). Allophane is found on Earth in moist, temperate volcanic soils, such as those in Japan, New Zealand, and Sweden (Wada, 1989; Parfitt, 1990; Gustafsson et al., 1998). In Fe-rich soils, Fe can substitute for some or most of the Al, producing Fe-substituted allophane or a related mineral known as hisingerite (approximately $\text{Fe}^{3+}_2\text{Si}_2\text{O}_5(\text{OH})_4 \cdot (\text{H}_2\text{O})$, Henmi et al., 1980). Like allophane, hisingerite is poorly ordered and tends to form aggregates of hollow, porous nano-spherules in soils (Ingles and Willoughby, 1967), but the nano-spherules are much larger (~200 Å in diameter as per Shayan, 1984). Although much research has been done on the structure of allophane (e.g. Ohashi et al., 2002; Montarges-Pelletier et al., 2005; Iyoda et al., 2012; Bishop et al., 2013), few data exist on its dissolution kinetics (Abidin et al., 2004), and to our knowledge no dissolution rates have been measured for hisingerite.

By determining the rates and conditions under which analogs for the martian amorphous soil component persist, dissolve, and form secondary alteration phases, we can place constraints on the characteristics and longevity of liquid water that was present in Gale Crater after the formation of these amorphous materials. We performed dissolution experiments of synthetic allophane, Fe-substituted allophane, and hisingerite at acidic, near-neutral, and alkaline conditions, and have characterized the

materials altered at low and high pH. We show that the dissolution rates of allophane, Fe-allophane, and hisingerite are much faster than those of crystalline phases with similar compositions, and that the dissolution rates of all three X-ray amorphous materials show only a small dependence on pH. We also present indirect evidence for secondary Fe- and Al-rich alteration phases from solution chemistry, and direct evidence of alteration to phyllosilicate-like phases at high pH from field-emission scanning transmission electron microscopy (FE-STEM). These results help us interpret the implications of the presence of these materials in Gale Crater and in other locations on the martian surface, and the possibility of detecting direct evidence of past aqueous alteration in returned martian samples.

2. Materials and methods

2.1 Synthesis procedures

Hisingerite, Fe-allophane, and allophane were synthesized following the methods of Baker et al. (2011, 2012). Plastic labware was used for all steps of the synthesis in order to avoid silica contamination from glass.

Syntheses were carried out using $\text{AlCl}_3 \cdot 6\text{H}_2\text{O}$ (reagent grade, Alfa Aesar), $\text{FeCl}_3 \cdot 6\text{H}_2\text{O}$ (ACS grade, Malinkrodt), and tetraethyl orthosilicate ($\geq 98\%$ purity, Acros Organics). Solutions of 0.1 M AlCl_3 and FeCl_3 were mixed, and tetraethyl orthosilicate (TEOS) was added. At this stage, TEOS is immiscible with water. While stirring, NaOH was added to the solution with a VWR variable speed ultra low flow syringe pump (Model 3384) at a rate of 25 mL/hour in order to hydrolyze TEOS and allow silica to bond with Al and Fe. A solution of NaOH was added until a molar ratio of 3:1 OH^- to Al+Fe was achieved in order to maximize allophane/hisingerite production and minimize the production of other phases (Denaix, 1993). For hisingerite, the molar Fe/Al/Si ratio was 0.5:0.5:1; for Fe-allophane, it was 0.01:0.99:1; and for allophane, it was 0:1:1. The precursor materials were stirred for one additional hour after addition of NaOH to ensure thorough mixing. They were then incubated without stirring at room temperature overnight to stabilize the suspension through colloid formation and proton release (Denaix, 1993; Montarges-Pelletier, 2005). The precursors were then heated in an oven at 95 °C for seven days to promote colloid formation. The samples were removed from the oven, cooled, and washed with deionized water to remove excess ions and alcohol from TEOS. Samples were washed by adding 25-45 mL of 18.2 M Ω deionized water, agitating them on a vortex analog mixer, centrifuging at 11,000 rpm for 5 minutes at 20 °C, and then pipetting off the supernatant. The washing process was repeated until the conductivity of the supernatant was <20 μmhos . The washed products were frozen in a -20 °C freezer for at least 24 hours, and then freeze-dried to create the final solid product. The final products were characterized by Fourier-transform infrared (FTIR) spectroscopy, scanning electron microscopy/energy dispersive X-ray

spectroscopy (SEM/EDS), field-emission SEM (FE-SEM), X-ray diffraction (XRD), field-emission scanning transmission electron microscopy (FE-STEM), and evolved gas analysis (EGA) as described in Section 2.3.

2.2 Characterization

2.2.1 FTIR

FTIR analyses were carried out on a Varian FTS 7000 FTIR spectrometer in the Inorganic Materials & Nanomaterials lab at UNLV. For all runs, the speed was 2.5 kHz, with 64 scans collected at a resolution of 4 cm⁻¹ over the 4,000-400 cm⁻¹ range. For each sample, the sample chamber was run through an open helium purge for ten minutes, followed by a closed helium purge for another ten minutes in order to minimize contamination from atmospheric gases. A background spectrum was obtained for each run, and this background spectrum was used as a correction for all sample spectra in order to remove absorptions due to CO₂ and other atmospheric gases. Data for synthetic allophane, Fe-substituted allophane, and hisingerite were compared with data from Wada (1989), Rampe et al. (2012), and Milliken et al. (2008), respectively, and contained all of the major features of each phase (see Results Section 3.1.1).

2.2.2 SEM/EDS

Freeze-dried aggregates of unaltered allophane, Fe-allophane, and hisingerite were placed on carbon tape atop aluminum sample plugs and carbon coated for analysis using a Denton Vacuum DV-502A carbon coater. SEM and EDS analyses were carried out on a JEOL scanning electron microscope model JSM-5610 with an Oxford ISIS EDS system in the Electron Microanalysis and Imaging Laboratory (EMiL) at UNLV. In addition, samples of altered synthetic hisingerite were examined with SEM under the same conditions to identify potential morphological changes due to dissolution.

Hisingerite exposed to pH ~4 solution for two days and hisingerite exposed to pH ~4 solution for one month were examined and compared to the unaltered hisingerite. Only hisingerite was examined in this way because it had the highest potential for forming Fe-rich alteration products.

2.2.3 FE-SEM

In order to reach sufficient magnifications to distinguish the nano-spherules characteristic of allophane and hisingerite, samples were examined on a JEOL JSM-6700F field-emission SEM with a magnification range of 500x to 430,000x (5 micrometer to 10 nanometer resolution) in the EMiL at UNLV. Sample preparation was the same as that for SEM/EDS analyses. A standard voltage of 15 kV was used, with a working distance of 8.4 ± 0.1 mm. Allophane was examined in secondary electron mode, whereas Fe-allophane and hisingerite were examined in backscatter mode for increased resolution of fine particles.

2.2.4 FE-STEM

Freeze-dried samples of allophane and hisingerite were gently crushed in an agate mortar and pestle to break up aggregates, suspended in ethanol, and droplet-deposited on amorphous holey-carbon films supported on 200 mesh transmission electron microscope (TEM) grids. Transmission electron microscopy was carried out using a JEOL JEM-2500SE analytical field-emission scanning transmission electron microscope (FE-STEM) at NASA Johnson Space Center. Both conventional and STEM bright-field imaging was used in order to identify major morphological features of the grains, such as nano-spherules. Assessment of features on the crystal structure scale, including those indicative of short- or long-range crystal order, was made using high-resolution lattice fringe imaging (HRTEM). Major element composition of grains was assessed by energy-dispersive X-ray spectroscopy (EDS) analyses, including acquisition of element maps obtained through EDS compositional spectrum imaging.

Both unreacted hisingerite and allophane and hisingerite and allophane reacted at pH = 3 and pH = 10 for up to 181 days (for complete experimental details, including the initial and final pH of each experiment, as well as the total time the experiment ran, see supplemental material) were examined by FE-STEM in order to characterize crystallinity, morphology, and to identify alteration features and secondary phases due to reaction.

2.2.5 XRD

Samples were run on a PANalytical X'Pert Pro MPD 3040 instrument using a traditional spinner stage at NASA Johnson Space Center. Cu K α radiation was used for allophane and hisingerite, while Co K α radiation was used for Fe-allophane. The scan was conducted at 45 kV, 40 mA, from 2° to 80° 2 θ with a step size of 0.02° 2 θ , 100 seconds per step. Before analysis, samples were crushed gently in an agate mortar and pestle to break up aggregates, but were not sieved. Aluminum sample holders were used for all samples.

2.2.6 EGA

Evolved gas analysis was conducted in order to compare our synthetic materials with those measured in Gale Crater by the Sample Analysis at Mars (SAM) instrument on the Curiosity rover to check the appropriateness of our synthetic materials as martian analogs. EGA was conducted under conditions similar to those utilized by SAM. The analyses were conducted on a Netzsch STA 449 F1 Jupiter simultaneous thermal analyzer, coupled to a Pfeiffer ThermoStar GSD 320 quadrupole mass spectrometer at NASA Johnson Space Center. The temperature range was from 40 °C to 1050 °C with a ramp rate of 35 °C per minute. The carrier gas was helium, with a flow rate of 20 mL per minute, and the pressure was 30 mbar. Approximately 10 mg of sample was used for each run, and samples were run in duplicate. No special preparation of samples was conducted for EGA after freeze-drying.

2.2.7 BET surface area and particle size analysis

Approximately 400 mg each of synthetic allophane, Fe-allophane, and hisingerite, sieved to <355 μm , was prepared for particle size analysis and determination of Brunauer-Emmett-Teller (BET) specific surface area (SSA). Particle size analysis was conducted on a Microtrac Bluewave S4640 particle size analyzer at NASA Johnson Space Center. Samples were dispersed in ethanol and sonicated prior to analysis. Analyses were run in duplicate to increase accuracy. BET SSA was determined using a Micromeritics TriStar II 3020 surface area and porosity instrument at NASA Johnson Space Center. N_2 was used as the analysis adsorptive. Analyses were conducted in duplicate to allow estimates of uncertainty.

For allophane, the average BET SSA was $385.7658 \pm 0.1466 \text{ m}^2 \text{ g}^{-1}$ and the average particle size was $170.6 \pm 2.1 \text{ }\mu\text{m}$. For Fe-allophane, the average BET SSA was $350.2424 \pm 10.6735 \text{ m}^2 \text{ g}^{-1}$ and the average particle size was $135.5 \pm 0.6 \text{ }\mu\text{m}$. For hisingerite, the average BET SSA was $507.4815 \pm 0.2155 \text{ m}^2 \text{ g}^{-1}$ and the average particle size was $167.8 \pm 5.8 \text{ }\mu\text{m}$. The average BET SSA for each material was used to normalize the calculated initial dissolution rates to surface area. The complete results of particle size analyses and BET SSA analyses are given in the supplemental material (**Table S4**).

2.3 Dissolution experiments

Dissolutions of allophane, Fe-allophane, and hisingerite were carried out at pH = 3, 5, 7, and 10. Suspensions were prepared by adding 0.15 g of sample in acid-washed 250 mL polypropylene bottles containing 180 mL of 0.01 M NaCl solution. The pH was adjusted with 1.5 M HNO_3 or 1 M NaOH. The suspensions were shaken in a shaker water bath at $25.0 \pm 0.1 \text{ }^\circ\text{C}$ at 50 rpm for the entirety of each experiment. Each experiment was run in duplicate with a blank at each pH condition.

Solution aliquots (10 mL each) were taken periodically based on expected dissolution rates and

preliminary experiments. 8 mL of each sample aliquot was filtered through a 0.2 μm filter and acidified with 1% v/v high purity HNO_3 . The pH of the solution was measured from the remaining 2 mL of unfiltered sample aliquot. Experimental conditions for each experiment, including initial and final pH and total reaction time, are given in **Tables S5-S36** in the supplemental material. At the end of the experiments, the solution was decanted from the dissolution vessels, and the solid material was centrifuged at 11,000 rpm for 5 minutes, washed twice with deionized water to remove excess NaCl, and then frozen for at least 24 hours before freeze-drying for analysis by SEM and FE-STEM.

2.3.1 Solution chemistry

Elemental analyses for dissolved Fe, Al, and Si were conducted via flame atomic absorption spectroscopy on a Thermo Scientific iCE 3000 Series AA Spectrometer. Dissolved Fe was measured using an air-acetylene flame, and dissolved Al and Si were measured using an air-acetylene-nitrous oxide flame. Fe samples were treated with CaCO_3 to reduce interference and Al samples were treated with KCl to control ionization following the methods of Eaton et al. (2005). Method blanks were also run to check for possible contamination, and 18.2 M Ω deionized water was used as an instrument blank.

3. Results

3.1 Characterization of unreacted materials

3.1.1 FTIR

Infrared spectra obtained with FTIR analyses, shown below in **Figure 1**, were consistent with allophane, Fe-allophane, and hisingerite. All samples had bands at 3400 cm^{-1} , 1645 cm^{-1} , 1030 cm^{-1} , and 940 cm^{-1} , and weak bands at 825 cm^{-1} and 620 cm^{-1} . The band positions were close to previously published results (e.g. Wada, 1989; Montarges-Pelletier et al., 2005; Milliken et al., 2008; Rampe et al., 2012; Bishop et al., 2013), and varied from the literature values by less than 50 cm^{-1} . Montarges-Pelletier et al. (2005) showed that peak positions in FTIR spectra of allophanes vary significantly with Si/Al ratio, which may account for the wide range of values seen in the literature for allophane and hisingerite spectra.

The broad band at 3400 cm^{-1} is due to stretching vibration of H_2O molecules. The energy and short lifetime of the vibrational state is typical for free water, indicating that this band is likely due to adsorbed water (Wada, 1989; Montarges-Pelletier et al., 2005). The band centered at 1645 cm^{-1} is assigned to bending vibration of H_2O molecules, although this band is much sharper than the stretching modes from structural and/or adsorbed water (Ohashi et al., 2002, Montarges-Pelletier et al., 2005). Based on the low intensity of the sharp H_2O bending band, compared with the properties of the H_2O stretching band, we conclude that most of the water in our synthetic materials is likely adsorbed rather than structural. Bands at 1030 cm^{-1} and 940 cm^{-1} are due to Si-O-Al stretching. Bands due to OH and/or Al-O bending exist at 825 cm^{-1} and 620 cm^{-1} , although they are difficult to distinguish in this dataset due to noise (Bishop et al., 2013).

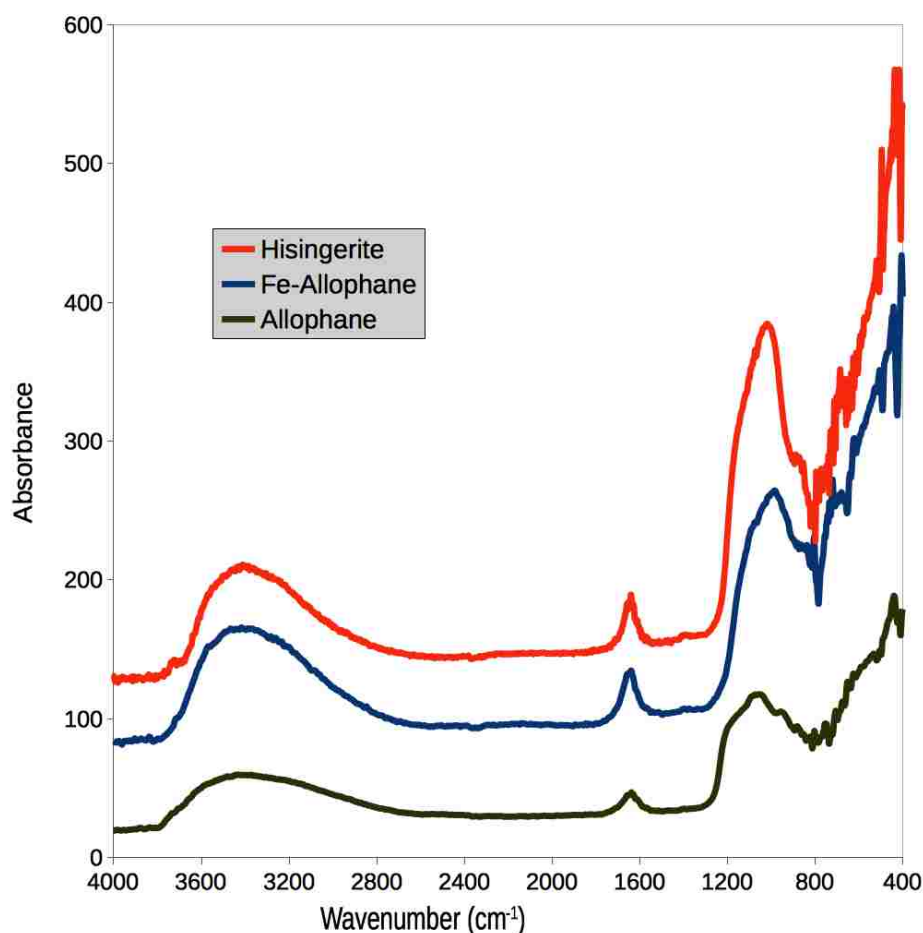


Figure 1. FTIR spectra of allophane, Fe-substituted allophane, and hisingerite. The spectra are offset for clarity.

3.1.2 SEM/EDS

In general, unreacted samples examined by SEM consisted of large, smooth grains $\sim 300\text{--}600\ \mu\text{m}$ in diameter coated with much smaller ($\sim 10\text{--}50\ \mu\text{m}$) flakes of "fluffy" material (Figures S6-S7, supplemental material). Semi-quantitative EDS analyses yielded mainly Al, Si, and Fe compositions consistent with synthesis ratios (**Table S2**, supplemental material). No major compositional differences were observed between the larger, smooth grains and the smaller, "fluffy" material. Cl was observed in a few samples, most likely the result of incomplete washing, but was not prevalent.

3.1.3 FE-SEM

FE-SEM analyses of unreacted material also showed that all samples contained large, smooth

chunks of material as well as small, "fluffy" aggregates (e.g. **Figure 2**; **Figures S10-S12** in supplemental material). Often the smaller, "fluffy" grains were attached to or associated with the larger, smoother grains. The "fluffy" texture is most likely due to individual allophane or hisingerite nano-spherules. The large, smooth grains are likely also aggregates of nano-spherules, since EDS analyses (see above) revealed no significant compositional differences between large and small grains. These aggregates may have been compacted into more coherent grains by centrifugation during the washing process.

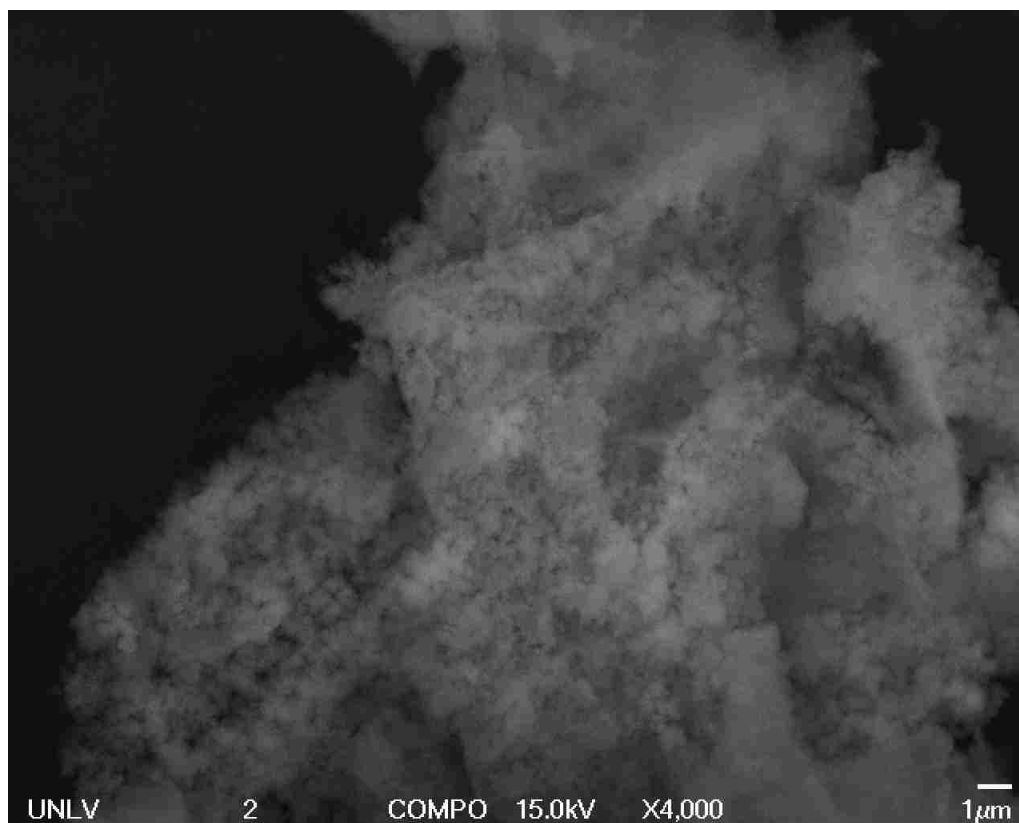


Figure 2. Synthetic Fe-allophane imaged by FE-SEM. Nano-spherules are distinguishable in the "fluffy" texture of the aggregate. Similar textures were observed in allophane and hisingerite samples (supplemental material).

3.1.4 FE-STEM

Particles with nano-spherule structures, indicative of allophane and hisingerite, were observed in the TEM subsamples of the unreacted synthetic samples (**Figure 3**; **Figure S1**, supplemental material). Such nano-spherules have previously been observed in samples of natural allophane (e.g. Wada, 1989;

Iyoda, 2012) and natural hisingerite (e.g. Eggleton and Tilley, 1998). Our synthetic hisingerite particles exhibited poorly-developed lattice fringes in some localized regions (**Figure 3c**), indicative of mid- to long-range order. However, the majority of hisingerite material was structurally disordered (i.e., amorphous) based on HRTEM images analyzed by Fourier-transform image processing. Our synthetic allophane did not show any lattice fringes, even when exposed to the electron beam for several minutes. Two different textures were observed in the allophane sample; one "fluffy," likely representing an aggregate of many individual nano-spherules, and one "smooth." These morphologies are consistent with those presented by Wada (1989) for natural allophane and Eggleton and Tilley (1998) for natural hisingerite.

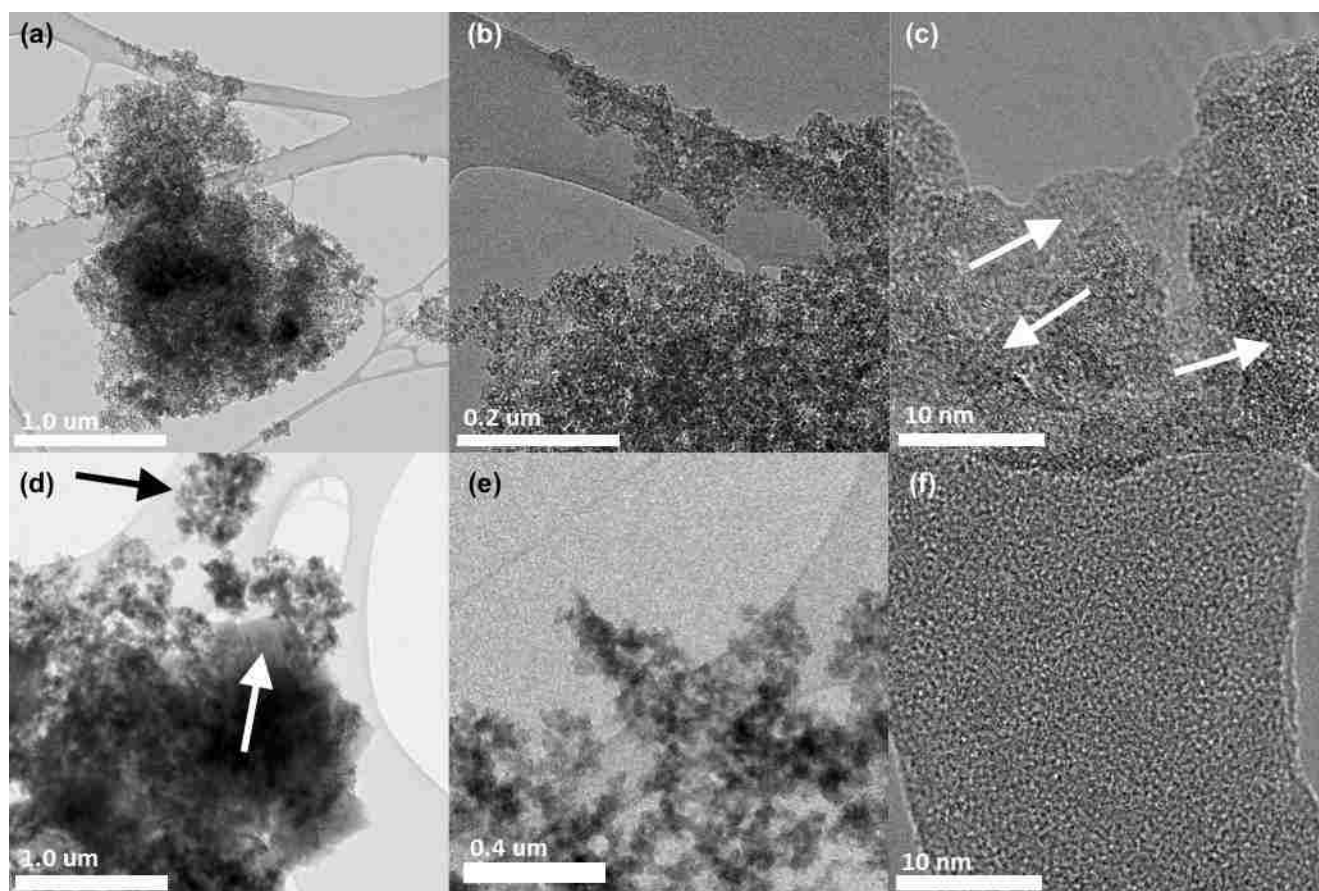


Figure 3. TEM images of synthetic unaltered hisingerite (a-c) and allophane (d-f). **a)** An agglomerate of synthetic hisingerite. **b)** A closer view of synthetic hisingerite agglomerate in (a). Nano-spherules are visible, especially along the edges of the agglomerate. **c)** A very high-magnification view of synthetic hisingerite. Lattice fringes (arrows) indicate some crystalline structure. **d)** An agglomerate of synthetic allophane. Nano-spherule-like structures are visible along the edges of the agglomerate. Both the "fluffy" (black arrow) and "smooth" (white arrow) textures are visible. **e)** A closer view of (d), showcasing the "fluffy" nano-spherule structures. **f)** Very high magnification of synthetic allophane. Note the lack of lattice fringes, indicating no long-range crystal structure

3.1.5 XRD

Synthetic allophane, Fe-allophane, and hisingerite all had similar diffraction patterns with elevated low background and broad peaks, indicating an abundance of small particles and nano-crystalline structure, respectively (van der Gaast and Vaars, 1981). Allophane had a prominent peak at 3.1 Å d-spacing, with a possible second peak at 7.2 Å; Fe-allophane had two peaks at 2.9 and 1.9 Å; and hisingerite had three peaks at 3.2, 2.7, and 1.5 Å (**Figure S17**).

The d-spacings obtained by XRD for synthesized allophane, Fe-allophane, and hisingerite are consistent with literature values for natural and synthetic allophane and hisingerite (e.g. Yoshinaga and

Aomine, 1962; Wada and Yoshinaga, 1969; Milliken and Bish, 2014). Mustoe (1966) summarizes the d-spacings of various natural hisingerite samples, indicating variations in d-spacings of up to 0.3 Å, as well as variability in the number of observed peaks. Therefore, considering the variability in natural samples, our synthetic materials have XRD patterns consistent with allophane, Fe-allophane, and hisingerite.

3.1.6 EGA

Hisingerite and allophane exhibited mass-18 (i.e., H₂O) release at ~130 °C, likely of adsorbed H₂O (**Figure S13**), consistent with previous laboratory measurements of water release from allophane. Release of O₂ (mass 32) occurred concurrently with H₂O release in all samples (**Figure S14**), and therefore is likely a result of fragmentation of released H₂O during ionization in the mass spectrometer. No CO₂ (mass 44) or SO₂ (mass 64) releases were observed from our synthetic materials, consistent with the absence of carbon and sulfur in the syntheses (**Figures S15, S16**).

Overall, these observations are consistent with previous measurements for allophane (e.g. Bish and Duffy, 1990; Rampe et al., 2016). Although we are not aware of any published EGA data for hisingerite, the observed concordance between allophane and hisingerite samples is consistent with the expectation that allophane and hisingerite would behave similarly under EGA conditions.

3.2 Dissolution experiments

3.2.1 Solution chemistry

The pH of dissolution experiments with low initial pH rose with time, the pH of the dissolution experiment with high initial pH decreased with time, and the pH of the near-neutral experiment remained near-neutral throughout the experiment (**Figure 4**). For all experiments, an initial rapid change in pH occurred, which then leveled off to a steady-state value. All experiments reached their steady-state pH within 18 days after the start of the experiment, and for all experiments except pH 5, hisingerite had the

lowest steady-state pH.

The initial rapid change in pH corresponded to an initial linear release of silica, which was used to calculate the dissolution rate (see Section 3.2.2 below). The pH at the final time point of this rapid-release phase was ~3.23-4.14 for experiments with initial pH = 3, ~5.98-6.47 for experiments with initial pH = 5, ~5.24-7.17 for experiments with initial pH = 7, and ~6.85-8.70 for experiments with initial pH = 10. The initial and final pH data for the rapid-release phase of dissolution are summarized below in **Table 1**. As seen in **Figure 4**, the final pH of the data used to calculate the rates was usually closer to the initial pH than to the steady-state pH of the experiment.

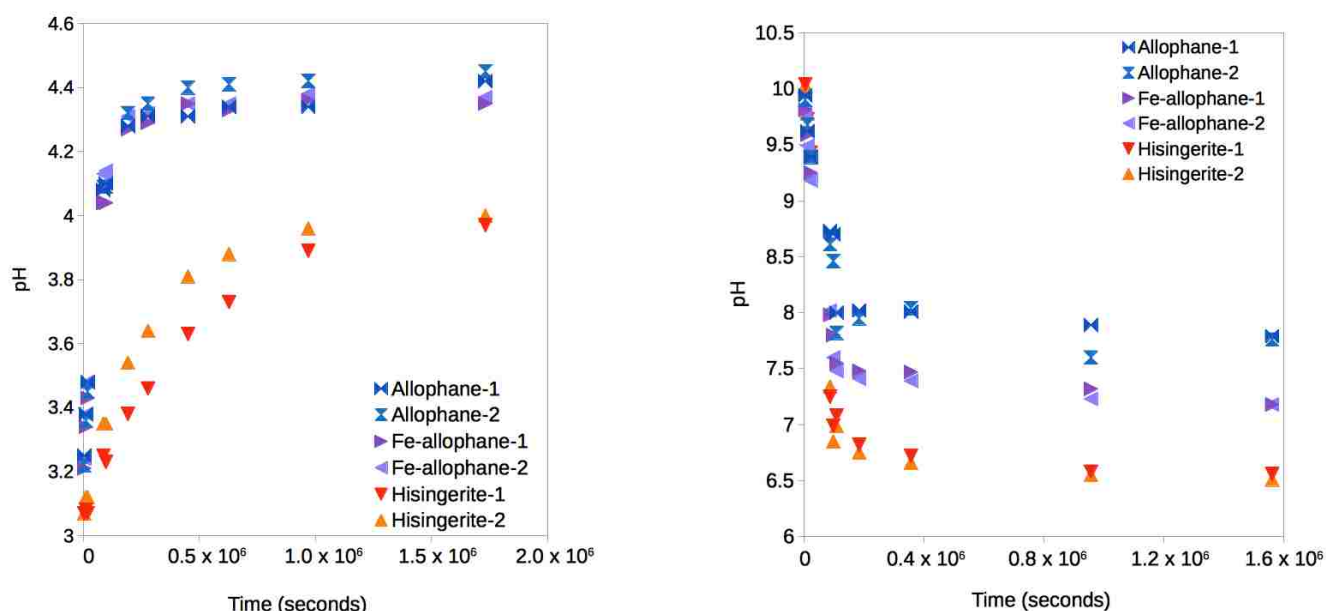


Figure 4. Observed change in solution pH with time for the initial pH = 3 (**left**) and initial pH = 10 (**right**) experiments. The experiments at pH 5 showed similar pH change to those at pH 3, in that the pH of all experiments rose with time until reaching a steady-state value. The experiments at pH 7 were somewhat similar to those at pH 10, in that the pH of hisingerite experiments decreased from pH ~7, although the pH of the Fe-allophane experiments remained relatively constant, and the pH of the allophane experiments increased slightly (data in supplemental material). Balanced chemical equations (see supplemental material **Section S8**) explain the observed pH changes.

In all experiments except hisingerite reacted at pH 3, Fe remained below the practical quantitation limit of the atomic absorption spectrometer (<0.2 ppm Fe) throughout the duration of the experiment. For hisingerite at pH 3, the concentration of Fe in solution first increased rapidly, then decreased more slowly (see **Figure S23**, supplemental material). Likewise, Al was only above the practical quantitation

limit (1.0 ppm) in the allophane, Fe-allophane, and hisingerite dissolution experiments carried out at pH 3. In these experiments, Al concentration similarly first rose rapidly, and then leveled off or decreased slowly as the pH approached steady-state (**Figure S23**).

For all experiments, Si concentrations were above detection at all time points. Si concentrations initially increased linearly, and then reached a steady concentration of ~ 0.2 - 0.5 mM within 18 days. The linear section of the Si release curve was used to calculate dissolution rates (see Section 3.2.2). During dissolution of hisingerite, Fe release was always below the ~ 0.5 :1 stoichiometric Fe/Si ratio, while Al release was initially higher than the ~ 0.5 :1 Al/Si stoichiometric ratio, and then decreased with time to approximately stoichiometric values (**Figure 5**). Allophane and Fe-allophane reacted at pH 3 also showed Al/Si ratios in solution that were initially above stoichiometric values and then decreased to below the ~ 1 :1 stoichiometric value (**Figure 5**). Solution chemistry for each time point for each experiment is reported in the supplemental material (Section S9).

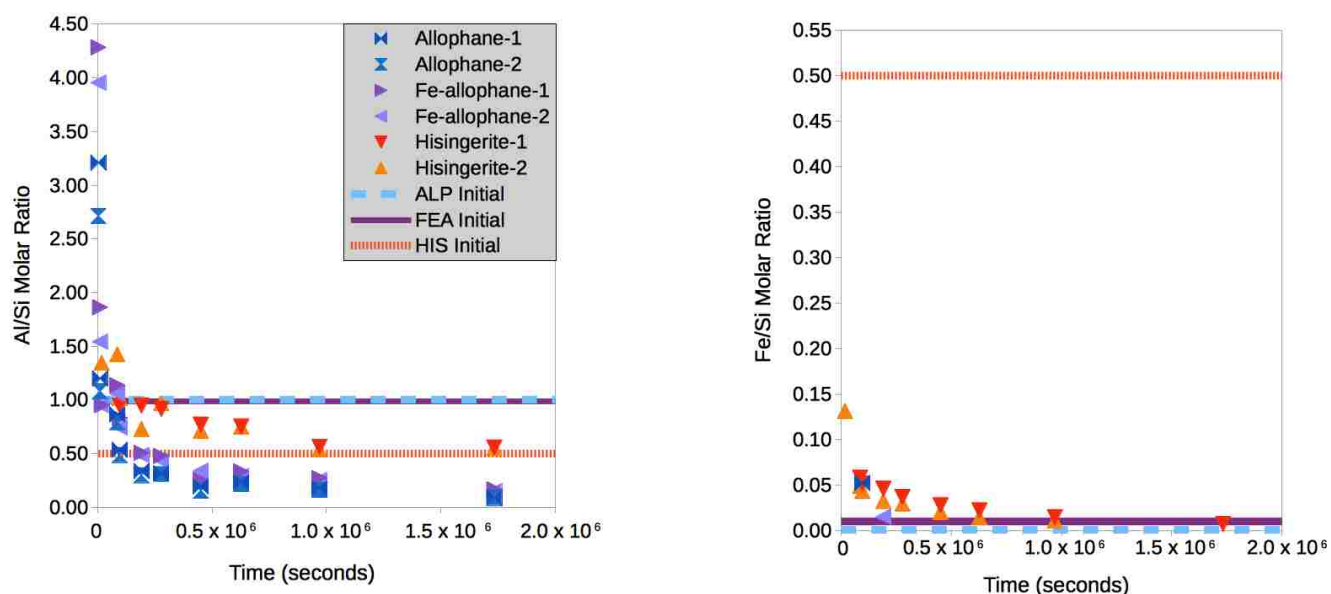


Figure 5. Al/Si ratio (**left**) and Fe/Si ratio (**right**) measured from solution in pH 3 experiments versus time. Points where Fe, Al, or Si were below detection are not plotted. ALP Initial, FEA Initial, and HIS Initial indicate the synthesis ratios of the unaltered allophane, Fe-allophane, and hisingerite, respectively.

3.2.2 Calculations

Dissolution rates were determined from moles Si released into solution with time. The Si concentration measured in solution was corrected for volume removed to moles Si released using the equation:

$$m_t = m_{(t-1)} + (c_t - c_{(t-1)})V_{(t-1)} \quad (1)$$

where m_t and $m_{(t-1)}$ are the moles Si released at times t and $t-1$, c_t and $c_{(t-1)}$ are the corresponding concentrations in mols L^{-1} , and $V_{(t-1)}$ is the volume of solution remaining at time $t-1$ (Welch and Ulmann, 2000).

Dissolution of all materials showed an initial linear rapid dissolution phase, followed by a slower phase that approaches steady conditions (**Figure 6**). The initial linear part of this curve, generally the first five to eight points, was fit with a linear regression, where the slope of the line was the silica release rate in mol s^{-1} . The dissolution rate was calculated using the following equation:

$$r_{diss} = \frac{\Delta m / \Delta t}{A \times M} \quad (2)$$

where r_{diss} is the dissolution rate in $\text{mol m}^{-2} \text{s}^{-1}$, $\Delta m / \Delta t$ is the silica release rate in mol s^{-1} , A is the average BET SSA of the material in $\text{m}^2 \text{g}^{-1}$, and M is the total mass of material in the reactor in g (**Table 1**). One of the duplicate experiments of Fe-allophane at pH 7 was excluded from the rate calculations due to anomalous experimental conditions (see supplemental material).

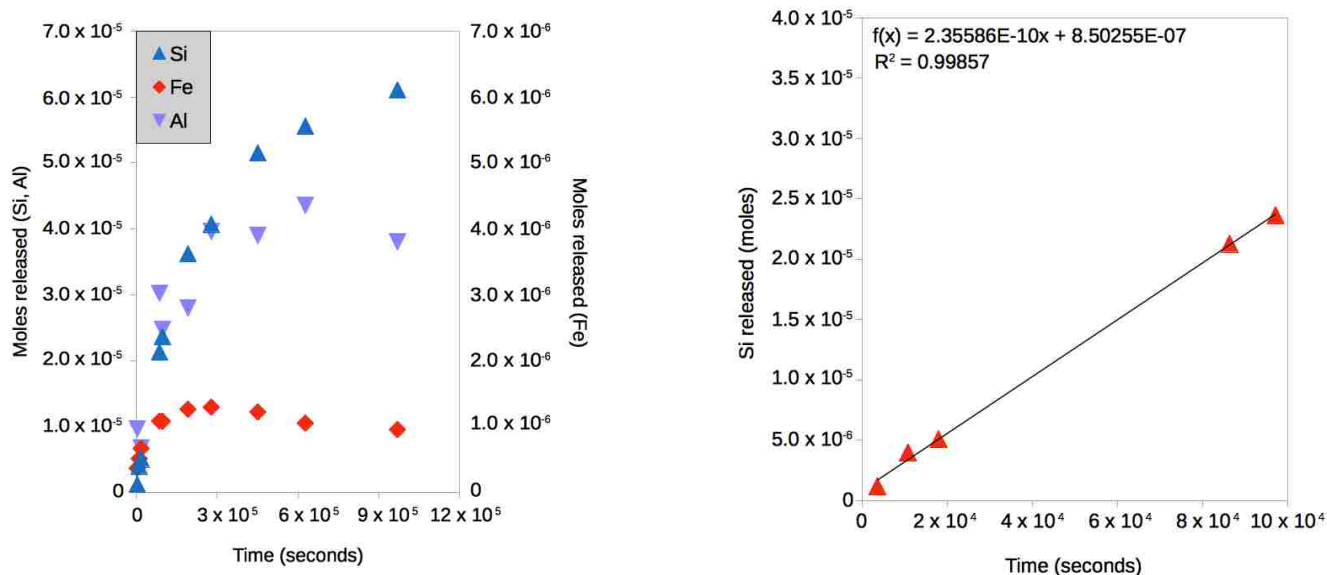


Figure 6. Typical shape of the Si, Al, and Fe release curves for allophane, Fe-allophane, and hisingerite dissolution (**left**) and the linear portion of the silica release curve (**right**) as exemplified by a hisingerite experiment with initial pH = 3. In general, hisingerite reached higher final Si, Al, and Fe concentrations than allophane or Fe-allophane. No Al or Fe release was observed in experiments at pH 5, 7, or 10. Full data sheets for all experiments are given in the supplemental material.

Rate law equations were determined by plotting the log of the dissolution rates from Equation (2) against the pH of the experiment, and then fitting the points with a linear regression. The resulting rate law equation was of the form:

$$\log r_{diss} = \log k_{diss} - n \times pH$$

where r_{diss} is the surface-area normalized dissolution rate, k_{diss} is the dissolution rate constant, and n is the reaction order with respect to H^+ . For allophane, $\log r_{diss} = -11.05 - 0.088 \times pH$; for Fe-allophane, $\log r_{diss} = -11.09 - 0.091 \times pH$; and for hisingerite, $\log r_{diss} = -11.49 - 0.032 \times pH$. The pH at the first time point was considered to be the pH of the experiment, since the majority of dissolution took place at or near that pH (see Section 3.2.1 and Section S9). The pH dependence for all phases was low; for allophane, $n = 0.088 \pm 0.014$; for Fe-allophane, $n = 0.091 \pm 0.026$; and for hisingerite, $n = 0.032 \pm 0.0089$. The error is the 1- σ standard deviation of n . The pH dependence of allophane and Fe-allophane were within uncertainty of each other, which is not surprising given the structural and compositional similarity of these phases. The pH dependence of hisingerite is lower than that of the allophane phases, consistent

with previous results for amorphous Al- and Fe-phosphates (Tu et al., 2014). Balanced chemical equations for each pH condition (Section S7) demonstrate the production or uptake of H^+ ions that explain these trends. While dissolution was not stoichiometric, the general trends described by the balanced chemical equations hold true; namely, that the pH dependence of hisingerite dissolution is less than that of allophane and Fe-allophane dissolution. The difference in pH dependence between the Al-rich and Fe-rich phases is also supported by the balanced equations for these reactions (supplemental material). The scatter in the experimental rate data is likely due to the small dependence of silica release rate on pH.

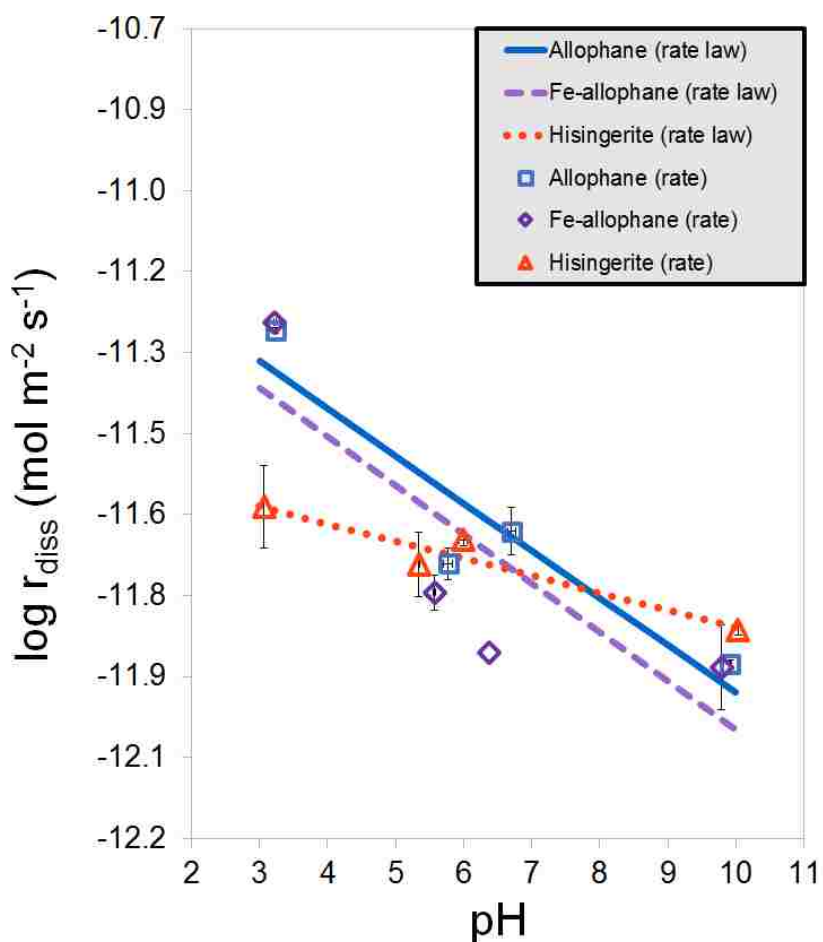


Figure 7. Average of the dissolution rates (points) and rate laws (lines) for allophane, Fe-allophane, and hisingerite at pH 3, 5, 7, and 10. Error bars represent the range of values for the dissolution rates. All experimental data are given in the supplemental material.

Table 1. Measured pH at the first time point (t_i), measured pH at the final time point of the data used to calculate the dissolution rates (t_f), dissolution rates (r_{diss}) and their 1- σ standard deviations (Std err) at each experimental pH condition for each material. The "-1" or "-2" suffix indicates duplicate experiments. Averages of the data are plotted in **Fig. 7** with rate laws. Shaded cells were omitted from the rate law calculation due to anomalous experimental conditions (see supplemental material **Table S20**). All solution compositions for each experiment at each time point are given in Supplemental Material (**Tables S5-S36**).

Material	pH 3				pH 5				pH 7				pH 10			
	pH at t_i	pH at t_f	r_{diss}^a $\times 10^{-12}$	Std err ^a $\times 10^{-12}$	pH at t_i	pH at t_f	r_{diss} $\times 10^{-12}$	Std err $\times 10^{-12}$	pH at t_i	pH at t_f	r_{diss} $\times 10^{-12}$	Std err $\times 10^{-12}$	pH at t_i	pH at t_f	r_{diss} $\times 10^{-12}$	Std err $\times 10^{-12}$
Allophane-1	3.25	4.10	5.44	0.509	5.84	6.47	2.17	0.144	6.76	7.17	2.11	0.245	9.94	8.70	1.35	0.145
Allophane-2	3.22	4.09	5.57	0.436	5.71	6.39	1.92	0.182	6.65	7.06	2.28	0.356	9.90	8.46	1.30	0.172
Fe-allophane-1	3.21	4.04	5.70	0.423	5.59	5.98	1.95	0.101	6.38	6.40	1.39	0.0846	9.81	7.80	1.09	0.172
Fe-allophane-2	3.24	4.14	5.72	0.627	5.56	6.05	1.67	0.271	6.37	6.42	1.00	0.610	9.78	7.60	1.16	0.128
Hisingerite-1	3.07	3.23	2.17	0.0995	5.33	6.56	2.33	0.103	5.94	5.27	2.29	0.158	10.04	6.99	1.57	0.150
Hisingerite-2	3.07	3.35	3.10	0.0676	5.35	6.46	1.77	0.218	6.05	5.24	2.31	0.132	10.03	6.85	1.50	0.265

^a r_{diss} and standard error have units of $\text{mol m}^{-2} \text{s}^{-1}$

3.3 Characterization of reacted materials

3.3.1 SEM/EDS

Analyses of hisingerite reacted for two days and hisingerite reacted for one month revealed that the texture of hisingerite grains tended to become more porous with increasing dissolution time, and the grains themselves tended to become smaller. **Figures S7-S9** (supplemental material) show representative SEM images of grains of each sample.

3.3.2 FE-STEM

Hisingerite that had been reacted at pH 10 for 2 months showed the formation of small ($\sim 2 \mu\text{m}$) linear features within the larger hisingerite aggregates (**Figure 8; Figure S3** in supplemental material). These features were interpreted as the rolled or curled edges of silicate sheets, possibly due to the inception of conversion to phyllosilicate. Overall, the material was still poorly crystalline, and the linear features did not demonstrate a higher degree of crystallinity than the surrounding masses, as demonstrated by their lack of lattice fringes. The linear features were also observed in hisingerite that was reacted at pH 3 for 6 months, although they were much less prevalent.

Only a few of these linear "edge-curl" features were observed in allophane that had been reacted

at pH 10 for 2 months (**Figure S4**, supplemental material). Allophane also maintained the morphological dichotomy between a "fluffy" texture and a "smooth" texture (**Figure 8**) seen in the unreacted material. The "smooth" texture was rapidly destroyed by the high-energy STEM beam, while the "fluffy" texture was more robust, suggesting a higher degree of hydration in the "smooth" material (**Figure S5**, supplemental material). This extreme beam-sensitivity was only observed in the altered material, but may also be true of the unaltered material.

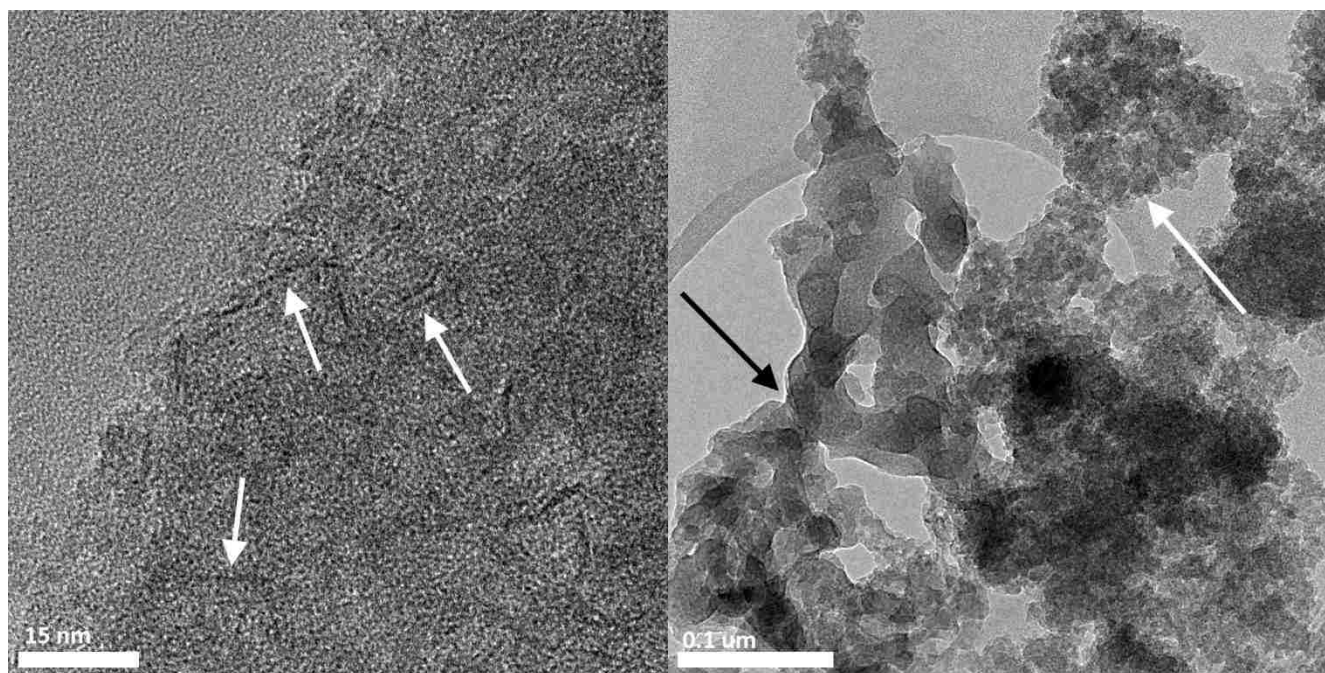


Figure 8. TEM images of synthetic hisingerite (**left**) and allophane (**right**), each reacted at ~pH 10 for 2 months. Edge-curl features were much less prevalent in the allophane sample than in the hisingerite. **Left:** Arrows indicate linear features that may represent the curled edges of incipient phyllosilicate-like sheets. **Right:** The "smooth" morphology is visible on the left (black arrow), while the "fluffy" morphology is on the right (white arrow).

4. Discussion

4.1 Comparison of synthetic amorphous materials to Mars

It is important to compare our synthetic materials directly to phases found on the martian surface to ensure that they are appropriate functional analogs. In the absence of returned samples, these synthetic analogs can also help us to understand properties of the martian amorphous soil component that cannot be examined with current remote instrumentation, such as dissolution kinetics, micro-morphology, and formation of secondary phases.

The contributions from the amorphous component in the XRD patterns obtained from the Rocknest, Cumberland, John Klein, and Windjana samples, which have been fit with allophane and basaltic glass, have a broad peak centered around $28^\circ 2\theta$ (Dehouck et al., 2014). Synthesized allophane, Fe-allophane, and hisingerite all have similarly broad peaks, likewise centered around $28^\circ 2\theta$, corresponding to a d-spacing at 2.9-3.2 Å (supplemental material **Figure S17**). Although other phases are likely present in the martian amorphous soil component, such as basaltic or rhyolitic glass, ferrihydrite, and amorphous sulfates, our phases are a good fit to the Gale Crater sites, indicating their relevance to the martian amorphous material. Other poorly crystalline phases, such as ferrihydrite and opal, have XRD peaks that are inconsistent with the Gale Crater data, with d-spacings that are either too small (2.58 Å for ferrihydrite, e.g. Schwertmann and Cornell, 2000) or too large (3.42-4.03 Å for opal, e.g. Smith, 1998) to fit the observed data from Gale Crater.

Mass-balance calculations performed by Dehouck et al. (2014) provided a range of possible compositions for the martian amorphous soil component. The range of possible SiO_2 , Al_2O_3 , and FeO_T contents are summarized below in **Table 2**, along with the SiO_2 , Al_2O_3 , and Fe_2O_3 contents of our synthetic materials. Vaniman et al. (2014) performed similar calculations to obtain the abundance of amorphous material in the Rocknest, Cumberland, and John Klein samples, but did not calculate possible compositions of the amorphous component.

Table 2. Putative SiO₂, Al₂O₃, and FeO_T contents, in weight percent, of the martian amorphous soil component, as calculated by Dehouck et al. (2014), compared with the values for our synthetic allophane, Fe-allophane, and hisingerite. “NA” = None Added during synthesis.

Oxide (wt%)	Mars amorphous soil component (Dehouck et al., 2014)	Synthetic allophane (this study)	Synthetic Fe-allophane (this study)	Synthetic hisingerite (this study)
SiO ₂	31.9-37.1	37.08	36.95	31.47
Al ₂ O ₃	2.8-5.9	62.92	62.7	26.7
FeO _T	23.7-27.7	0*	0.98*	41.8*
SO ₃	11.0-16.1	NA	NA	NA
Na ₂ O	3.6-4.4	NA	NA	NA
CaO	3.7-5.4	NA	NA	NA
P ₂ O ₅	2.1-3.1	NA	NA	NA
TiO ₂	2.1-2.9	NA	NA	NA
MgO	1.2-4.8	NA	NA	NA
Cl	1.4-2.0	NA	NA	NA
Cr ₂ O ₃	1.1-1.6	NA	NA	NA
MnO	0.9-1.4	NA	NA	NA
K ₂ O	0.8-1.1	NA	NA	NA

*Calculated as wt% Fe₂O₃

The compositions calculated by Dehouck et al. (2014) include SO₃ (~16%), Na₂O (~4.4%), CaO (~3.7%), and P₂O₅ (~3.1%), along with six other oxides (**Table 2**). This highlights the fact that the martian amorphous soil component likely does not consist of a single phase, but is rather a mixture of phases (e.g. Bish et al., 2014; Achilles et al., 2017). Although the Al contents of our materials are higher than that of the martian amorphous soil component, this may be due to the presence of other high-silica and high-Fe phases, such as high silica glasses and iron sulfates, in the martian samples, rather than being the result of a martian Fe-Al-silicate phase with vastly different elemental ratios.

The EGA data of our synthetic samples (**Figures S13-S16**), which were dominated by water release at ~130-150 °C, compared favorably to SAM-EGA data of samples from Gale Crater. SAM data from the Rocknest, Cumberland, John Klein, and Windjana samples showed a mass-18 H₂O release profile dominated by H₂O release around 200-300 °C, likely from hydrated sulfates and clays. However,

the H₂O release from these samples is too broad to be due solely to hydrated sulfates and clays, and requires contributions from amorphous phases with adsorbed water, such as allophane (Leshin et al., 2013; Sutter et al., 2017). Sutter et al. (2017) predict contributions from allophane and other amorphous phases below ~450 °C, with adsorbed water being released below ~200 °C, and Leshin et al. (2013) attribute water release ~110 °C to allophane.

Based on FTIR spectra (Section 3.1.1), the water in our synthetic samples seems to be primarily adsorbed, rather than chemically bound in the lattice, which may account for the observed difference. Therefore, although only a small fraction of the water release from samples at Gale Crater is attributed to amorphous materials, our samples agree well with that component.

Based on the results of these analyses and current data, our synthetic allophane, Fe-allophane, and hisingerite are appropriate analogs for the Mars amorphous soil component. XRD analyses indicate that our synthetic materials have similar d-spacings to the materials found on Mars; their compositions are consistent with fractions of the martian amorphous soil component; and EGA analyses indicate that they have water adsorption properties consistent with martian amorphous materials. Therefore, the properties of our synthetic materials, such as dissolution rates, micromorphology, and secondary products can be used to help us better understand the amorphous materials that are present on Mars.

4.2 Dissolution rates and rate laws

The dissolution rates measured for allophane, Fe-allophane, and hisingerite are very similar to each other (within 10%, see **Figure 7**), and are approximately an order of magnitude faster than dissolution rates measured for crystalline clay minerals of similar compositions, such as nontronite (Gainey et al., 2014; Steiner et al., 2016) and kaolinite (Carroll-Webb & Walther, 1990; Huertas et al., 1999; Cama et al., 2002) (**Figure 9**). This is consistent with trends observed for other amorphous or poorly crystalline materials; amorphous Al and Fe phosphates dissolve more rapidly than crystalline Al

and Fe phosphates (Huffman 1960; Tu et al., 2014), and amorphous silica dissolves more rapidly than quartz (Liang and Readey, 1987). Therefore, interactions between liquid water and poorly crystalline silicate phases, such as allophane and hisingerite, release cations and silica into solution more rapidly than well-crystalline phases with similar compositions.

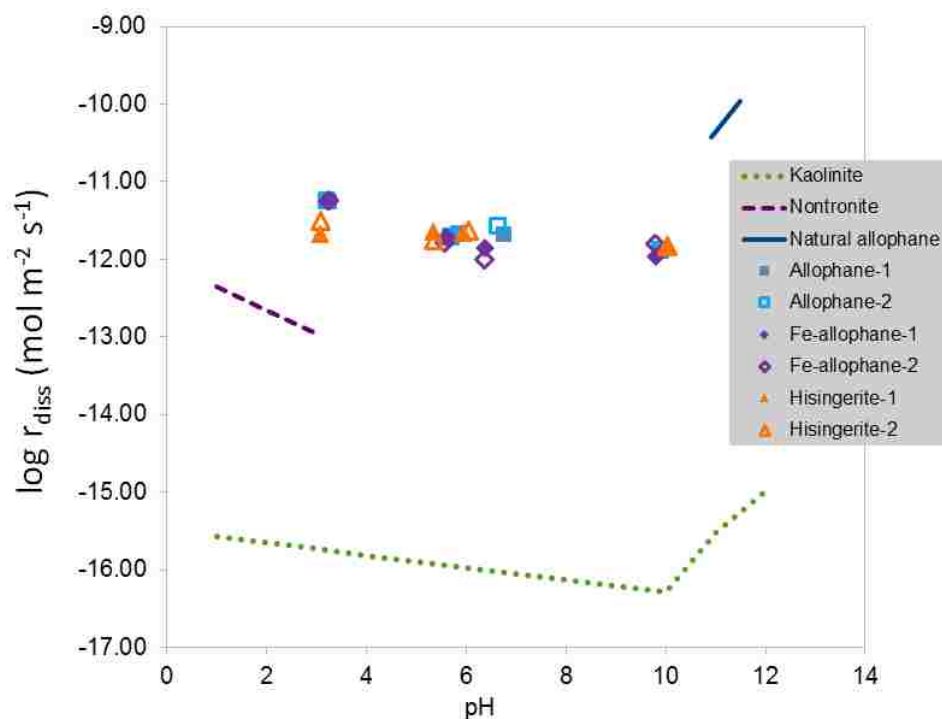


Figure 9. Comparison of the log of the dissolution rates of our synthetic allophane, Fe-allophane, and hisingerite (points) with rate laws for kaolinite (Carroll-Webb and Walther, 1990), nontronite (Gainey et al., 2014), and natural allophane (Abidin et al., 2004) (lines).

In addition, a very low dependence on H^+ is observed for all materials (hisingerite, $n = 0.032 \pm 0.0089$, Fe-allophane, $n = 0.091 \pm 0.026$, and allophane, $n = 0.088 \pm 0.014$). These dependences are much lower than for other silicates; for example, for kaolinite, $n = 0.78$ under acidic conditions (Palandri and Kharaka, 2004), and for nontronite, $n = 0.297$ under acidic conditions (Gainey et al., 2016).

The dissolution behavior of these phases—very similar dissolution rates, with very low reaction orders with respect to H^+ —may be explained by the structures of allophane and hisingerite, described by Iyoda et al. (2012) and Eggleton and Tilley (1998), respectively. Allophane consists of hollow, porous

nano-spherules ~ 5 nm (50 \AA) in diameter, formed from a rolled SiO_4 sheet surrounded by a gibbsite sheet (Iyoda et al., 2012; Wada, 1989). Gibbsite dissolution has a large reaction order with respect to H^+ ($n = 0.992$) (Palandri and Kharaka, 2004). However, dissolution of pure silica phases, such as amorphous silica or quartz, does not depend on pH under acidic conditions (e.g. Palandri and Kharaka and references therein). Therefore, if acidic conditions enhance dissolution of the gibbsite phases in allophane, but the gibbsite layer is a single layer on top of the silica sheet, we would expect dissolution rates based on Si release rates to be relatively insensitive to pH. These conditions are entirely consistent with our observations of Al release and dissolution rates based on silica release rates.

In hisingerite, a similar layered nano-spherule structure is observed (Shayan, 1984; Eggleton and Tilley, 1998). However, the layers occur in multiple concentric sheets, similar to the structure of true phyllosilicates, and form nano-spherules up to 200 \AA in diameter (Shayan, 1984). These multiple concentric layers may reduce the dissolution rate under acidic conditions by protecting inner layers of SiO_4 from species in solution. In addition, the balanced reactions for stoichiometric dissolution of these phases help explain the lower pH dependence of hisingerite than the allophanes.

Release of Fe and Al from our synthetic materials was non-stoichiometric (**Figure 5**), with all steady-state ratios below stoichiometric values. This non-stoichiometric dissolution indicates that the altered material is likely more Al- and Fe-rich than the starting material. Al (and Fe if present) is first leached rapidly from the gibbsite sheet in the nano-spherules (supplemental material **Tables S29-S36**), and then concentrations decrease, consistent with reprecipitation of a secondary phase.

4.4 Secondary phases and altered material

Allophane and hisingerite are generally considered to occur as intermediates in the formation of more stable phases, such as kaolinite and nontronite (Wada, 1989). The lifetime of allophane in soils ranges from $\sim 2,000$ years in tropical climates (Bleeker and Parfitt, 1984) to $>30,000$ years in more

temperate zones, such as central Japan (Nagasawa, 1978). During the weathering process, opaline silica and Al or Fe complexes alter to allophane and/or hisingerite, which are then converted to imogolite or halloysite, and then to more mature layer silicates (Wada, 1989). However, despite the studies examining these large-scale transitions, little work has examined the incipient weathering of poorly crystalline phases such as allophane and hisingerite. Our work shows that under alkaline conditions, phyllosilicate precursor phases form rapidly from allophane and hisingerite, on the order of a few months under laboratory conditions.

FE-STEM analyses of hisingerite reacted for 2 months at pH 10 showed linear "edge-curl" features that were not present in the unreacted materials (**Figure 3, Figure 8; Figures S1-S5**, supplemental material). The alternating layers of silica and aluminum in hisingerite may act as an incipient phyllosilicate structure and precursor phase to the formation of clay minerals under alkaline conditions. At low pH, fewer of these linear features were observed. This may be because conditions at low pH may be less favorable to phyllosilicate formation, or because the samples from pH 3 experiments examined with FE-STEM were reacted for a longer time than those at pH 10 and enough of the hisingerite may have dissolved to remove phyllosilicate-like structures.

As described above, allophane and Fe-allophane do not have the same alternating layers of silica and aluminum as hisingerite (Iyoda et al., 2012), and also show fewer phyllosilicate-like "edge-curl" features than hisingerite. Because the allophanes contain few incipient phyllosilicate characteristics (e.g. a tetrahedral Si_2O_5 sheet), they may be less likely to develop phyllosilicate precursor phases when exposed to alkaline conditions.

4.5 Implications of experiments for Mars

Our dissolution experiments with poorly crystalline allophanes and hisingerite demonstrate rapid initial dissolution and separation of silica and Fe-rich phases across the range of pH conditions. Silica

tends to enter solution from allophane, Fe-allophane, and hisingerite, while Fe either rapidly re-precipitates or does not enter solution at all. FE-STEM analyses of reacted materials show diagnostic linear features that are not seen in unreacted material, which are more prevalent at alkaline pH than at acidic pH. In the event that samples containing hisingerite or allophane are returned from Mars, therefore, it might be possible to observe similar features that indicate interaction with past liquid water (on the order of months to years). The rapid alteration of poorly crystalline silicate materials could be a useful tool for examining very short-lived episodes of water-rock interaction; on timescales where more crystalline materials would show little to no chemical, mineralogical, or morphological change due to interaction with water, poorly crystalline materials may be significantly altered.

In light of the rapid dissolution rates of allophane, Fe-allophane, and hisingerite, the continued presence of allophanic materials in returned samples from Mars would indicate that interactions of liquid water with the amorphous component were limited. Although the dissolution rates of all three materials are fastest at pH 3, and slower at more alkaline pH conditions, the range between the fastest and slowest dissolution rates spans less than an order of magnitude. Therefore, allophane or hisingerite on Mars would have dissolved rapidly if abundant liquid water was present, regardless of the water's pH.

The tendency of silica to enter solution from hisingerite while leaving Fe-containing phases behind may contribute to the silica-rich deposits (>50 wt% high-Si crystalline and amorphous materials) found in ancient mudstone and sandstone on the lower slopes of Mt. Sharp in Gale Crater, as well as the presence of Fe-rich deposits, such as those seen in Vera Rubin Ridge in Gale Crater (Rampe et al., 2017; Yen et al., 2017). If silica dissolved from hisingerite or other amorphous materials and was transported away by moving water, it would tend to re-precipitate in areas where the waters pooled, leaving Fe-rich deposits behind.

5. Conclusions

The presence of rapidly dissolving, poorly crystalline materials in Gale Crater indicates that interaction of water with these materials was limited after the X-ray amorphous materials formed. In the case of more prolonged interactions, we would expect the materials to have dissolved completely. Dissolution experiments with synthetic allophane, Fe-substituted allophane, and hisingerite in the range of pH 3-10 indicate rapid initial dissolution, approximately an order of magnitude faster than that of well-crystalline clay minerals of similar composition. The dissolution rates of all three materials showed little pH dependence across the experimental pH range. Therefore, the poorly crystalline, allophane-like materials in Gale Crater would have dissolved rapidly when exposed to liquid water regardless of the water's pH. Dissolution in Gale Crater would likely have proceeded significantly more slowly than in our experiments, due to the lower temperature and higher salinity expected for Mars' ancient waters as well as generally slower dissolution rates in the field than in the laboratory, extending the possible duration of water-rock interaction at Gale.

Under the experimental conditions studied here, allophane, Fe-allophane, and hisingerite tend to dissolve non-stoichiometrically, with silica entering solution much more readily than Fe. This behavior may contribute to silica-rich deposits found in parts of the Murray formation in Gale Crater; silica may have dissolved out of poorly crystalline materials, been transported to spots where the water pooled, and subsequently precipitated when concentrations exceeded saturation.

Examinations made with FE-STEM of reacted hisingerite and allophane revealed morphological changes due to dissolution after only a few months. Such morphological changes may be a useful tool for examinations of returned martian soil samples combined with the enrichment of Fe expected during weathering.

Because of the rapid reaction rates of allophane, Fe-allophane, and hisingerite with water, examination of these materials may be critical to understanding the characteristics of very short-lived

martian waters. These phases may provide insight into the duration of short-lived liquid water in Gale Crater by allowing examination of aqueous alteration features at a finer timescale than that provided by well-crystalline, aqueously altered minerals. With continued investigation and characterization, we may be able to use the properties of the Mars amorphous soil component to constrain and elucidate the characteristics of Gale Crater's most recent waters.

APPENDIX

S1. TEM



Figure S1: Diffraction pattern from an agglomerate of unaltered synthetic hisingerite, obtained during TEM investigations. Diffuse rings are visible, indicating nanocrystalline structure. Diffractograms were not obtained for synthetic allophane due to its lack of lattice fringes, indicating no long-range order.

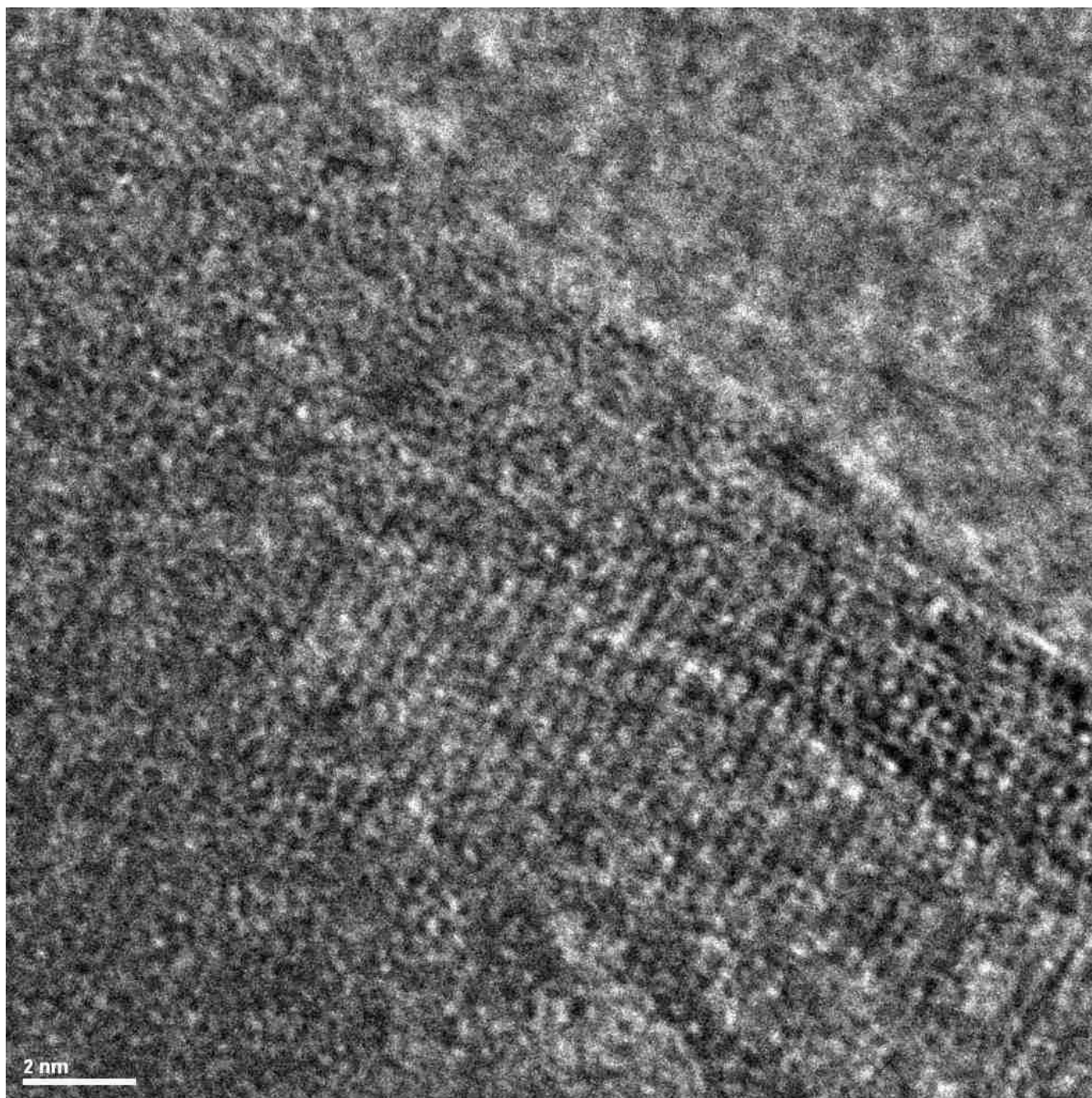


Figure S2: TEM image of incipient phyllosilicate structure developing from poorly-crystalline hisingerite reacted at pH 3 for 112 days. Some phyllosilicate-like structures, like the one above, were observed.

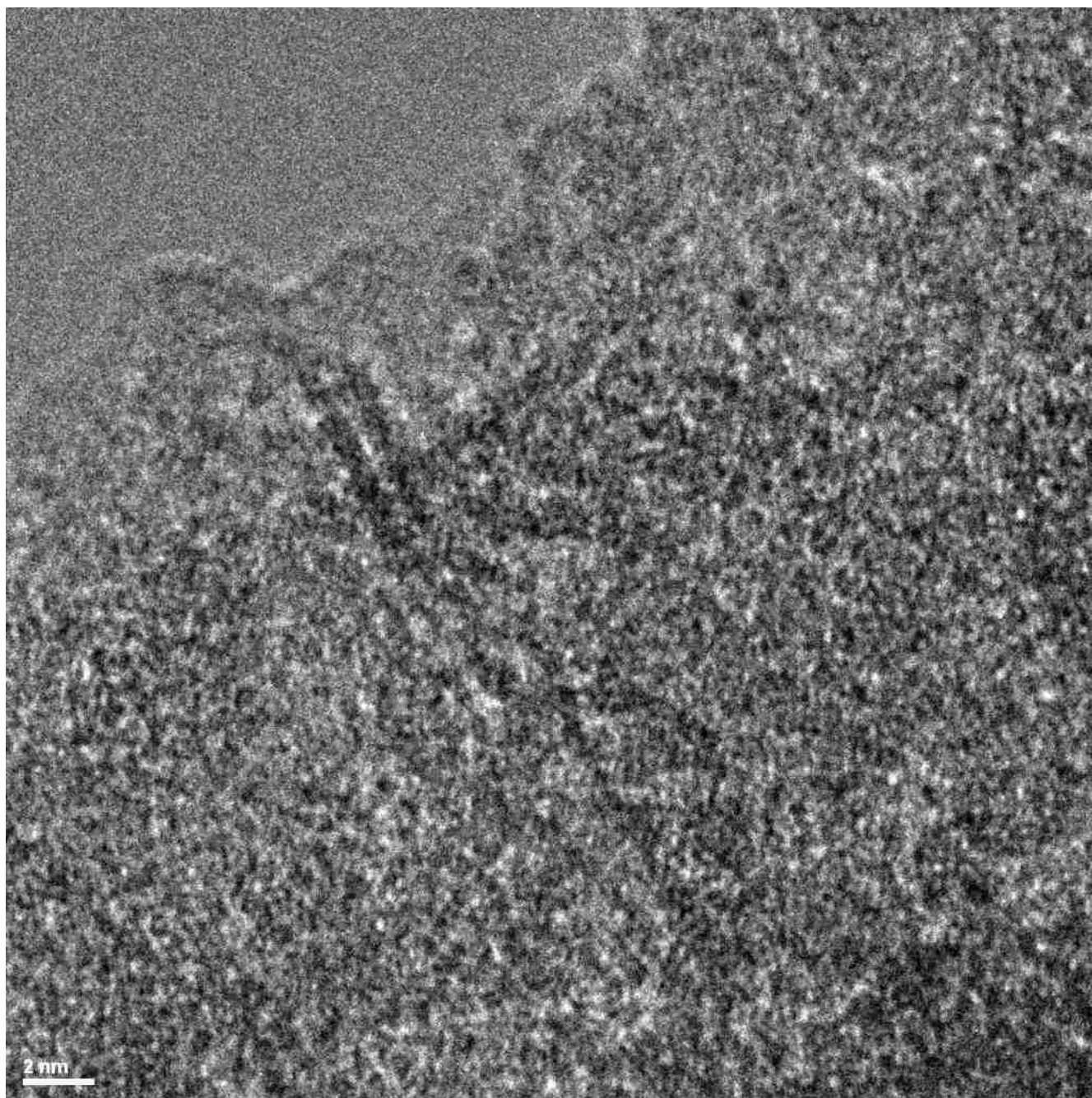


Figure S3: TEM image of hisingerite agglomerate grain reacted at pH 10 for 57 days that contains several incipient phyllosilicate structures. Some grains (e.g. **Figure 8**) were much richer in incipient phyllosilicate structures than the one shown here.

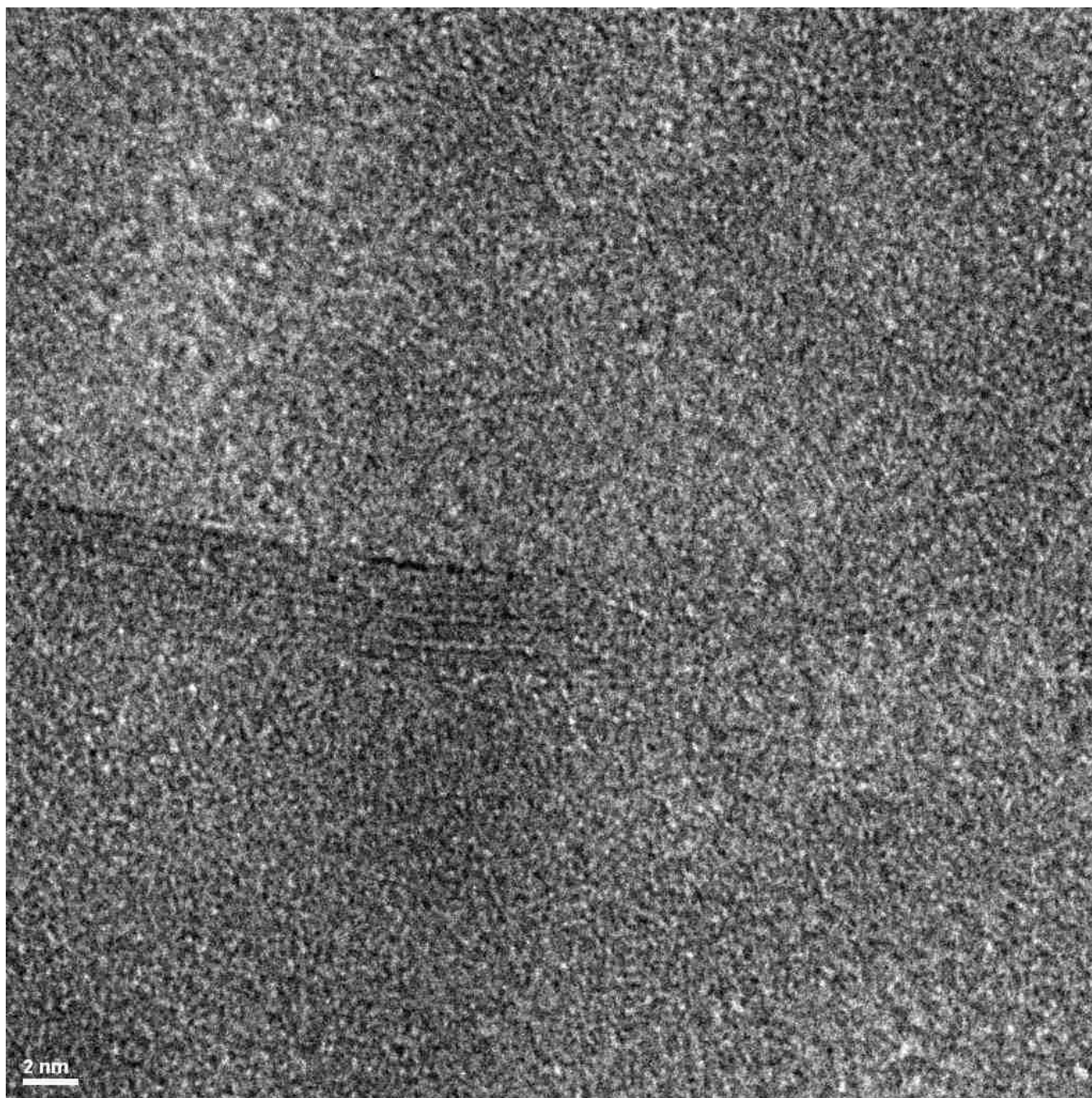


Figure S4: TEM of allophane reacted at pH 10 for 57 days. While incipient phyllosilicate structures were seen in this sample, they were much less abundant than in hisingerite reacted at pH 10 for the same amount of time.

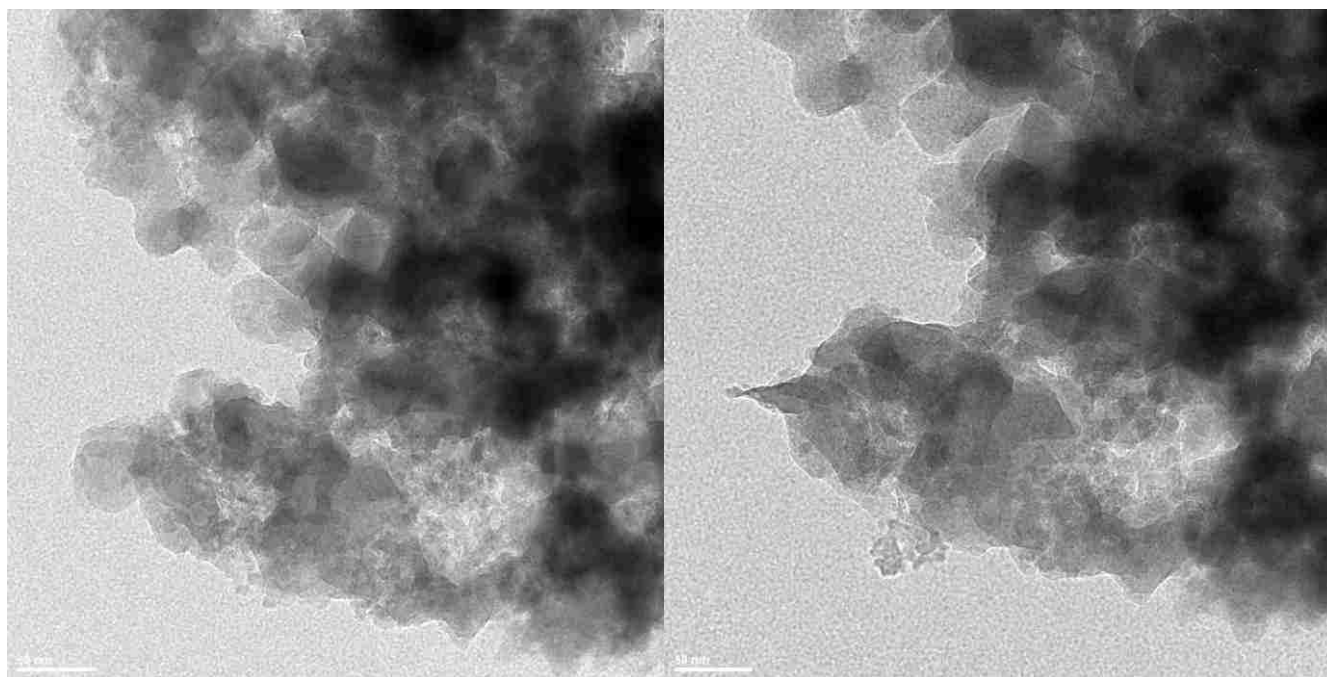


Figure S5: TEM image of allophane reacted at pH 10 for 57 days, showcasing the beam-sensitive nature of the "smooth" material. The image on the left was taken before exposing the material to the high-energy STEM beam. The image on the right was taken after exposing the material to the STEM beam for less than one minute.

S2. SEM/EDS of unaltered and altered samples

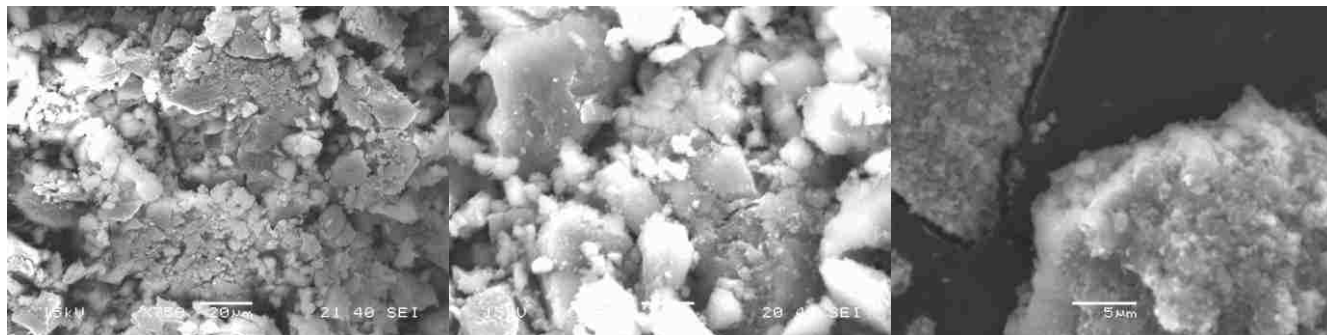


Figure S6: SEM images of unaltered synthetic allophane (left), Fe-allophane (center), and hisingerite (right). The "fluffy" texture of the grains is indicative of nanoball structures.

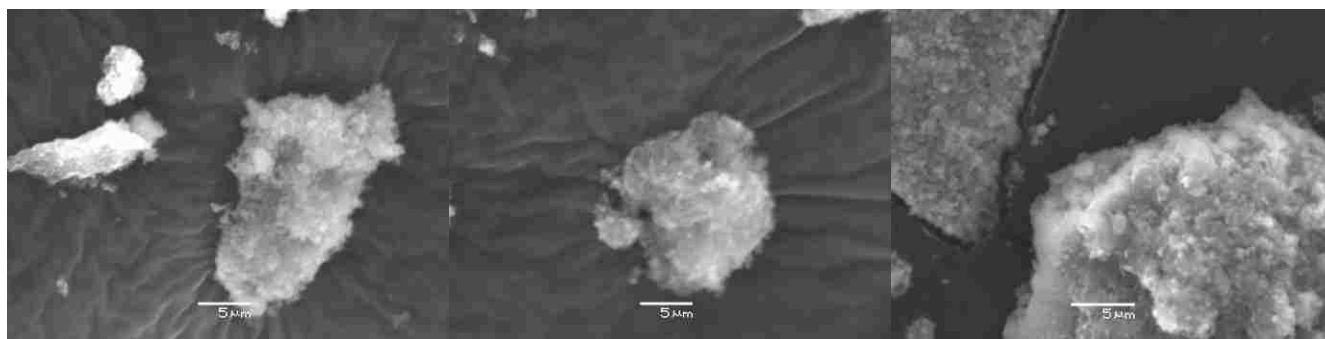


Figure S7: SEM of unaltered hisingerite. At this scale, nanoballs (~5 nm in diameter) cannot be discerned; however, the 'fluffy' texture of the grains is indicative of the presence of nanoballs.

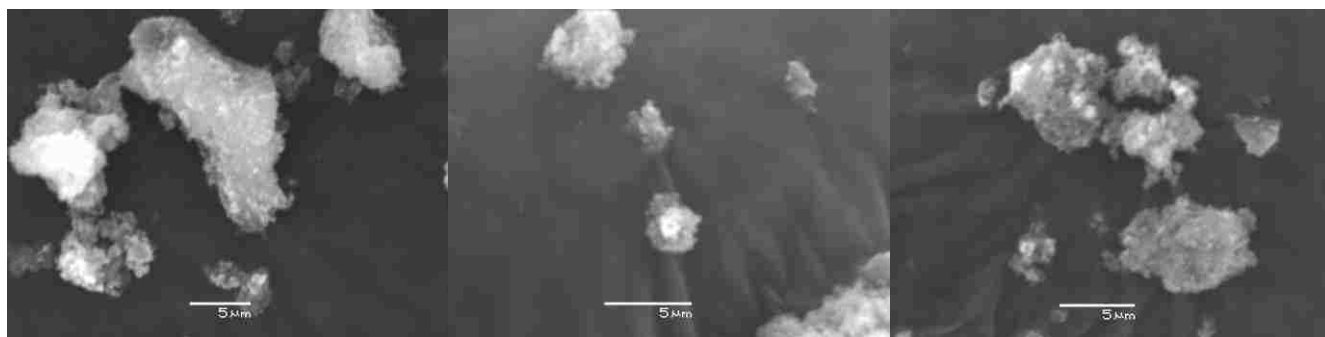


Figure S8: SEM of hisingerite reacted in 0.1M NaCl solution at pH ~4 for two days. Although selected grains are smaller than those in the unaltered hisingerite, overall grain-size distribution did not appear significantly different.

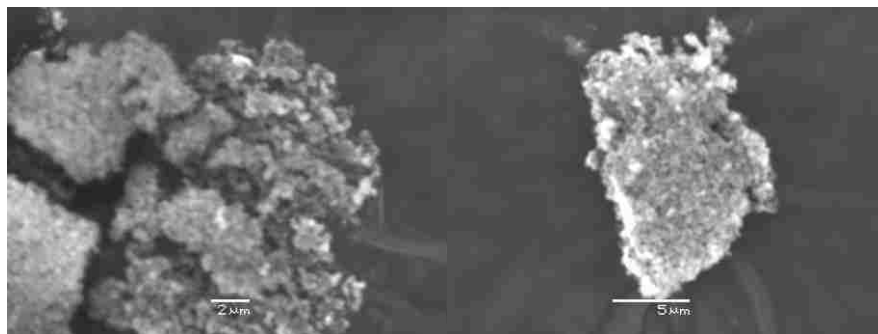


Figure S9: SEM of hisingerite reacted in 0.1M NaCl solution at pH ~4 for one month.

S3. FE-SEM of unaltered samples

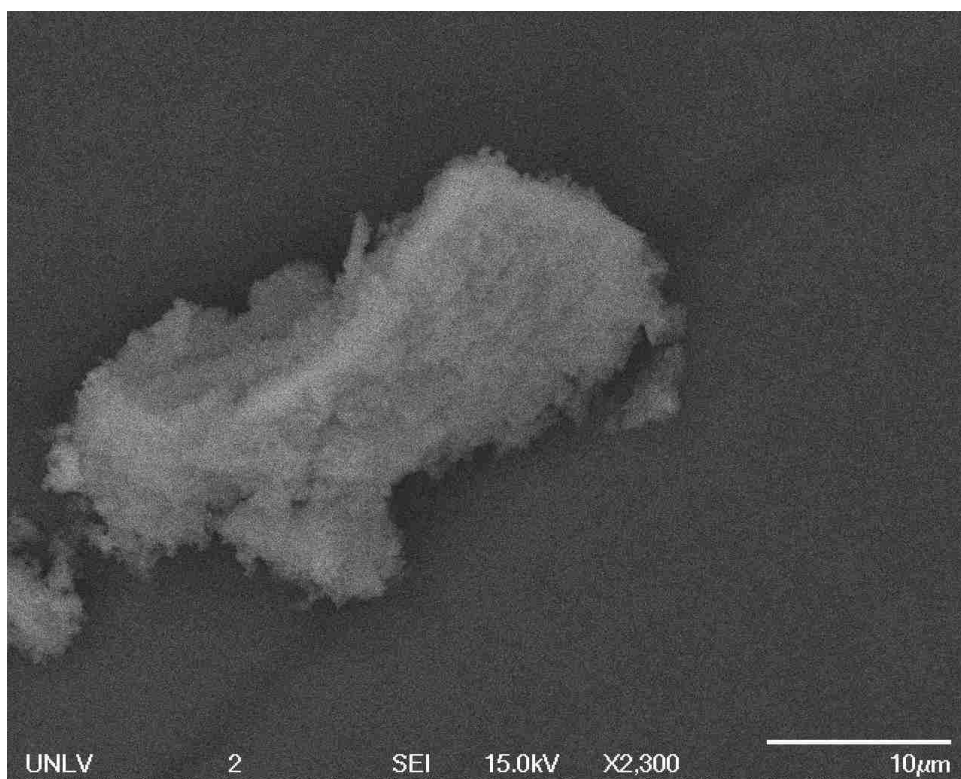


Figure S10: FE-SEM image of synthetic allophane. The "fluffy" texture of this grain indicates that it is an aggregate of nanoballs, each ~5 nm in diameter.

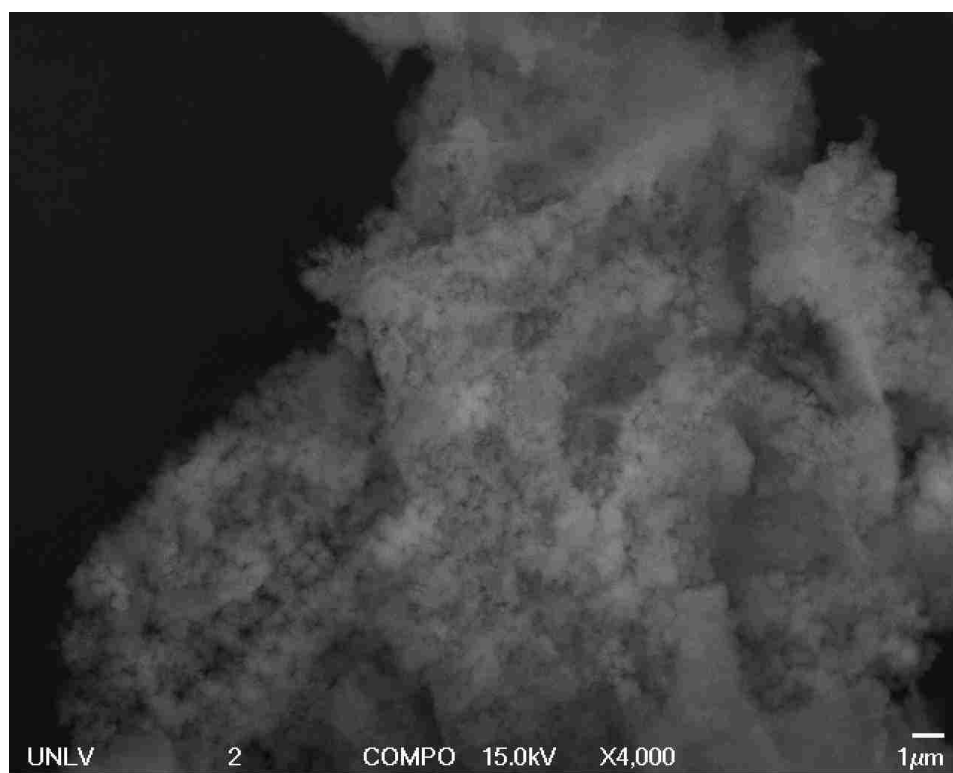


Figure S11: Synthetic Fe-allophane examined by FE-SEM. Nanoballs are clearly distinguishable in the "fluffy" texture of the aggregate.

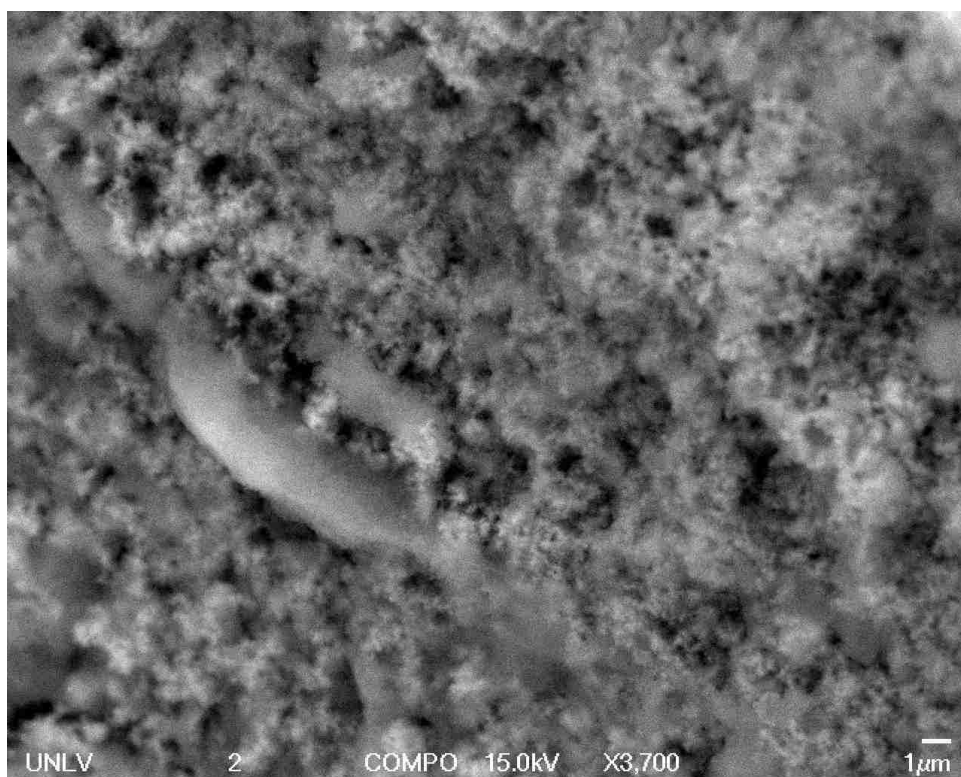


Figure S12: An image of synthetic hisingerite obtained with FE-SEM. Nanoballs are distinguishable across the entire surface of this large aggregate, as well as patches of "smooth" texture. The two textures did not appear to be compositionally different, as per earlier SEM/EDS analyses.

S4. EGA of unaltered samples

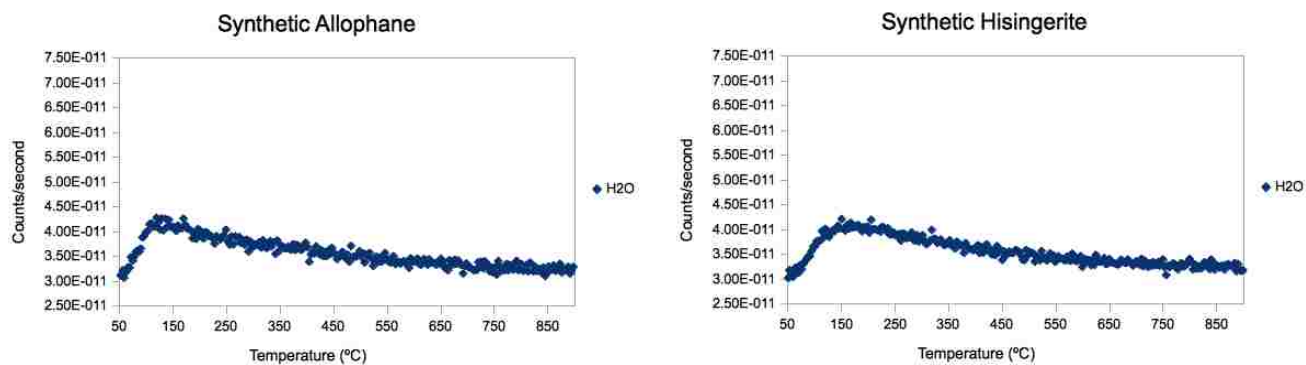


Figure S13: Mass-18 H₂O release from **a)** synthetic allophane, and **b)** synthetic hisingerite. The peak around 130-150 °C agrees well with other literature values for allophane EGA (Bish and Duffy, 1990).

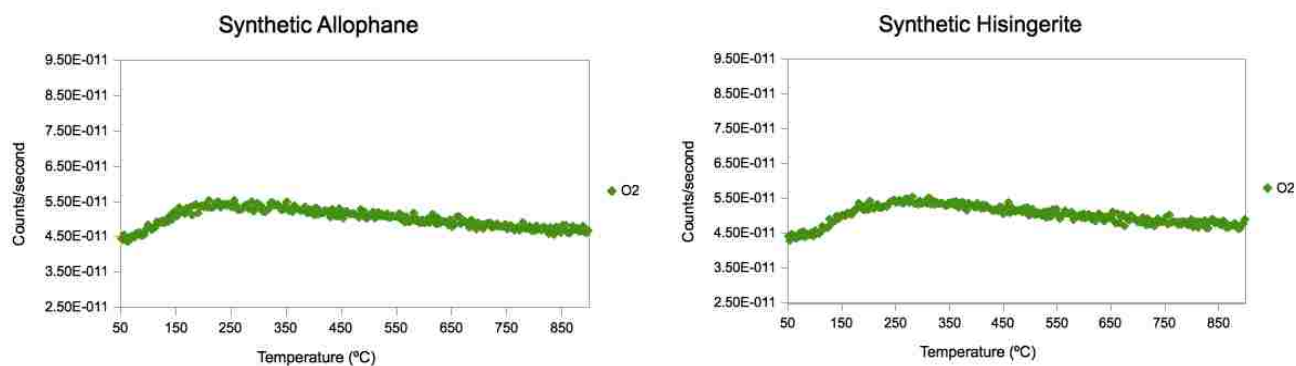


Figure S14: Mass-32 O₂ release from **a)** synthetic allophane, and **b)** synthetic hisingerite. Because the O₂ release occurs concurrently with the H₂O release, it is likely that the O₂ release is due to fragmentation of water in the mass spectrometer.

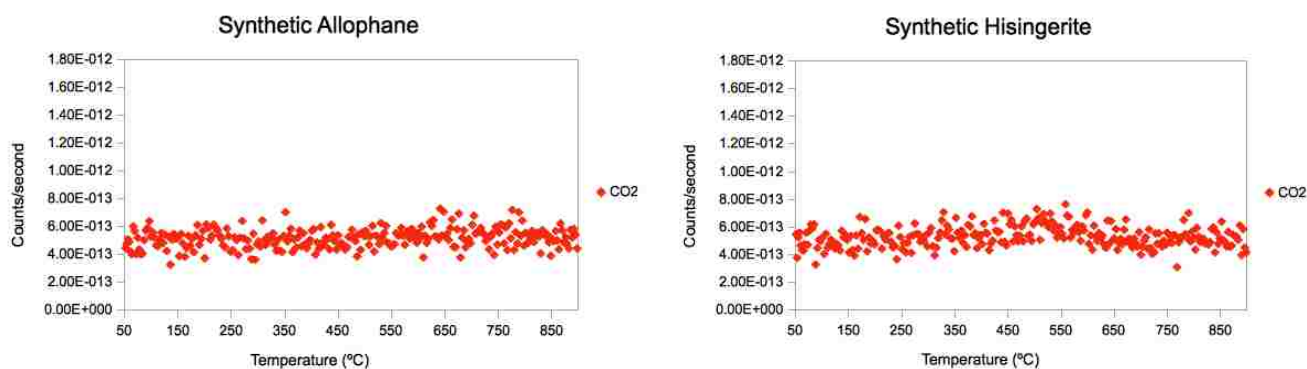


Figure S15: Mass-44 CO₂ release from **a)** synthetic allophane, and **b)** synthetic hisingerite. No releases were observed, indicating no structural or adsorbed CO₂.

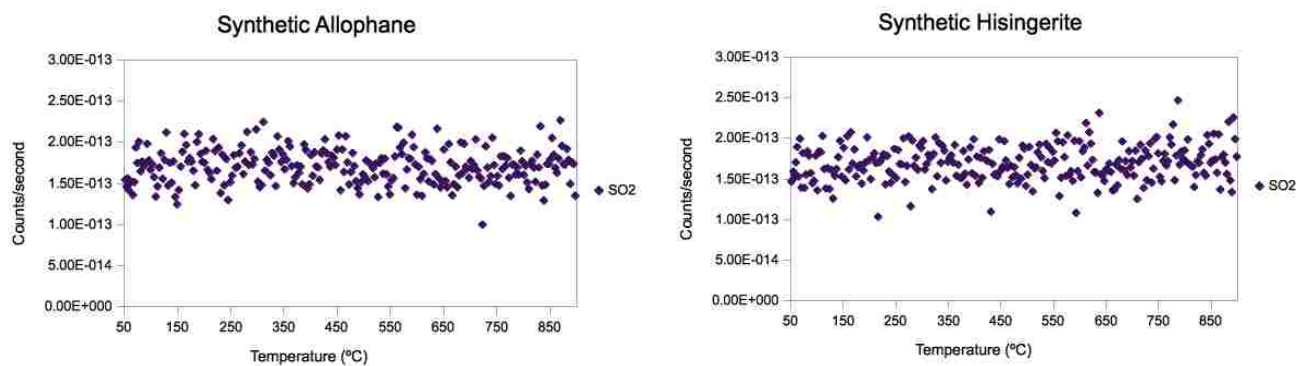


Figure S16: Mass-64 SO₂ release from **a)** synthetic allophane, and **b)** synthetic hisingerite. No releases were observed, consistent with the lack of S-bearing compounds in the synthesis process.

S5. XRD

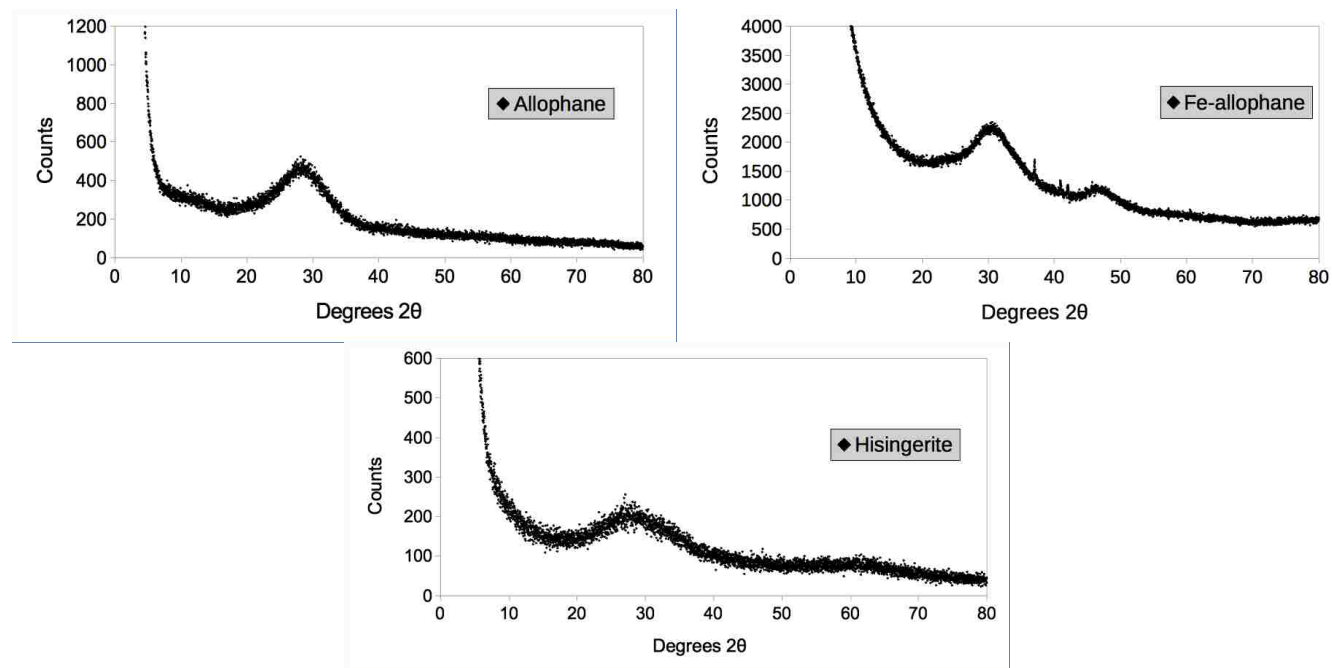


Figure S17: XRD patterns of synthetic allophane, Fe-allophane, and hisingerite. All samples show elevated low background indicative of small particle sizes. **a)** Synthetic allophane. A single broad peak, indicative of nanocrystalline structure, is visible at 3.1 Å. There is a possible second d-spacing around 7.2 Å. **b)** Synthetic Fe-allophane. Broad peaks occur at 2.9 Å and 1.9 Å. Small, sharp peaks are likely due either to contaminants, such as NaCl from the synthesis process, or to poor grain-size sorting in the sample. **c)** Synthetic hisingerite. Broad peaks are visible around 3.2 and 1.5 Å, with a possible shoulder at 2.7 Å.

S6. Dissolution

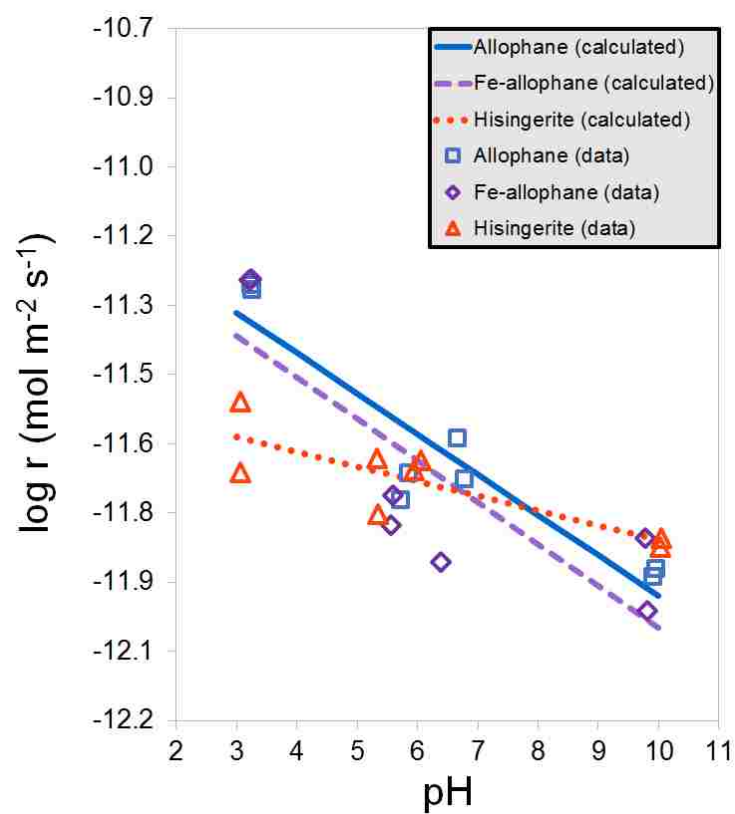


Figure S18. Dissolution rates and rate laws for allophane, Fe-allophane, and hisingerite. Rate data are plotted as open points, and calculated rate laws are plotted as lines.

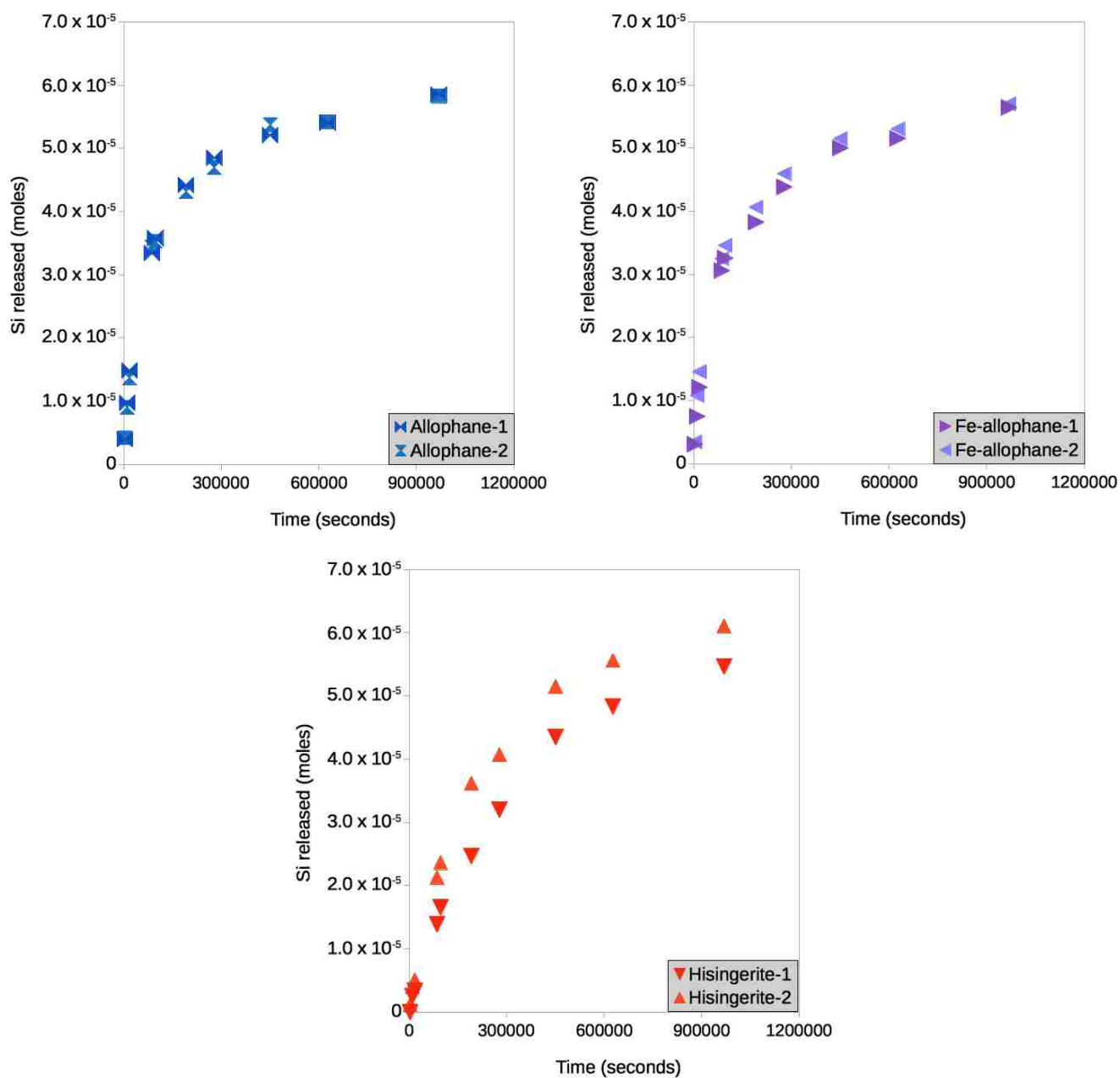


Figure S19. Silica release from allophane, Fe-allophane, and hisingerite duplicates at pH 3.

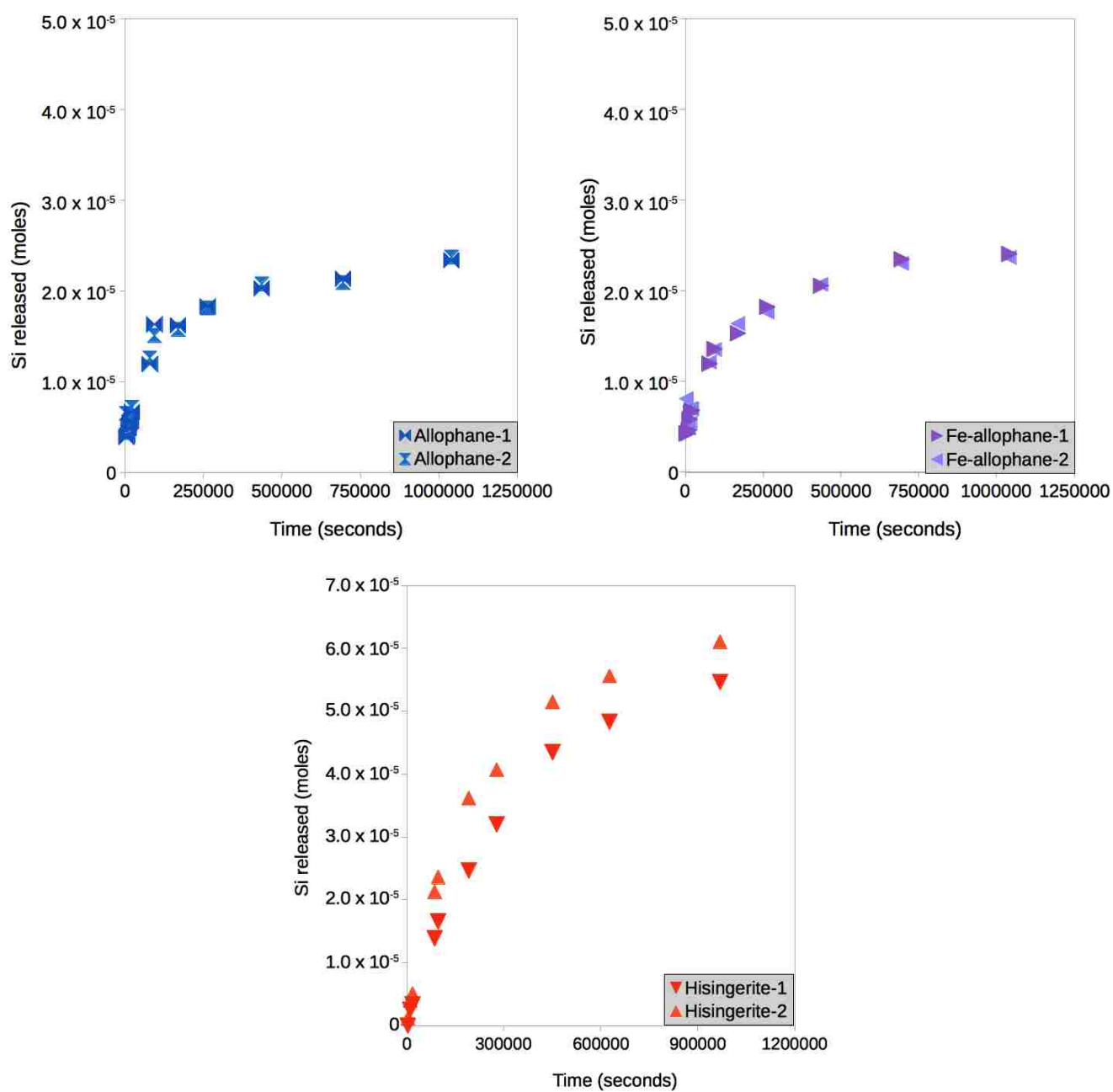


Figure S20. Silica release from allophane, Fe-allophane, and hisingerite duplicates at pH 5.

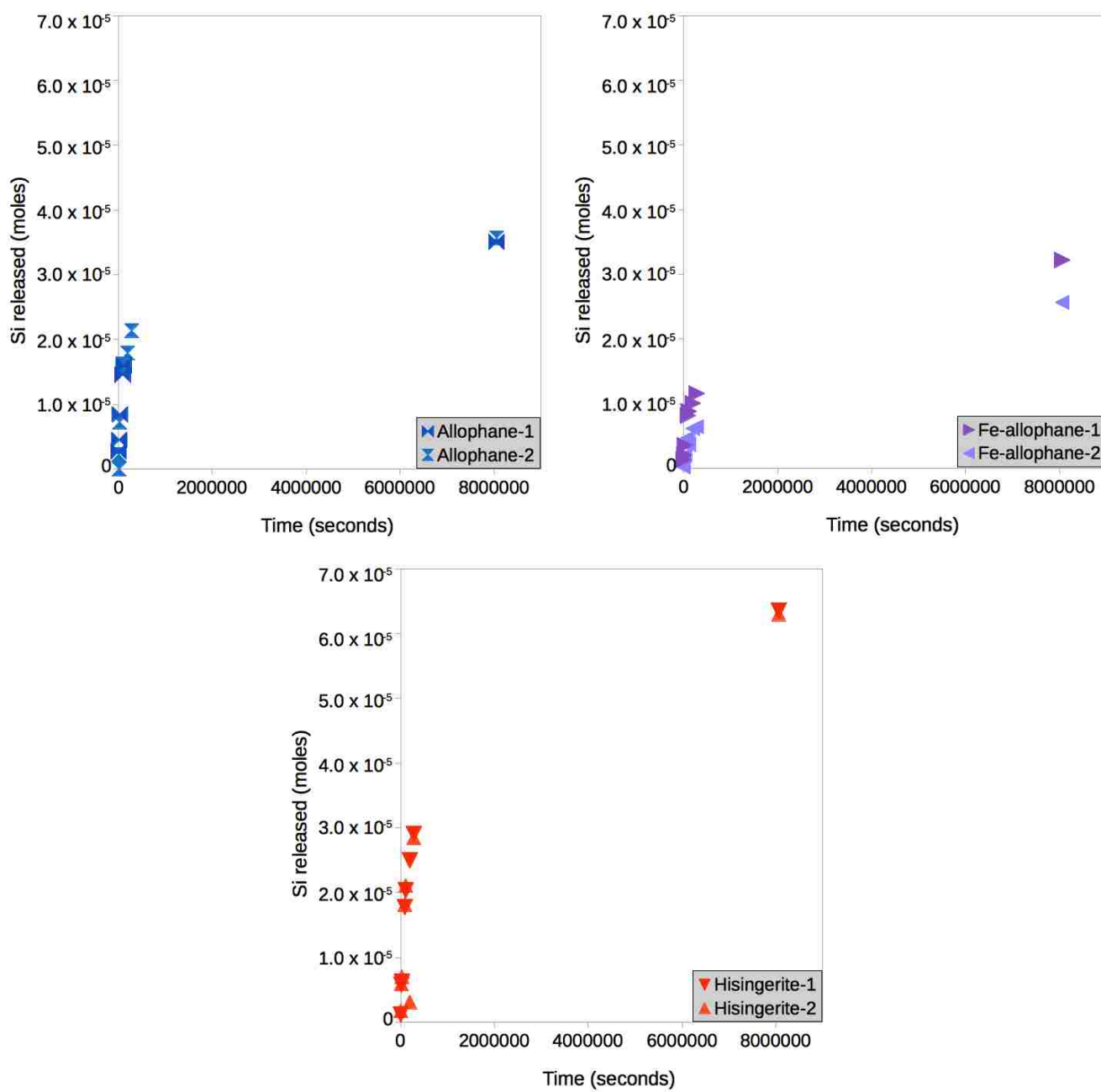


Figure S21. Silica release from allophane, Fe-allophane, and hisingerite duplicates at pH 8.

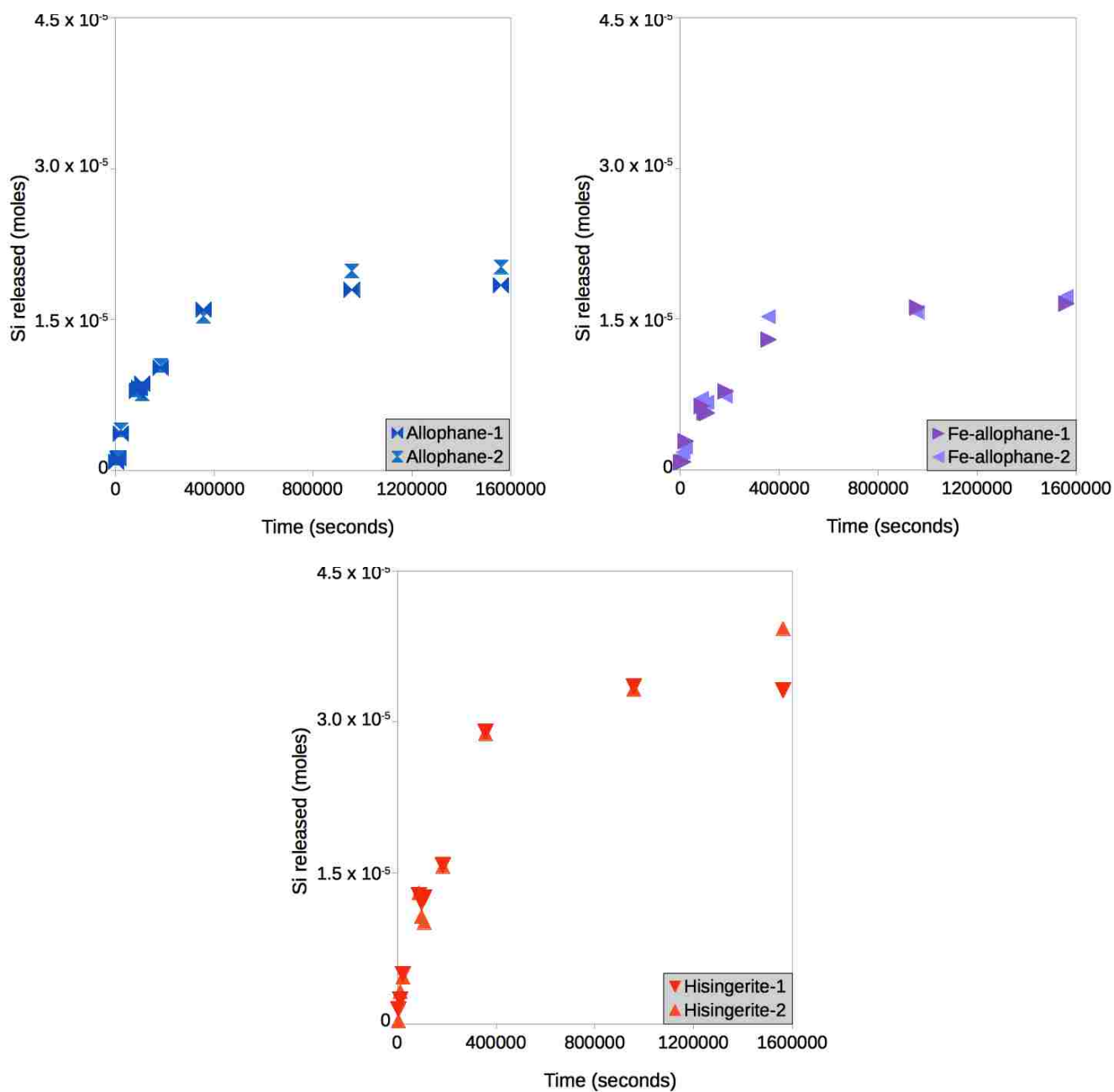


Figure S22. Silica release from allophane, Fe-allophane, and hisingerite duplicates at pH 10.

Tables S4-S27 (Section S9 below) show silica concentration in solution and solution pH for each experiment at each time point.

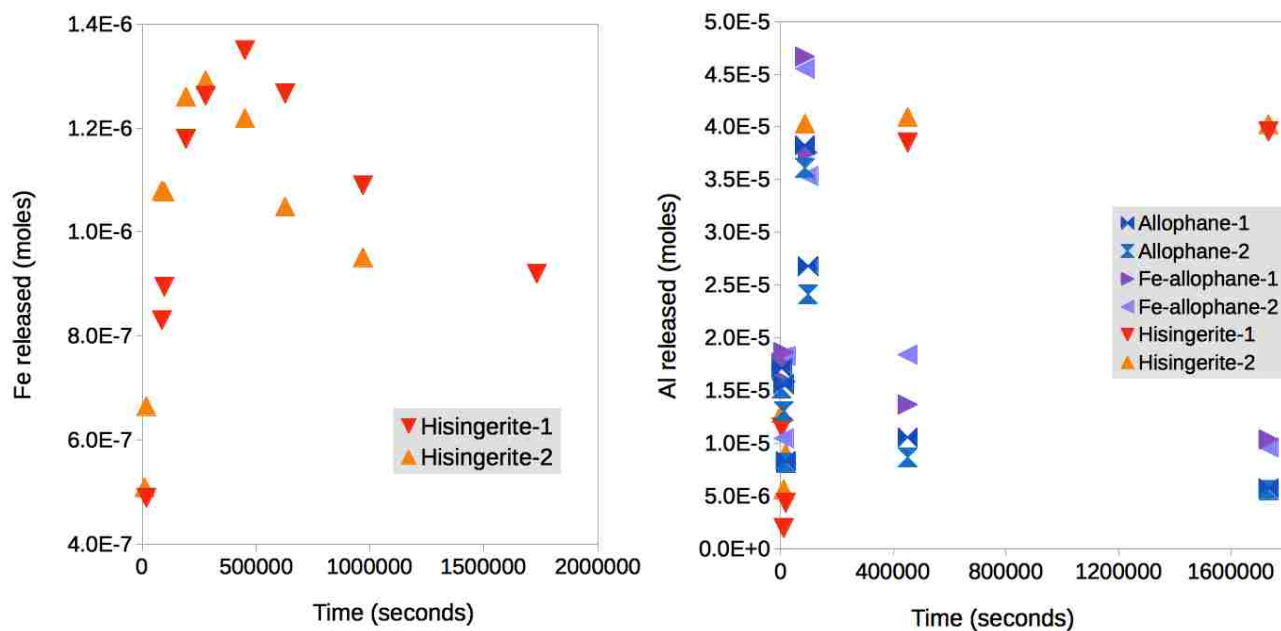
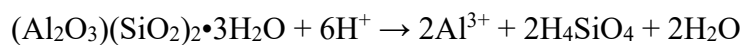


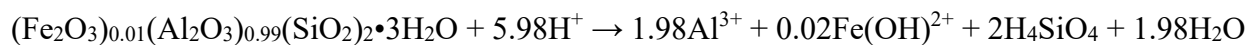
Figure S23. Moles of Fe released into solution with time for hisingerite at pH 3 (left) and moles of Al released into solution with time for allophane, Fe-allophane, and hisingerite at pH 3 (right).

S7. Balanced chemical equations

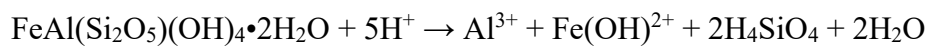
S7.1 Allophane at pH 3



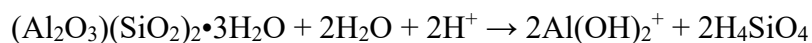
S7.2 Fe-allophane at pH 3



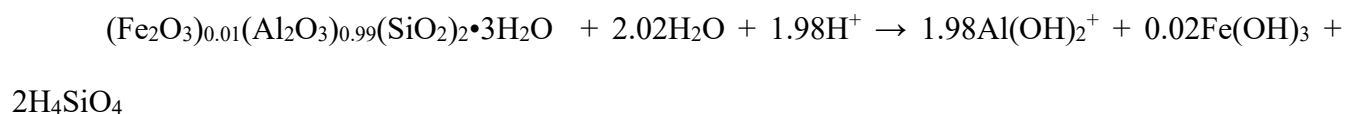
S7.3 Hisingerite at pH 3



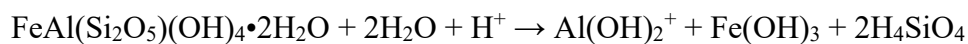
S7.4 Allophane at pH 5



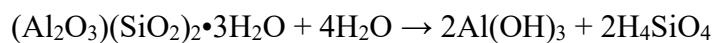
S7.5 Fe-allophane at pH 5



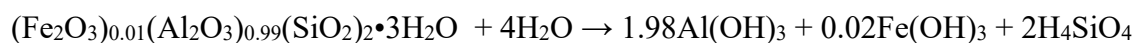
S7.6 Hisingerite at pH 5



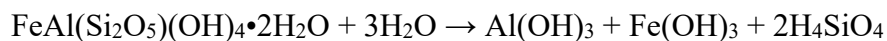
S7.7 Allophane at pH 7



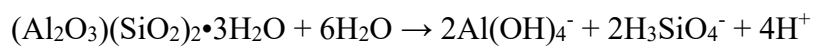
S7.9 Fe-allophane at pH 7



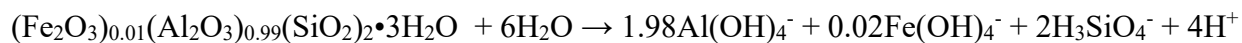
S7.10 Hisingerite at pH 7



S7.11 Allophane at pH 10



S7.12 Fe-allophane at pH 10



S7.13 Hisingerite at pH 10



S8. Supplemental Tables

S8.1 TEM

Table S1. Table of experiments examined by TEM for the presence of alteration products.

Experiment	Initial pH	Final pH	Total Experiment Time
Hisingerite at pH 3	3.01	4.78	181 days
Hisingerite at pH 10	10.36	6.39	57 days
Allophane at pH 10	10.36	8.59	57 days
Allophane at pH 3 (TBD)	3.01	4.35	112 days

S8.2 SEM/EDS

Table S2. EDS results from selected grains of unaltered synthetic allophane, Fe-allophane, and hisingerite. Values were obtained by averaging the atomic percentages for each element from either 3 or 4 EDS spectra taken from multiple grains within each sample. The total values are low due to the presence of a large amount of water in the samples.

Sample ID	% Si (avg)	% Fe (avg)	% Al (avg)	% Na (avg)	% Cl (avg)	% O (avg)
Allophane	11.36	N/A	10.51	4.74	N/A	62.54
Fe-allophane	10.26	N/A	8.71	4.30	N/A	63.66
Hisingerite	2.29	1.43	1.11	0.39	0.39	65.47

Table S3. EDS results from selected grains of unaltered synthetic hisingerite (Hisingerite-0), synthetic hisingerite reacted at pH ~4 for approximately 2 days (Hisingerite-2d), and synthetic hisingerite reacted at pH ~4 for approximately 4 months (Hisingerite-4mo). Values were obtained by averaging the atomic percentages for each element from either 2 or 3 EDS spectra taken from multiple grains within each sample. Decreasing Si, Fe, and Al values and increasing O values may indicate that the material becomes more hydrous with increasing reaction time. The total values are low due to the presence of a large amount of water in the samples.

Sample ID	Reaction Time (hours)	Final pH	% Si (avg)	% Fe (avg)	% Al (avg)	% Na (avg)	% Cl (avg)	% O (avg)
Hisingerite-0	0	N/A	2.29	1.43	1.11	0.39	0.39	65.47
Hisingerite-2d	46	5.35	1.32	0.75	0.66	0.53	N/A	66.06
Hisingerite-4mo	739	6.54	0.85	0.65	0.46	0.46	0.12	66.14

S8.3 BET surface area and particle size analyses

Table S4. Particle size analysis and BET specific surface areas for allophane, Fe-allophane, and hisingerite. Duplicates are denoted by the "-1" and "-2" suffixes.

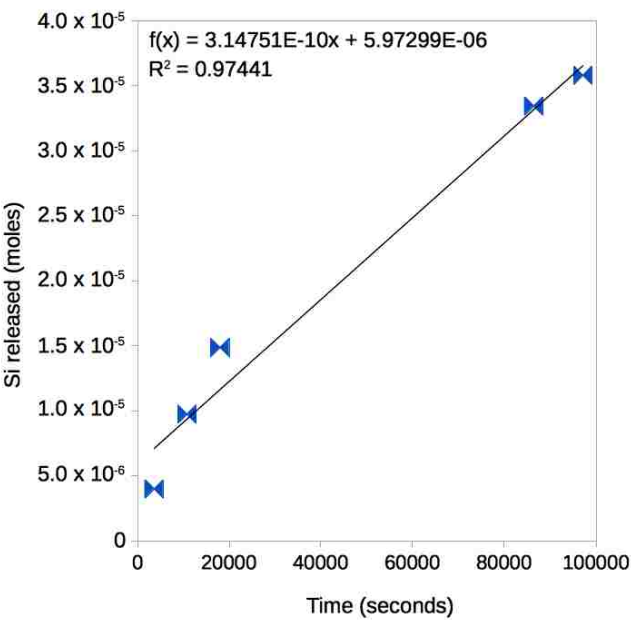
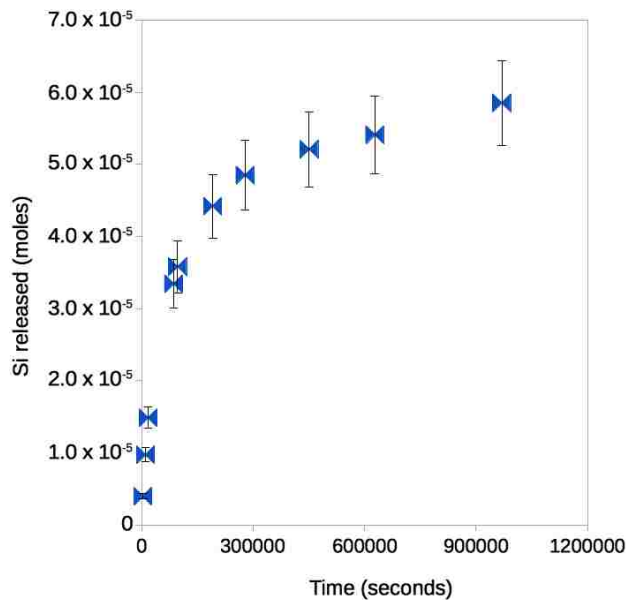
Material	Mass (mg)	Particle Size (μm)	BET SSA (m^2/g)
Allophane-1	408.5	168.5	385.6192
Allophane-2	408.5	172.7	385.9124
Fe-allophane-1	400.8	134.9	410.8675
Fe-allophane-2	400.8	136.0	389.5205
Hisingerite-1	402.0	162.0	507.2660
Hisingerite-2	402.0	173.5	507.6969

Table S5. Dissolved silica analysis for experiment Al+Si-p3-1

Material: Allophane **Initial pH:** 3.01 **Solution:** 0.01M NaCl **Specific Surface Area (BET):** 385.6192 m²/g
Batch ID: Al+Si-p3-1 **Material mass:** 0.1501 g **Total Surface Area (BET):** 57.8814 m²
N/A = no analysis.

Time (sec)	pH	Volume (mL)	Concentration Si (ppm)	Moles Si released
0	3.01	180		0
3600	3.25	170	0.623436987	3.99561 x 10 ⁻⁶
10800	3.38	160	1.52098346	9.74798 x 10 ⁻⁶
18000	3.48	150	2.36682487	1.48678 x 10 ⁻⁵
86400	4.08	140	5.62654066	3.34381 x 10 ⁻⁵
97200	4.10	130	6.06910753	3.58017 x 10 ⁻⁵
192000	4.28	120	7.75413609	4.42012 x 10 ⁻⁵
278400	4.31	110	8.67957306	4.84848 x 10 ⁻⁵
451200	4.31	100	9.52142048	5.20818 x 10 ⁻⁵
627600	4.34	90	10.028264	5.40669 x 10 ⁻⁵
969600	4.34	80	11.2719841	5.84952 x 10 ⁻⁵
1732800	4.42	70	15.0064335	7.04622 x 10 ⁻⁵

Si Release



Analytical uncertainty is 10%.

Linear Fit

Regression analysis		Std. Error
R Squared	0.97441	N/A
Si release rate	3.15 x 10 ⁻¹⁰	2.94 x 10 ⁻¹¹

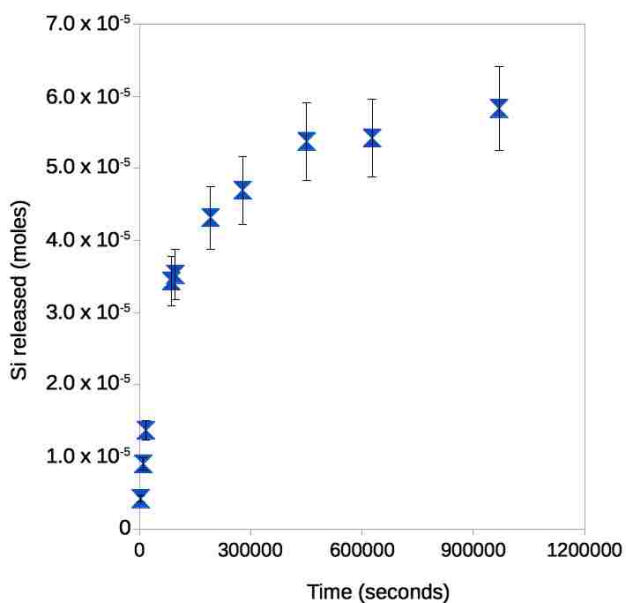
Diss. Rate Mineral (R_{diss}) 5.44 x 10⁻¹² mol m⁻² s⁻¹
Uncertainty of fit 5.09 x 10⁻¹³ mol m⁻² s⁻¹

Table S6. Dissolved silica analysis for experiment Al+Si-p3-2

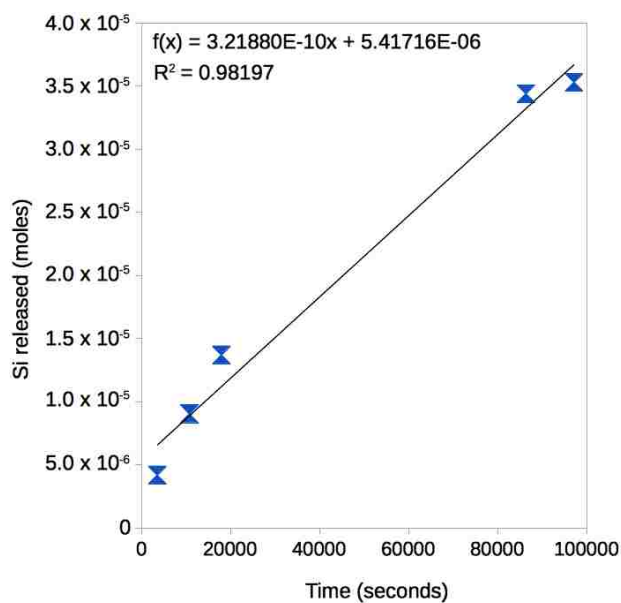
Material: Allophane **Initial pH:** 3.01 **Solution:** 0.01M NaCl **Specific Surface Area (BET):** 385.6192 m²/g
Batch ID: Al+Si-p3-2 **Material mass:** 0.1499 g **Total Surface Area (BET):** 57.8043 m²
N/A = no analysis.

Time (sec)	pH	Volume (mL)	Concentration Si (ppm)	Moles Si released
0	3.01	180		0
3600	3.25	170	0.654747009	4.19627 x 10 ⁻⁶
10800	3.38	160	1.40991044	9.03612 x 10 ⁻⁶
18000	3.48	150	2.18204594	1.37098 x 10 ⁻⁵
86400	4.08	140	5.81133604	3.43855 x 10 ⁻⁵
97200	4.10	130	5.97960806	3.52842 x 10 ⁻⁵
192000	4.28	120	7.55599737	4.31421 x 10 ⁻⁵
278400	4.31	110	8.37674141	4.69411 x 10 ⁻⁵
451200	4.31	100	9.96673489	5.37347 x 10 ⁻⁵
627600	4.34	90	10.0855904	5.42002 x 10 ⁻⁵
969600	4.34	80	11.2310944	5.82788 x 10 ⁻⁵
1732800	4.42	70	14.8543186	6.98894 x 10 ⁻⁵

Si Release



Linear Fit



Analytical uncertainty is 10%.

Regression analysis		Std. Error
<i>R Squared</i>	0.98197	N/A
<i>Si release rate</i>	3.22 x 10 ⁻¹⁰	2.52 x 10 ⁻¹¹

Diss. Rate Mineral (R_{diss}) 5.57 x 10⁻¹² mol m⁻² s⁻¹
Uncertainty of fit 4.36 x 10⁻¹³ mol m⁻² s⁻¹

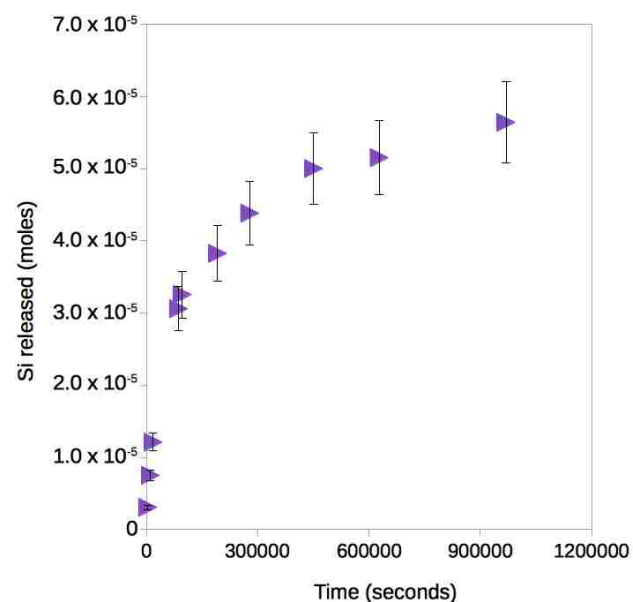
Table S7. Dissolved silica analysis for experiment 1:99-p3-1

Material: Fe-allophane **Initial pH:** 3.01 **Solution:** 0.01M NaCl **Specific Surface Area (BET):** 350.2424 m²/g
Batch ID: 1:99-p3-1 **Material mass:** 0.1503 g **Total Surface Area (BET):** 52.6414 m²

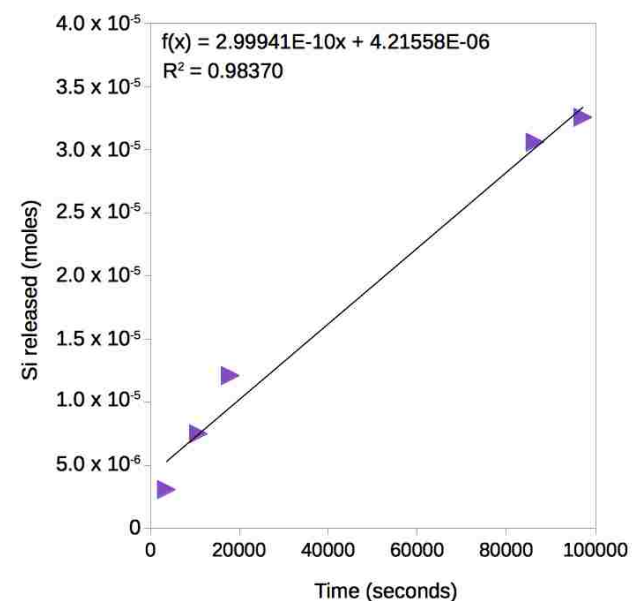
N/A = no analysis..

Time (sec)	pH	Volume (mL)	Concentration Si (ppm)	Moles Si released
0	3.01	180		0
3600	3.21	170	0.481400609	3.08530 x 10 ⁻⁶
10800	3.34	160	1.17056489	7.50215 x 10 ⁻⁶
18000	3.43	150	1.93203735	1.21113 x 10 ⁻⁵
86400	4.04	140	5.17693949	3.05972 x 10 ⁻⁵
97200	4.04	130	5.54620028	3.25693 x 10 ⁻⁵
192000	4.27	120	6.68937826	3.82678 x 10 ⁻⁵
278400	4.29	110	7.89358568	4.38417 x 10 ⁻⁵
451200	4.35	100	9.34075451	5.00250 x 10 ⁻⁵
627600	4.33	90	9.72676373	5.15369 x 10 ⁻⁵
969600	4.36	80	11.100379	5.64277 x 10 ⁻⁵
1732800	4.35	70	14.5511656	6.74857 x 10 ⁻⁵

Si Release



Linear Fit



Analytical uncertainty is 10%.

Regression analysis		Std. Error
R Squared	0.98370	N/A
Si release rate	3.00 x 10 ⁻¹⁰	2.23 x 10 ⁻¹¹

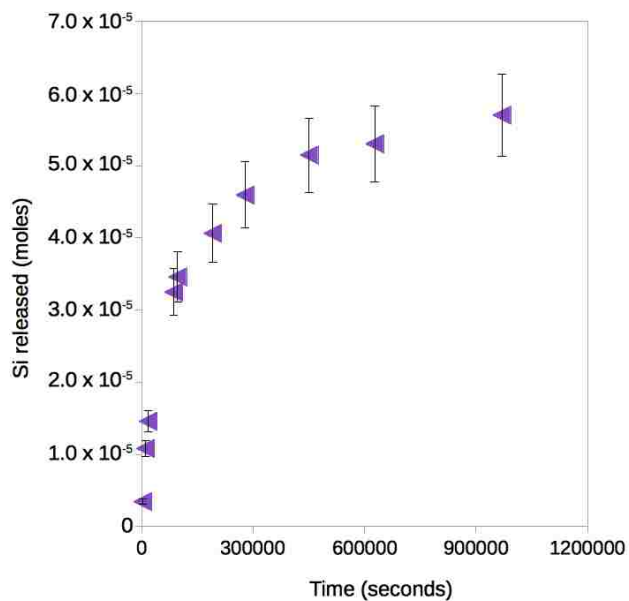
Diss. Rate Mineral (R_{diss}) $5.70 \times 10^{-12} \text{ mol m}^{-2} \text{ s}^{-1}$
Uncertainty of fit $4.23 \times 10^{-13} \text{ mol m}^{-2} \text{ s}^{-1}$

Table S8. Dissolved silica analysis for experiment 1:99-p3-2

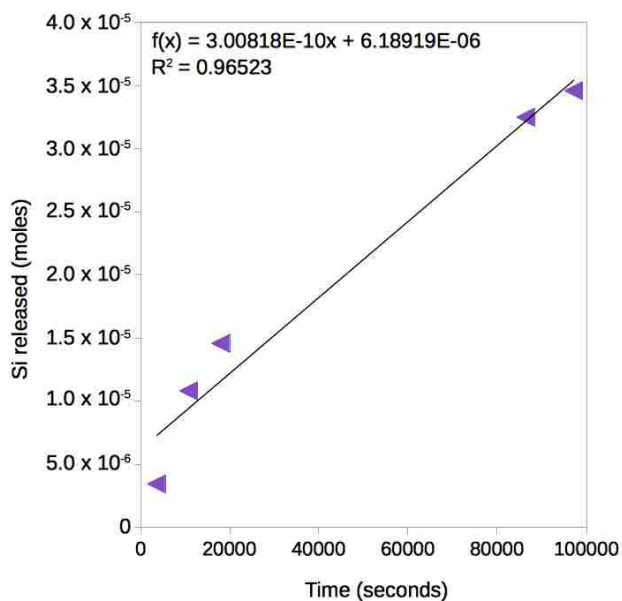
Material: Fe-allophane **Initial pH:** 3.01 **Solution:** 0.01M NaCl **Specific Surface Area (BET):** 350.2424 m²/g
Batch ID: 1:99-p3-2 **Material mass:** 0.1502 g **Total Surface Area (BET):** 52.6064 m²
N/A = no analysis.

Time (sec)	pH	Volume (mL)	Concentration Si (ppm)	Moles Si released
0	3.01	180		0
3600	3.24	170	0.537692487	3.44607 x 10 ⁻⁶
10800	3.38	160	1.68774545	1.08168 x 10 ⁻⁵
18000	3.48	150	2.30930901	1.45791 x 10 ⁻⁵
86400	4.13	140	5.45357418	3.24916 x 10 ⁻⁵
97200	4.14	130	5.84632969	3.45892 x 10 ⁻⁵
192000	4.31	120	7.05799818	4.06291 x 10 ⁻⁵
278400	4.32	110	8.20371151	4.59323 x 10 ⁻⁵
451200	4.35	100	9.50206566	5.14798 x 10 ⁻⁵
627600	4.35	90	9.89772892	5.30294 x 10 ⁻⁵
969600	4.38	80	11.0138454	5.70034 x 10 ⁻⁵
1732800	4.37	70	14.9179258	6.95140 x 10 ⁻⁵

Si Release



Linear Fit



Analytical uncertainty is 10%.

<i>Regression analysis</i>		<i>Std. Error</i>
<i>R Squared</i>	0.96523	N/A
<i>Si release rate</i>	3.01 x 10 ⁻¹⁰	3.30 x 10 ⁻¹¹

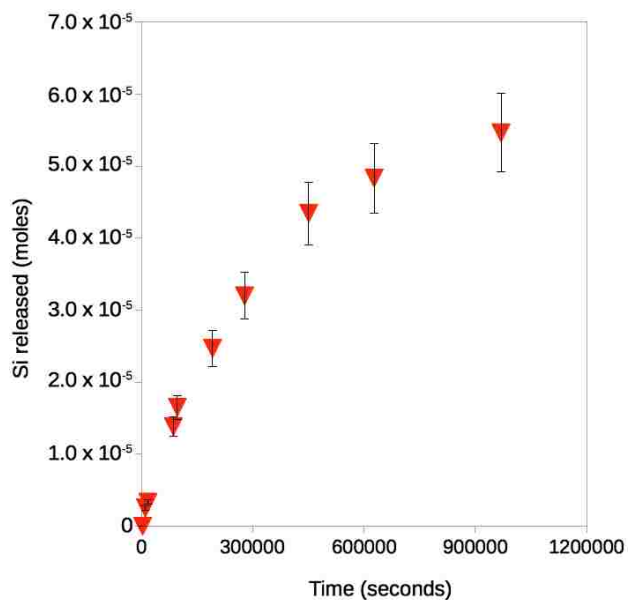
Diss. Rate Mineral (R_{diss}) 5.72 x 10⁻¹² mol m⁻² s⁻¹
Uncertainty of fit 6.27 x 10⁻¹³ mol m⁻² s⁻¹

Table S9. Dissolved silica analysis for experiment 50:50-p3-1

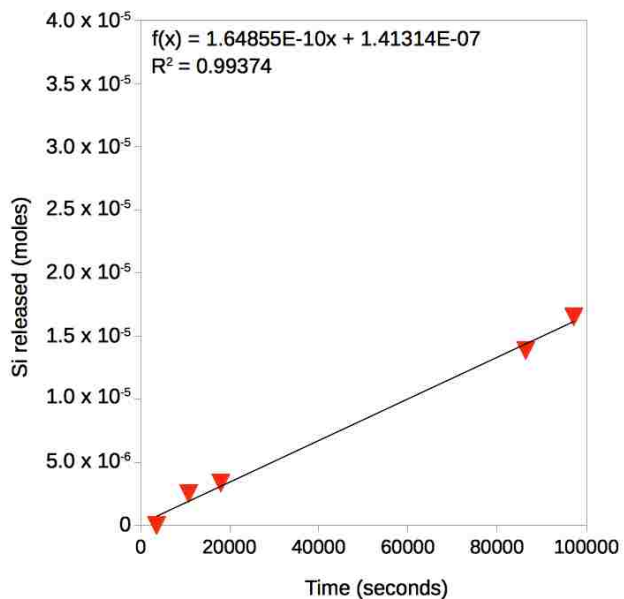
Material: Hisingerite **Initial pH:** 3.01 **Solution:** 0.01M NaCl **Specific Surface Area (BET):** 507.2660 m²/g
Batch ID: 50:50-p3-1 **Material mass:** 0.1496 g **Total Surface Area (BET):** 75.8870 m²
N/A = no analysis.

Time (sec)	pH	Volume (mL)	Concentration Si (ppm)	Moles Si released
0	3.01	180		0
3600	3.07	170	0.00156035565	1.00003 x 10 ⁻⁸
10800	3.08	160	0.394710779	2.52970 x 10 ⁻⁶
18000	3.07	150	0.534033298	3.37301 x 10 ⁻⁶
86400	3.25	140	2.37560797	1.38643 x 10 ⁻⁵
97200	3.23	130	2.87626314	1.65382 x 10 ⁻⁵
192000	3.38	120	4.51006603	2.46823 x 10 ⁻⁵
278400	3.46	110	6.09357595	3.20120 x 10 ⁻⁵
451200	3.63	100	8.7730999	4.34607 x 10 ⁻⁵
627600	3.73	90	10.017025	4.83326 x 10 ⁻⁵
969600	3.89	80	11.7869749	5.46346 x 10 ⁻⁵
1732800	3.97	70	16.6151543	7.01065 x 10 ⁻⁵

Si Release



Linear Fit



Analytical uncertainty is 10%.

<i>Regression analysis</i>		<i>Std. Error</i>
<i>R Squared</i>	0.99374	N/A
<i>Si release rate</i>	1.65 x 10 ⁻¹⁰	7.55 x 10 ⁻¹²

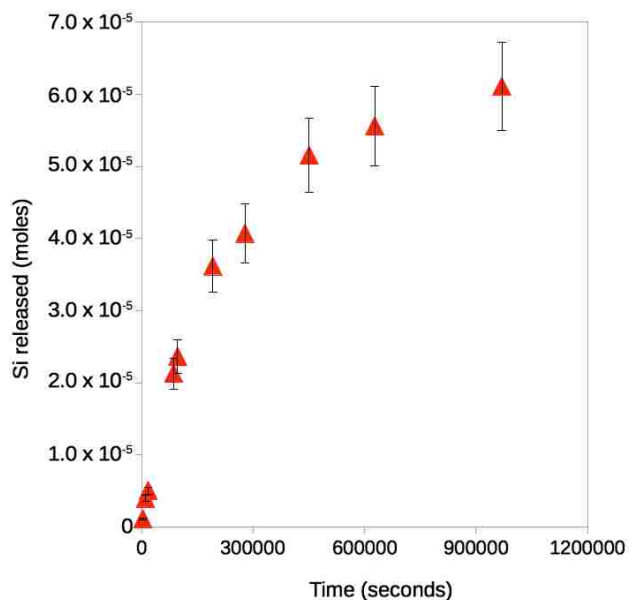
Diss. Rate Mineral (R_{diss}) 2.17 x 10⁻¹² mol m⁻² s⁻¹
Uncertainty of fit 9.95 x 10⁻¹⁴ mol m⁻² s⁻¹

Table S10. Dissolved silica analysis for experiment 50:50-p3-2

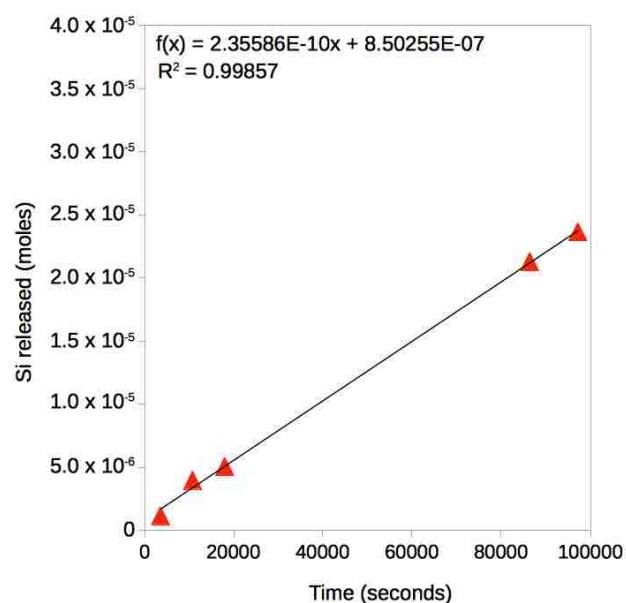
Material: Hisingerite **Initial pH:** 3.01 **Solution:** 0.01M NaCl **Specific Surface Area (BET):** 507.2660 m²/g
Batch ID: 50:50-p3-2 **Material mass:** 0.1503 g **Total Surface Area (BET):** 76.2421 m²
N/A = no analysis..

Time (sec)	pH	Volume (mL)	Concentration Si (ppm)	Moles Si released
0	3.01	180		0
3600	3.07	170	0.182102174	1.16709 x 10 ⁻⁶
10800	3.12	160	0.620425761	3.97631 x 10 ⁻⁶
18000	3.12	150	0.801653802	5.07327 x 10 ⁻⁶
86400	3.35	140	3.64720654	2.12841 x 10 ⁻⁵
97200	3.35	130	4.08778906	2.36372 x 10 ⁻⁵
192000	3.54	120	6.60463142	3.61831 x 10 ⁻⁵
278400	3.64	110	7.58110619	4.07029 x 10 ⁻⁵
451200	3.81	100	10.1077785	5.14985 x 10 ⁻⁵
627600	3.88	90	11.151597	5.55867 x 10 ⁻⁵
969600	3.96	80	12.6899385	6.10641 x 10 ⁻⁵
1732800	4.00	70	17.100256	7.51969 x 10 ⁻⁵

Si Release



Linear Fit



Analytical uncertainty is 10%.

Regression analysis		Std. Error
R Squared	0.99857	N/A
Si release rate	2.36 x 10 ⁻¹⁰	5.15 x 10 ⁻¹²

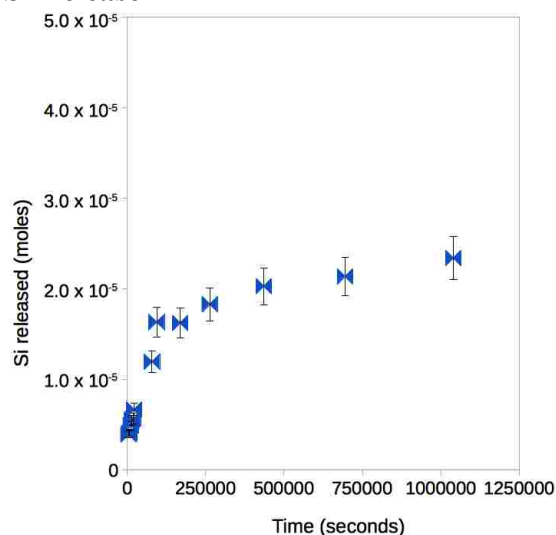
Diss. Rate Mineral (R_{diss}) $3.09 \times 10^{-12} \text{ mol m}^{-2} \text{ s}^{-1}$
 Uncertainty of fit $6.76 \times 10^{-14} \text{ mol m}^{-2} \text{ s}^{-1}$

Table S11. Dissolved silica analysis for experiment Al+Si-p5-1

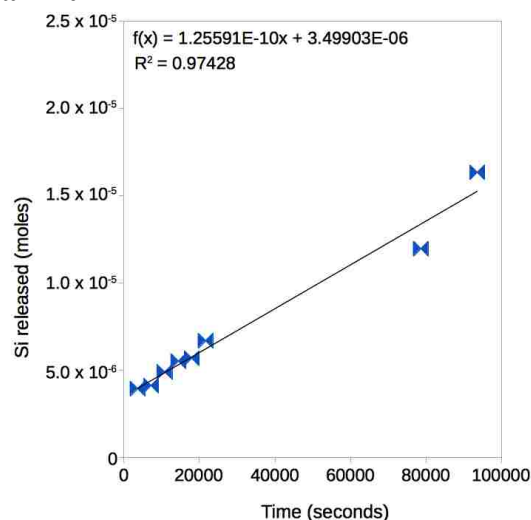
Material: Allophane **Initial pH:** 5.04 **Solution:** 0.01M NaCl **Specific Surface Area (BET):** 385.6192 m²/g
Batch ID: Al+Si-p5-1 **Material mass:** 0.1496 g **Total Surface Area (BET):** 57.766 m²
N/A = no analysis.

Time (sec)	pH	Volume (mL)	Concentration Si (ppm)	Moles Si released
0	5.04	180		0
3600	5.84	170	0.61379	3.9338 x 10 ⁻⁶
7200	5.87	160	0.64217	4.1156 x 10 ⁻⁶
10800	5.90	150	0.77116	4.8964 x 10 ⁻⁶
14400	6.11	140	0.87969	5.5147 x 10 ⁻⁶
18000	6.10	130	0.91104	5.6821 x 10 ⁻⁶
21600	6.32	120	1.11111	6.6794 x 10 ⁻⁶
78600	6.50	110	2.25139	1.1957 x 10 ⁻⁵
93600	6.47	100	3.27573	1.6334 x 10 ⁻⁵
169200	6.56	90	3.25261	1.6244 x 10 ⁻⁵
262800	6.67	80	3.83064	1.8302 x 10 ⁻⁵
435600	6.72	70	4.45403	2.0299 x 10 ⁻⁵
694800	6.89	60	4.82977	2.1370 x 10 ⁻⁵
1040400	6.85	50	5.64941	2.3413 x 10 ⁻⁵

Si Release



Linear Fit



Analytical uncertainty is 10%.

Regression analysis		Std. Error
<i>R Squared</i>	0.97428	N/A
<i>Si release rate</i>	1.26 x 10 ⁻¹⁰	8.33 x 10 ⁻¹²

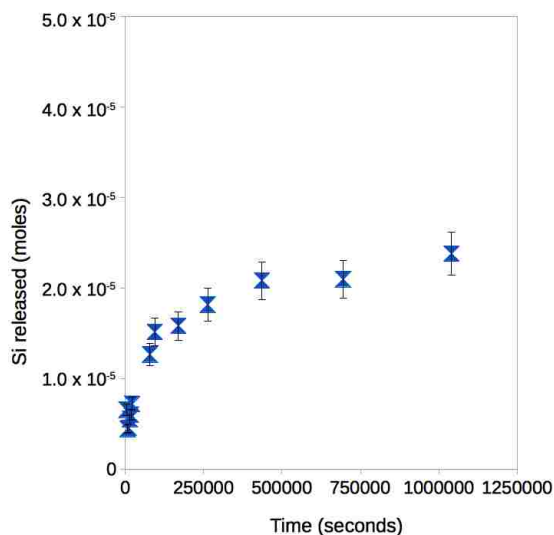
Diss. Rate Mineral (R_{diss}) 2.17 x 10⁻¹² mol m⁻² s⁻¹
Uncertainty of fit 1.44 x 10⁻¹³ mol m⁻² s⁻¹

Table S12. Dissolved silica analysis for experiment Al+Si-p5-2

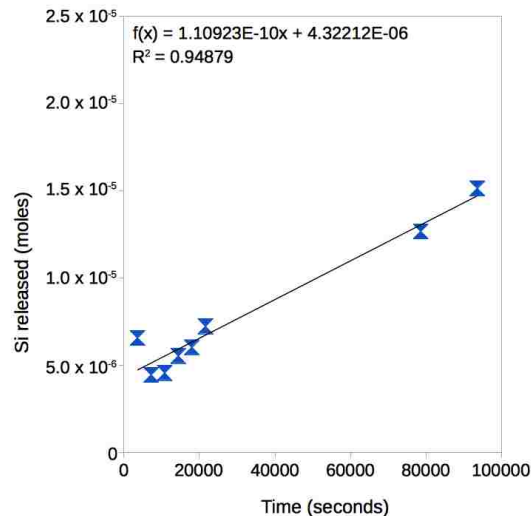
Material: Allophane **Initial pH:** 5.04 **Solution:** 0.01M NaCl **Specific Surface Area (BET):** 385.6192 m²/g
Batch ID: Al+Si-p5-2 **Material mass:** 0.1501 g **Total Surface Area (BET):** 57.881 m²
N/A = no analysis.

Time (sec)	pH	Volume (mL)	Concentration Si (ppm)	Moles Si released
0	5.04	180		0
3600	5.71	170	1.02201	6.5501 x 10 ⁻⁶
7200	5.77	160	0.69032	4.4242 x 10 ⁻⁶
10800	5.80	150	0.71039	4.5457 x 10 ⁻⁶
14400	5.94	140	0.88213	5.5241 x 10 ⁻⁶
18000	6.00	130	0.97530	6.0217 x 10 ⁻⁶
21600	6.00	120	1.21505	7.2168 x 10 ⁻⁶
78600	6.42	110	2.38875	1.2650 x 10 ⁻⁵
93600	6.39	100	2.96964	1.5132 x 10 ⁻⁵
169200	6.57	90	3.14124	1.5804 x 10 ⁻⁵
262800	6.59	80	3.80099	1.8153 x 10 ⁻⁵
435600	6.76	70	4.63123	2.0816 x 10 ⁻⁵
694800	6.78	60	4.68390	2.0964 x 10 ⁻⁵
1040400	6.83	50	5.80981	2.3770 x 10 ⁻⁵

Si Release



Linear Fit



Analytical uncertainty is 10%.

<i>Regression analysis</i>		<i>Std. Error</i>
<i>R Squared</i>	0.94879	N/A
<i>Si release rate</i>	1.11 x 10 ⁻¹⁰	1.05 x 10 ⁻¹¹

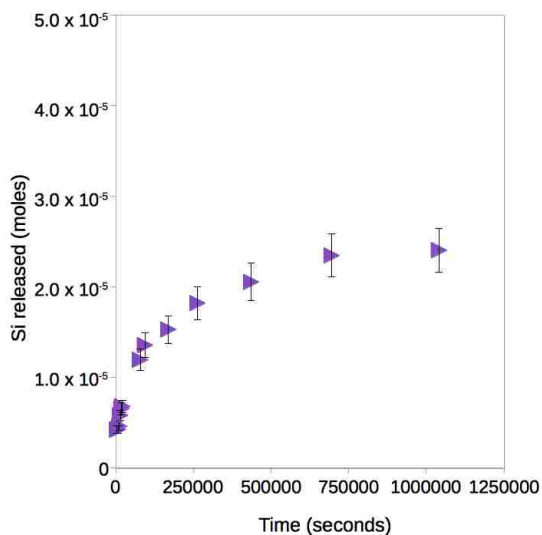
Diss. Rate Mineral (R_{diss}) 1.92 x 10⁻¹² mol m⁻² s⁻¹
Uncertainty of fit 1.82 x 10⁻¹³ mol m⁻² s⁻¹

Table S13. Dissolved silica analysis for experiment 1:99-p5-1

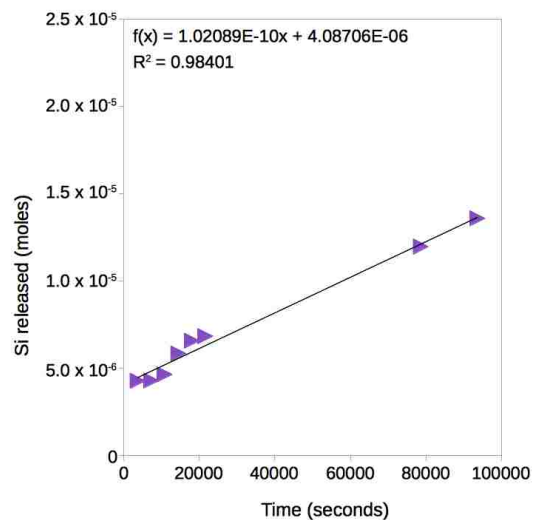
Material: Fe-allophane **Initial pH:** 5.04 **Solution:** 0.01M NaCl **Specific Surface Area (BET):** 350.2424 m²/g
Batch ID: 1:99-p5-1 **Material mass:** 0.1498 g **Total Surface Area (BET):** 52.466 m²
N/A = no analysis.

Time (sec)	pH	Volume (mL)	Concentration Si (ppm)	Moles Si released
0	5.04	180		0
3600	5.59	170	0.66661	4.2723 x 10 ⁻⁶
7200	5.57	160	0.66922	4.2890 x 10 ⁻⁶
10800	5.54	150	0.72749	4.6418 x 10 ⁻⁶
14400	5.71	140	0.93762	5.8398 x 10 ⁻⁶
18000	5.65	130	1.07461	6.5705 x 10 ⁻⁶
21600	5.81	120	1.12704	6.8318 x 10 ⁻⁶
78600	6.05	110	2.23641	1.1967 x 10 ⁻⁵
93600	5.98	100	2.61468	1.3583 x 10 ⁻⁵
169200	6.13	90	3.05807	1.5320 x 10 ⁻⁵
262800	6.17	80	3.87508	1.8229 x 10 ⁻⁵
435600	6.19	70	4.60542	2.0569 x 10 ⁻⁵
694800	6.26	60	5.63096	2.3490 x 10 ⁻⁵
1040400	6.37	50	5.86422	2.4072 x 10 ⁻⁵

Si Release



Linear Fit



Analytical uncertainty is 10%.

Regression analysis		Std. Error
<i>R Squared</i>	0.98401	N/A
<i>Si release rate</i>	1.02 x 10 ⁻¹⁰	5.31 x 10 ⁻¹²

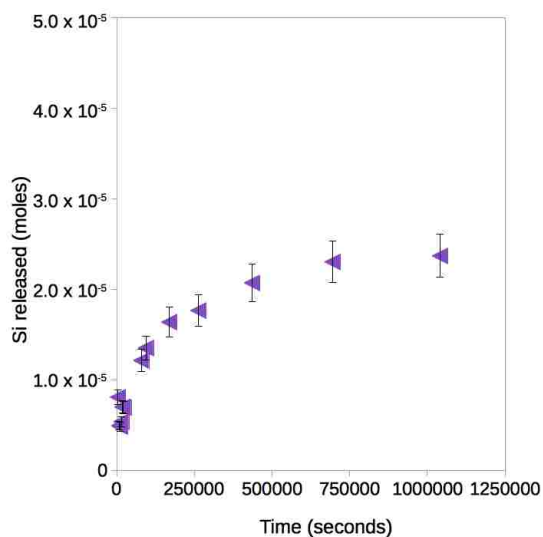
Diss. Rate Mineral (R_{diss}) 1.95 x 10⁻¹² mol m⁻² s⁻¹
Uncertainty of fit 1.01 x 10⁻¹³ mol m⁻² s⁻¹

Table S14. Dissolved silica analysis for experiment 1:99-p5-2

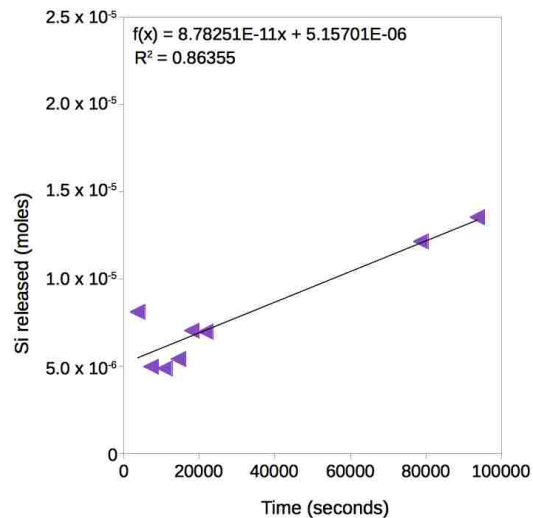
Material: Fe-allophane **Initial pH:** 5.04 **Solution:** 0.01M NaCl **Specific Surface Area (BET):** 350.2424 m²/g
Batch ID: 1:99-p5-2 **Material mass:** 0.1499 g **Total Surface Area (BET):** 52.501 m²
N/A = no analysis.

Time (sec)	pH	Volume (mL)	Concentration Si (ppm)	Moles Si released
0	5.04	180		0
3600	5.56	170	1.26441	8.1036 x 10 ⁻⁶
7200	5.55	160	0.77553	4.9703 x 10 ⁻⁶
10800	5.49	150	0.75806	4.8646 x 10 ⁻⁶
14400	5.67	140	0.85282	5.4044 x 10 ⁻⁶
18000	5.68	130	1.15778	7.0332 x 10 ⁻⁶
21600	5.72	120	1.14451	6.6971 x 10 ⁻⁶
78600	6.01	110	2.26313	1.2145 x 10 ⁻⁵
93600	6.05	100	2.25757	1.3531 x 10 ⁻⁵
169200	6.03	90	3.31736	1.6389 x 10 ⁻⁵
262800	6.11	80	3.67665	1.7669 x 10 ⁻⁵
435600	6.19	70	4.63010	2.0724 x 10 ⁻⁵
694800	6.19	60	5.44277	2.3039 x 10 ⁻⁵
1040400	6.27	50	5.70910	2.3703 x 10 ⁻⁵

Si Release



Linear Fit



Analytical uncertainty is 10%.

Regression analysis		Std. Error
<i>R Squared</i>	0.86355	N/A
<i>Si release rate</i>	8.78 x 10 ⁻¹¹	1.43 x 10 ⁻¹¹

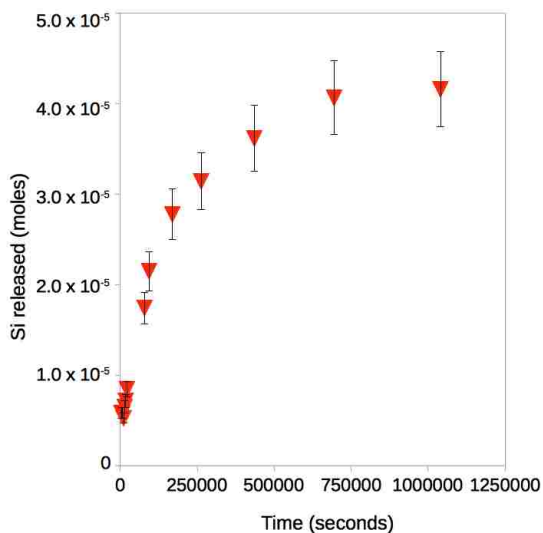
Diss. Rate Mineral (R_{diss}) 1.67 x 10⁻¹² mol m⁻² s⁻¹
Uncertainty of fit 2.71 x 10⁻¹³ mol m⁻² s⁻¹

Table S15. Dissolved silica analysis for experiment 50:50-p5-1

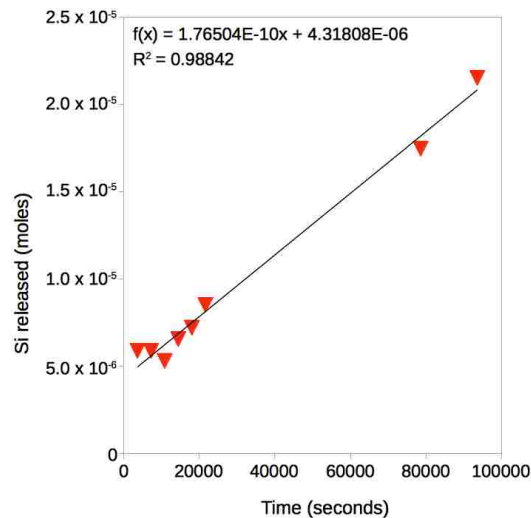
Material: Hisingerite **Initial pH:** 5.04 **Solution:** 0.01M NaCl **Specific Surface Area (BET):** 507.2660 m²/g
Batch ID: 50:50-p5-1 **Material mass:** 0.1496 g **Total Surface Area (BET):** 75.887 m²
N/A = no analysis.

Time (sec)	pH	Volume (mL)	Concentration Si (ppm)	Moles Si released
0	5.04	180		0
3600	5.33	170	0.91638	8.1036 x 10 ⁻⁶
7200	5.51	160	0.91530	4.9703 x 10 ⁻⁶
10800	5.63	150	0.82197	4.8646 x 10 ⁻⁶
14400	6.01	140	1.04073	5.4044 x 10 ⁻⁶
18000	5.89	130	1.16415	7.0332 x 10 ⁻⁶
21600	5.94	120	1.42513	6.6971 x 10 ⁻⁶
78600	6.47	110	3.36038	1.2145 x 10 ⁻⁵
93600	6.56	100	4.30817	1.3531 x 10 ⁻⁵
169200	6.78	90	5.91635	1.6389 x 10 ⁻⁵
262800	6.83	80	6.93831	1.7669 x 10 ⁻⁵
435600	6.95	70	8.41950	2.0724 x 10 ⁻⁵
694800	6.96	60	9.98684	2.3039 x 10 ⁻⁵
1040400	7.06	50	10.36728	2.3703 x 10 ⁻⁵

Si Release



Linear Fit



Analytical uncertainty is 10%.

Regression analysis		Std. Error
<i>R Squared</i>	0.98842	N/A
<i>Si release rate</i>	1.77 x 10 ⁻¹⁰	7.80 x 10 ⁻¹²

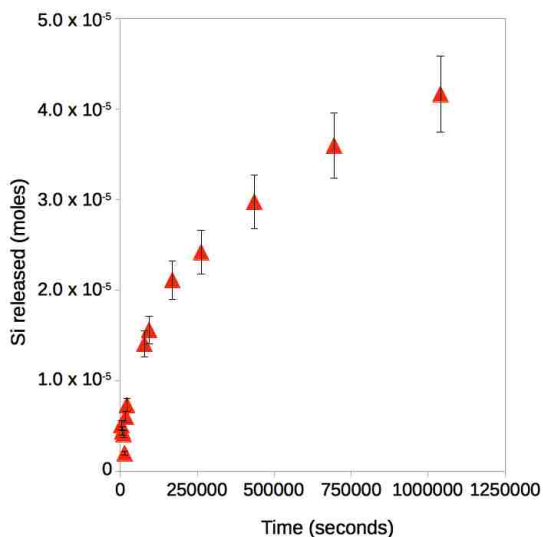
Diss. Rate Mineral (R_{diss}) 2.33 x 10⁻¹² mol m⁻² s⁻¹
Uncertainty of fit 1.03 x 10⁻¹³ mol m⁻² s⁻¹

Table S16. Dissolved silica analysis for experiment 50:50-p5-2

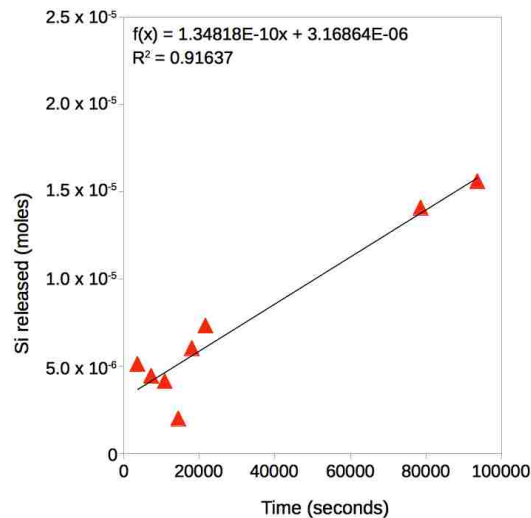
Material: Hisingerite **Initial pH:** 5.04 **Solution:** 0.01M NaCl **Specific Surface Area (BET):** 507.2660 m²/g
Batch ID: 50:50-p5-2 **Material mass:** 0.1501 g **Total Surface Area (BET):** 76.141 m²
N/A = no analysis.

Time (sec)	pH	Volume (mL)	Concentration Si (ppm)	Moles Si released
0	5.04	180		0
3600	5.35	170	0.79987	5.1264 x 10 ⁻⁶
7200	5.50	160	0.69402	4.4480 x 10 ⁻⁶
10800	5.51	150	0.64202	4.1332 x 10 ⁻⁶
14400	5.74	140	0.26866	2.0062 x 10 ⁻⁶
18000	5.85	130	1.02319	6.0360 x 10 ⁻⁶
21600	5.93	120	1.28075	7.3199 x 10 ⁻⁶
78600	6.49	110	2.74231	1.4085 x 10 ⁻⁵
93600	6.46	100	3.09740	1.5602 x 10 ⁻⁵
169200	6.64	90	4.50155	2.1102 x 10 ⁻⁵
262800	6.78	80	5.37456	2.4210 x 10 ⁻⁵
435600	6.87	70	7.10158	2.9744 x 10 ⁻⁵
694800	6.96	60	9.28816	3.5973 x 10 ⁻⁵
1040400	7.06	50	11.57553	4.1674 x 10 ⁻⁵

Si Release



Linear Fit



Analytical uncertainty is 10%.

<i>Regression analysis</i>		<i>Std. Error</i>
<i>R Squared</i>	0.91637	N/A
<i>Si release rate</i>	1.35 x 10 ⁻¹⁰	1.66 x 10 ⁻¹¹

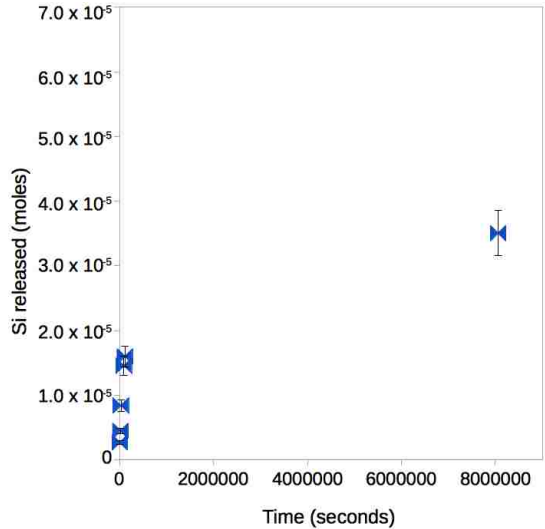
Diss. Rate Mineral (R_{diss}) 1.77 x 10⁻¹² mol m⁻² s⁻¹
Uncertainty of fit 2.18 x 10⁻¹³ mol m⁻² s⁻¹

Table S17. Dissolved silica analysis for experiment Al+Si-p8-1

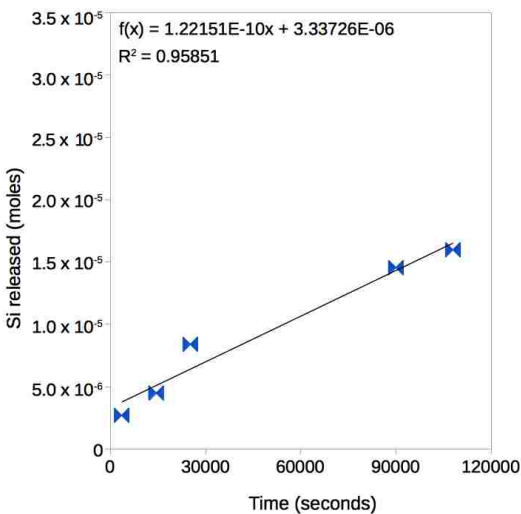
Material: Allophane **Initial pH:** 6.99 **Solution:** 0.01M NaCl **Specific Surface Area (BET):** 385.6192 m²/g
Batch ID: Al+Si-p8-1 **Material mass:** 0.1500 g **Total Surface Area (BET):** 57.8429 m²
N/A = no analysis.

Time (sec)	pH	Volume (mL)	Concentration Si (ppm)	Moles Si released
0	6.99	180		0
3600	6.76	170	0.42231	2.70659 x 10 ⁻⁶
14400	7.16	160	0.70033	4.48840 x 10 ⁻⁶
25200	6.95	150	1.34712	8.40337 x 10 ⁻⁶
90000	7.12	140	2.42705	1.45557 x 10 ⁻⁵
108000	7.17	130	2.69658	1.59952 x 10 ⁻⁵
194400	7.22	120	N/A	N/A
280800	7.36	110	N/A	N/A
8060400	7.20	100	8.20587254	3.50609 x 10 ⁻⁵

Si Release



Linear Fit



Analytical uncertainty is 10%.

<i>Regression analysis</i>		<i>Std. Error</i>
<i>R Squared</i>	0.95851	N/A
<i>Si release rate</i>	1.22 x 10 ⁻¹⁰	1.47 x 10 ⁻¹¹

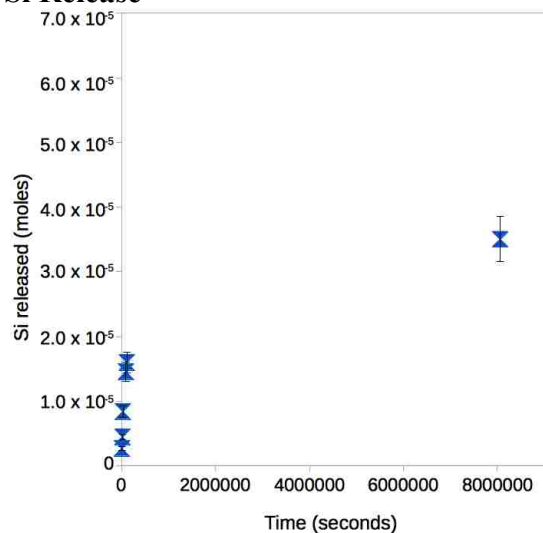
Diss. Rate Mineral (R_{diss}) 2.11 x 10⁻¹² mol m⁻² s⁻¹
Uncertainty of fit 2.45 x 10⁻¹³ mol m⁻² s⁻¹

Table S18. Dissolved silica analysis for experiment Al+Si-p8-2

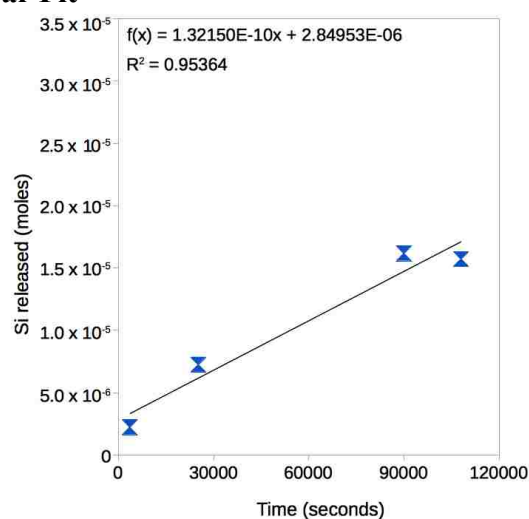
Material: Allophane **Initial pH:** 6.99 **Solution:** 0.01M NaCl **Specific Surface Area (BET):** 385.6192 m²/g
Batch ID: Al+Si-p8-2 **Material mass:** 0.1502 g **Total Surface Area (BET):** 57.9200 m²
N/A = no analysis.

Time (sec)	pH	Volume (mL)	Concentration Si (ppm)	Moles Si released
0	6.99	180		0
3600	6.65	170	0.34720	2.22519 x 10 ⁻⁶
14400	6.75	160	N/A	N/A
25200	6.7	150	1.19857	7.25491 x 10 ⁻⁶
90000	7.01	140	2.76481	1.61776 x 10 ⁻⁵
108000	7.06	130	2.67765	1.57121 x 10 ⁻⁵
194400	7.24	120	3.11976	1.79159 x 10 ⁻⁵
280800	7.2	110	3.86712	2.13752 x 10 ⁻⁵
8060400	7.2	100	7.21570396	3.56825 x 10 ⁻⁵

Si Release



Linear Fit



Analytical uncertainty is 10%.

Regression analysis		Std. Error
<i>R Squared</i>	0.95364	N/A
<i>Si release rate</i>	1.32 x 10 ⁻¹⁰	2.06 x 10 ⁻¹¹

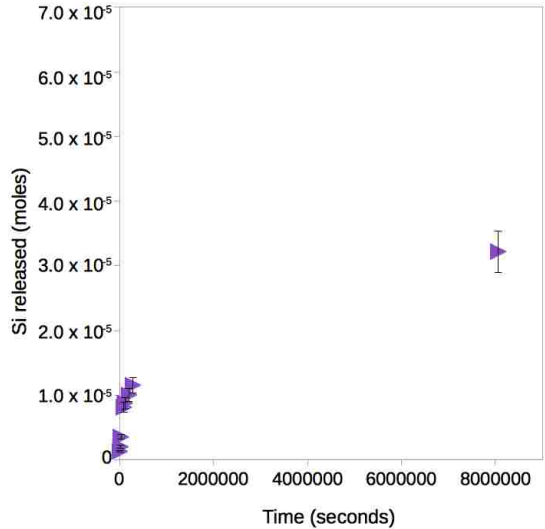
Diss. Rate Mineral (R_{diss}) 2.28 x 10⁻¹² mol m⁻² s⁻¹
Uncertainty of fit 3.56 x 10⁻¹³ mol m⁻² s⁻¹

Table S19. Dissolved silica analysis for experiment 1:99-p8-1

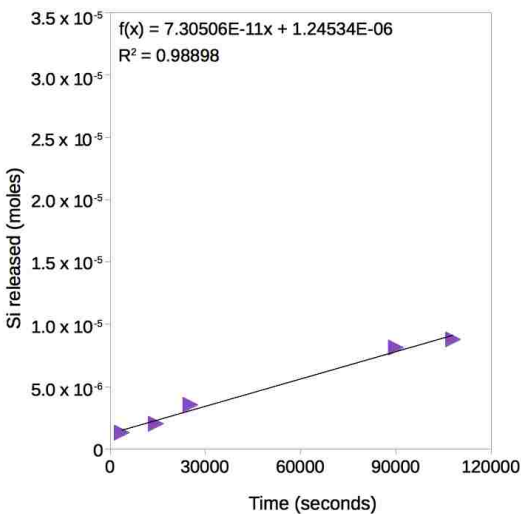
Material: Fe-allophane **Initial pH:** 6.99 **Solution:** 0.01M NaCl **Specific Surface Area (BET):** 350.2424 m²/g
Batch ID: 1:99-p8-1 **Material mass:** 0.1502 g **Total Surface Area (BET):** 52.6064 m²
N/A = no analysis.

Time (sec)	pH	Volume (mL)	Concentration Si (ppm)	Moles Si released
0	6.99	180		0
3600	6.38	170	0.20628	1.32206 x 10 ⁻⁶
14400	6.37	160	0.31738	2.03407 x 10 ⁻⁶
25200	6.37	150	0.56756	3.54841 x 10 ⁻⁶
90000	6.36	140	1.37401	8.14270 x 10 ⁻⁶
108000	6.4	130	1.49695	8.79925 x 10 ⁻⁶
194400	6.44	120	1.74751	1.00483 x 10 ⁻⁵
280800	6.4	110	2.07447	1.15617 x 10 ⁻⁵
8060400	6.4	100	6.90833	3.22151 x 10 ⁻⁵

Si Release



Linear Fit



Analytical uncertainty is 10%.

Regression analysis		Std. Error
<i>R Squared</i>	0.98898	N/A
<i>Si release rate</i>	7.31 x 10 ⁻¹¹	4.45 x 10 ⁻¹²

Diss. Rate Mineral (R_{diss}) 1.39 x 10⁻¹² mol m⁻² s⁻¹
Uncertainty of fit 8.46 x 10⁻¹⁴ mol m⁻² s⁻¹

Table S20. Dissolved silica analysis for experiment 1:99-p8-2

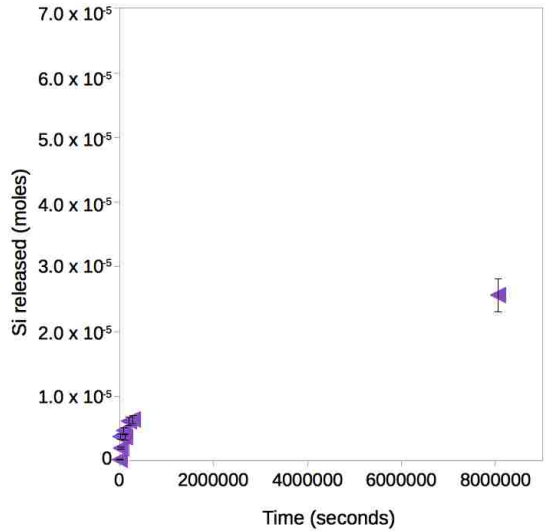
**This experiment was omitted from the final dataset due to the anomalous mass, high standard error, and poor R^2 value.

Material: Fe-allophane **Initial pH:** 6.99 **Solution:** 0.01M NaCl **Specific Surface Area (BET):** 350.2424 m²/g
Batch ID: 1:99-p8-2 **Material mass:** 0.0737 g **Total Surface Area (BET):** 25.8129 m²

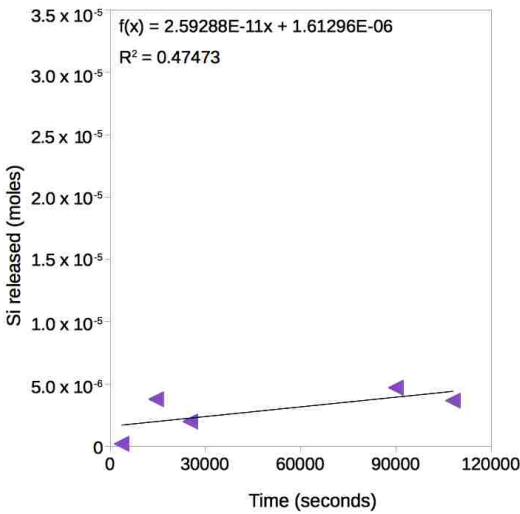
N/A = no analysis.

Time (sec)	pH	Volume (mL)	Concentration Si (ppm)	Moles Si released
0	6.99	180		0
3600	6.37	170	0.03077	1.97219×10^{-7}
14400	6.37	160	0.58864	3.77259×10^{-6}
25200	6.4	150	0.29342	1.98567×10^{-6}
90000	6.35	140	0.77023	4.70196×10^{-6}
108000	6.42	130	0.57539	3.66139×10^{-6}
194400	6.41	120	1.07378	6.14575×10^{-6}
280800	6.42	110	1.13292	6.41948×10^{-6}
8060400	6.24	100	5.63154	2.56406×10^{-5}

Si Release



Linear Fit



Analytical uncertainty is 10%.

Regression analysis		Std. Error
<i>R Squared</i>	0.47473	N/A
<i>Si release rate</i>	2.59×10^{-11}	1.57×10^{-11}

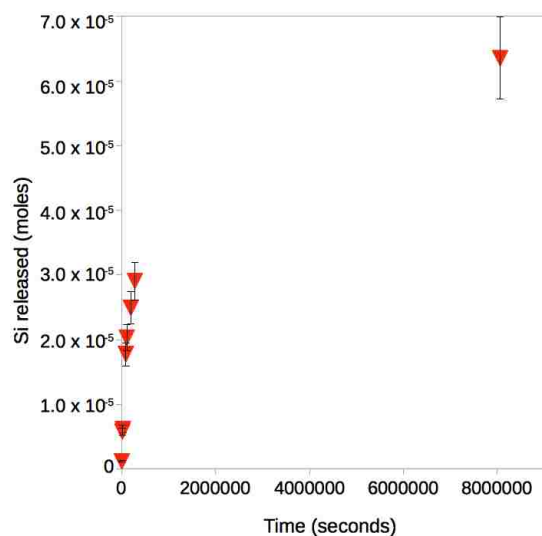
Diss. Rate Mineral (R_{diss}) $1.00 \times 10^{-12} \text{ mol m}^{-2} \text{ s}^{-1}$
Uncertainty of fit $6.10 \times 10^{-13} \text{ mol m}^{-2} \text{ s}^{-1}$

Table S21. Dissolved silica analysis for experiment 50:50-p8-1

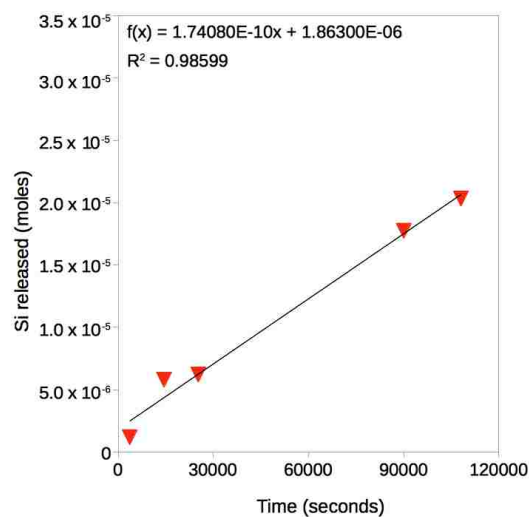
Material: Hisingerite **Initial pH:** 6.99 **Solution:** 0.01M NaCl **Specific Surface Area (BET):** 507.2660 m²/g
Batch ID: 50:50-p8-1 **Material mass:** 0.1497 g **Total Surface Area (BET):** 75.9377 m²
N/A = no analysis.

Time (sec)	pH	Volume (mL)	Concentration Si (ppm)	Moles Si released
0	6.99	180		0
3600	5.94	170	0.18687	1.19763 x 10 ⁻⁶
14400	5.70	160	0.90425	5.79531 x 10 ⁻⁶
25200	5.42	150	0.97387	6.21672 x 10 ⁻⁶
90000	5.24	140	3.00071	1.77634 x 10 ⁻⁵
108000	5.27	130	3.48126	2.03300 x 10 ⁻⁵
194400	5.22	120	4.40980	2.49585 x 10 ⁻⁵
280800	5.21	110	5.29977	2.90780 x 10 ⁻⁵
8060400	5.00	100	13.36705	6.35467 x 10 ⁻⁵

Si Release



Linear Fit



Analytical uncertainty is 10%.

<i>Regression analysis</i>		<i>Std. Error</i>
<i>R Squared</i>	0.98599	N/A
<i>Si release rate</i>	1.74 x 10 ⁻¹⁰	1.20 x 10 ⁻¹¹

Diss. Rate Mineral (R_{diss}) 2.29 x 10⁻¹² mol m⁻² s⁻¹

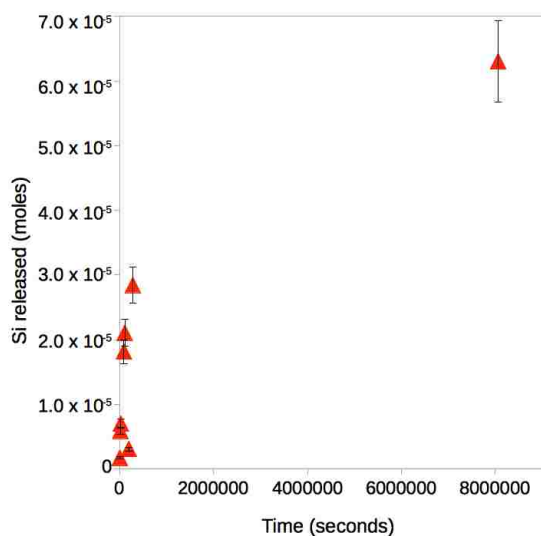
Uncertainty of fit 1.58 x 10⁻¹³ mol m⁻² s⁻¹

Table S22. Dissolved silica analysis for experiment 50:50-p8-2

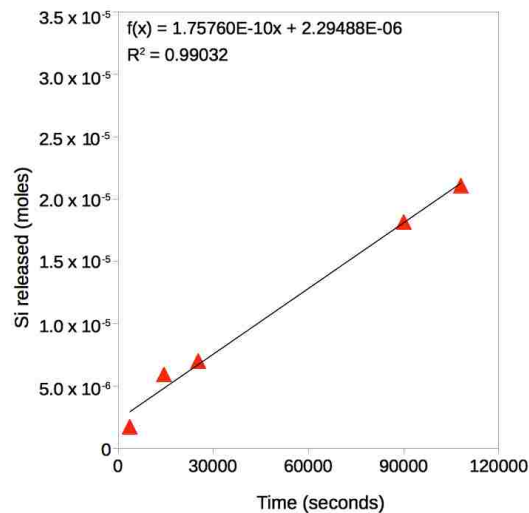
Material: Hisingerite **Initial pH:** 6.99 **Solution:** 0.01M NaCl **Specific Surface Area (BET):** 507.2660 m²/g
Batch ID: 50:50-p8-2 **Material mass:** 0.1499 g **Total Surface Area (BET):** 76.0392 m²
N/A = no analysis.

Time (sec)	pH	Volume (mL)	Concentration Si (ppm)	Moles Si released
0	6.99	180		0
3600	6.05	170	0.27037	1.73277 x 10 ⁻⁶
14400	5.69	160	0.92160	5.90655 x 10 ⁻⁶
25200	5.46	150	1.10247	7.00132 x 10 ⁻⁶
90000	5.24	140	3.05910	1.81480 x 10 ⁻⁵
108000	5.24	130	3.60788	2.10790 x 10 ⁻⁵
194400	5.19	120	N/A	N/A
280800	5.20	110	5.47730	2.84474 x 10 ⁻⁵
8060400	5.08	100	13.57007	6.30251 x 10 ⁻⁵

Si Release



Linear Fit



Analytical uncertainty is 10%.

<i>Regression analysis</i>		<i>Std. Error</i>
<i>R Squared</i>	0.99032	N/A
<i>Si release rate</i>	1.76 x 10 ⁻¹⁰	1.00 x 10 ⁻¹¹

Diss. Rate Mineral (R_{diss}) 2.31 x 10⁻¹² mol m⁻² s⁻¹

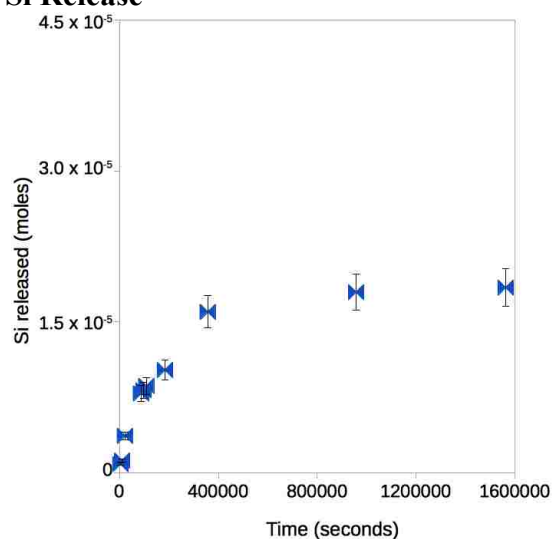
Uncertainty of fit 1.32 x 10⁻¹³ mol m⁻² s⁻¹

Table S23. Dissolved silica analysis for experiment Al+Si-p10.3-1

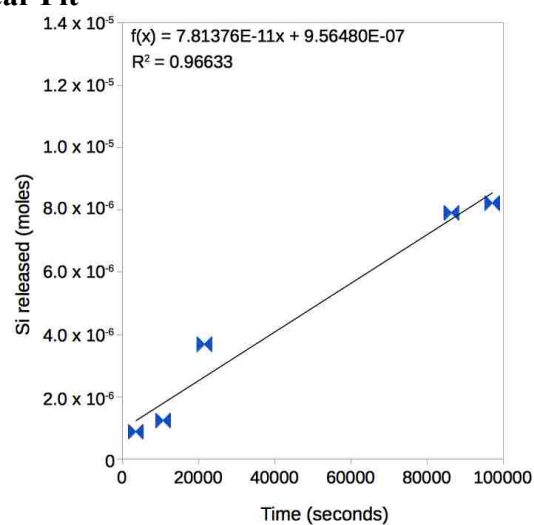
Material: Allophane **Initial pH:** 10.36 **Solution:** 0.01M NaCl **Specific Surface Area (BET):** 385.6192 m²/g
Batch ID: Al+Si-p10.3-1 **Material mass:** 0.1504 g **Total Surface Area (BET):** 57.9971 m²
N/A = no analysis.

Time (sec)	pH	Volume (mL)	Concentration Si (ppm)	Moles Si released
0	10.36	180		0
3600	9.94	170	0.13828	8.8625 x 10 ⁻⁷
10800	9.62	160	0.19394	1.2430 x 10 ⁻⁶
21600	9.39	150	0.57550	3.6884 x 10 ⁻⁶
86400	8.73	140	1.23329	7.9041 x 10 ⁻⁶
97200	8.70	130	1.28252	8.2196 x 10 ⁻⁶
108000	8.00	120	1.34882	8.6446 x 10 ⁻⁶
183600	8.02	110	1.59671	1.0233 x 10 ⁻⁵
356400	8.01	100	2.49581	1.5996 x 10 ⁻⁵
957300	7.89	90	2.80389	1.7970 x 10 ⁻⁵
1562100	7.79	80	2.87474	1.8424 x 10 ⁻⁵

Si Release



Linear Fit



Analytical uncertainty is 10%.

<i>Regression analysis</i>		<i>Std. Error</i>
<i>R Squared</i>	0.96633	N/A
<i>Si release rate</i>	7.81 x 10 ⁻¹¹	8.42 x 10 ⁻¹²

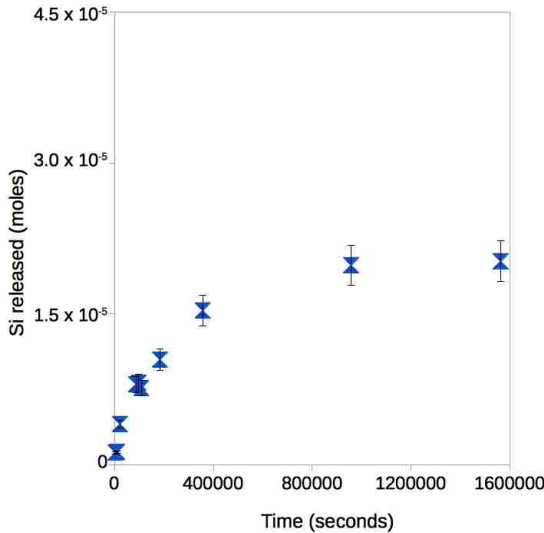
Diss. Rate Mineral (R_{diss}) 1.35 x 10⁻¹² mol m⁻² s⁻¹
Uncertainty of fit 1.45 x 10⁻¹³ mol m⁻² s⁻¹

Table S24. Dissolved silica analysis for experiment Al+Si-p10.3-2

Material: Allophane **Initial pH:** 10.36 **Solution:** 0.01M NaCl **Specific Surface Area (BET):** 385.6192 m²/g
Batch ID: Al+Si-p10.3-2 **Material mass:** 0.1502 g **Total Surface Area (BET):** 57.9200 m²
N/A = no analysis.

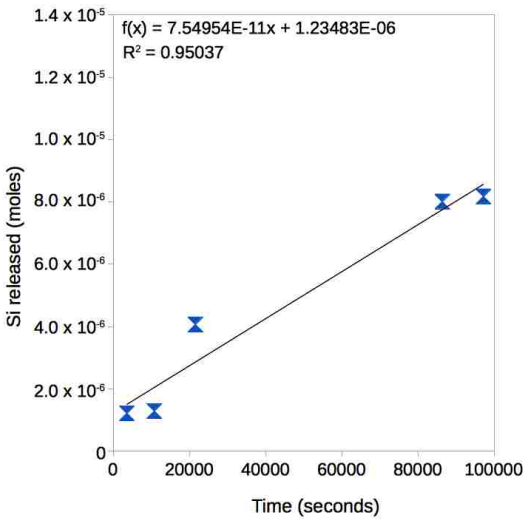
Time (sec)	pH	Volume (mL)	Concentration Si (ppm)	Moles Si released
0	10.36	180		0
3600	9.90	170	0.18916	1.2123 x 10 ⁻⁶
10800	9.62	160	0.20052	1.2851 x 10 ⁻⁶
21600	9.39	150	0.63471	4.0679 x 10 ⁻⁶
86400	8.61	140	1.25017	8.0124 x 10 ⁻⁶
97200	8.46	130	1.27559	8.1753 x 10 ⁻⁶
108000	7.82	120	1.18912	7.6210 x 10 ⁻⁶
183600	7.95	110	1.63182	1.0458 x 10 ⁻⁵
356400	8.04	100	2.39583	1.5355 x 10 ⁻⁵
957300	7.60	90	3.09747	1.9852 x 10 ⁻⁵
1562100	7.76	80	3.15923	2.0248 x 10 ⁻⁵

Si Release



Analytical uncertainty is 10%.

Linear Fit



Regression analysis		Std. Error
<i>R Squared</i>	0.95037	N/A
<i>Si release rate</i>	7.55×10^{-11}	9.96×10^{-12}

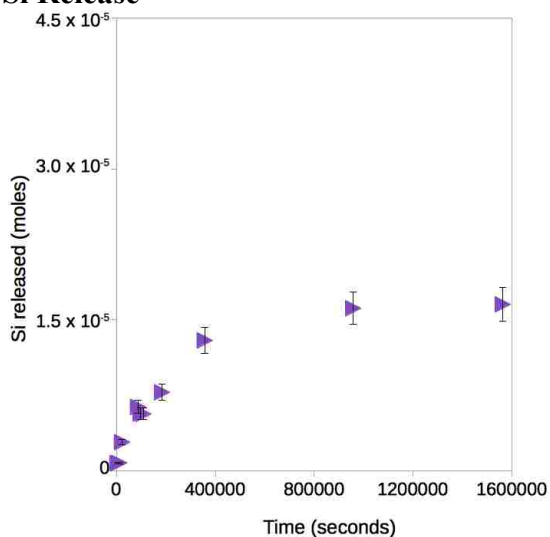
Diss. Rate Mineral (R_{diss}) $1.30 \times 10^{-12} \text{ mol m}^{-2} \text{ s}^{-1}$
Uncertainty of fit $1.72 \times 10^{-13} \text{ mol m}^{-2} \text{ s}^{-1}$

Table S25. Dissolved silica analysis for experiment 1:99-p10.3-1

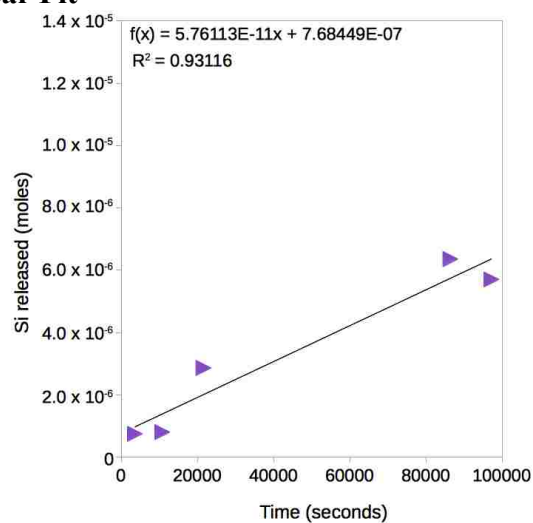
Material: Fe-allophane **Initial pH:** 10.36 **Solution:** 0.01M NaCl **Specific Surface Area (BET):** 350.2424 m²/g
Batch ID: 1:99-p10.3-1 **Material mass:** 0.1503 g **Total Surface Area (BET):** 52.6414 m²
N/A = no analysis.

Time (sec)	pH	Volume (mL)	Concentration Si (ppm)	Moles Si released
0	10.36	180		0
3600	9.81	170	0.11607	7.5308×10^{-7}
10800	9.59	160	0.12619	8.0873×10^{-7}
21600	9.25	150	0.35463	2.8661×10^{-6}
86400	7.98	140	0.99220	6.3590×10^{-6}
97200	7.80	130	0.89042	5.7067×10^{-6}
108000	7.55	120	0.88463	5.6696×10^{-6}
183600	7.48	110	1.22009	7.8196×10^{-6}
356400	7.47	100	2.02449	1.2975×10^{-5}
957300	7.32	90	2.52143	1.6160×10^{-5}
1562100	7.18	80	2.58314	1.6555×10^{-5}

Si Release



Linear Fit



Analytical uncertainty is 10%.

Regression analysis		Std. Error
<i>R Squared</i>	0.93116	N/A
<i>Si release rate</i>	5.76×10^{-11}	9.04×10^{-12}

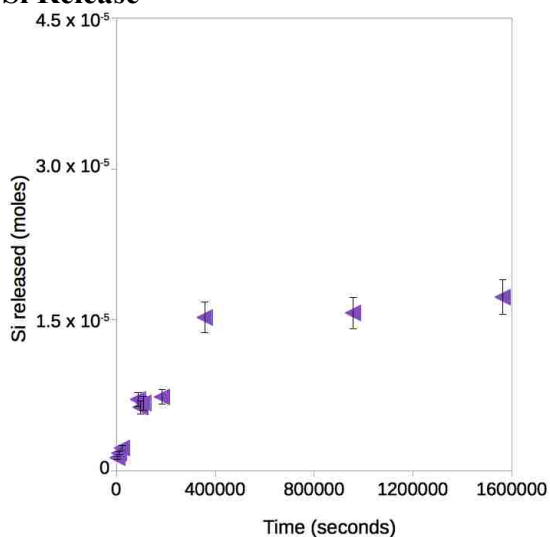
Diss. Rate Mineral (R_{diss}) $1.09 \times 10^{-12} \text{ mol m}^{-2} \text{ s}^{-1}$
Uncertainty of fit $1.72 \times 10^{-13} \text{ mol m}^{-2} \text{ s}^{-1}$

Table S26. Dissolved silica analysis for experiment 1:99-p10.3-2

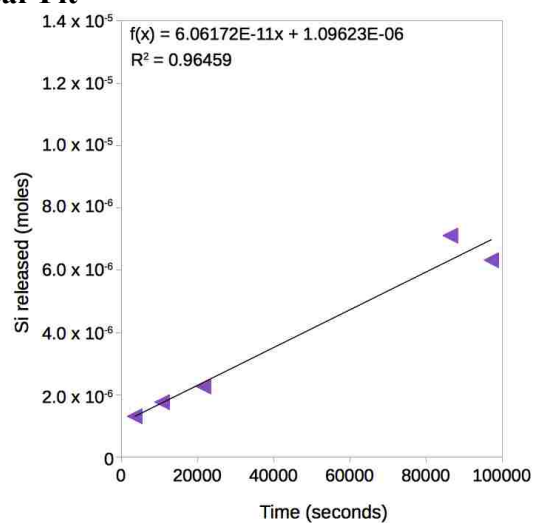
Material: Fe-allophane **Initial pH:** 10.36 **Solution:** 0.01M NaCl **Specific Surface Area (BET):** 350.2424 m²/g
Batch ID: 1:99-p10.3-2 **Material mass:** 0.1496 g **Total Surface Area (BET):** 52.3962 m²
N/A = no analysis.

Time (sec)	pH	Volume (mL)	Concentration Si (ppm)	Moles Si released
0	10.36	180		0
3600	9.78	170	0.11750	1.3155 x 10 ⁻⁶
10800	9.49	160	0.27599	1.7688 x 10 ⁻⁶
21600	9.18	150	0.76731	2.2728 x 10 ⁻⁶
86400	8.02	140	1.10943	7.1103 x 10 ⁻⁶
97200	7.60	130	0.98693	6.3252 x 10 ⁻⁶
108000	7.48	120	1.05290	6.7480 x 10 ⁻⁶
183600	7.41	110	1.14753	7.3545 x 10 ⁻⁶
356400	7.39	100	2.37914	1.5248 x 10 ⁻⁵
957300	7.23	90	2.4942	1.5698 x 10 ⁻⁵
1562100	7.18	80	2.69451	1.7269 x 10 ⁻⁵

Si Release



Linear Fit



Analytical uncertainty is 10%.

Regression analysis		Std. Error
<i>R Squared</i>	0.96459	N/A
<i>Si release rate</i>	6.06 x 10 ⁻¹¹	6.71 x 10 ⁻¹²

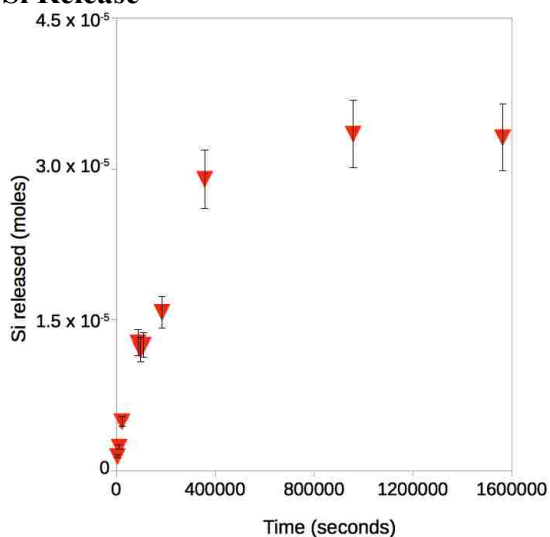
Diss. Rate Mineral (R_{diss}) 1.16 x 10⁻¹² mol m⁻² s⁻¹
Uncertainty of fit 1.28 x 10⁻¹³ mol m⁻² s⁻¹

Table S27. Dissolved silica analysis for experiment 50:50-p10.3-1

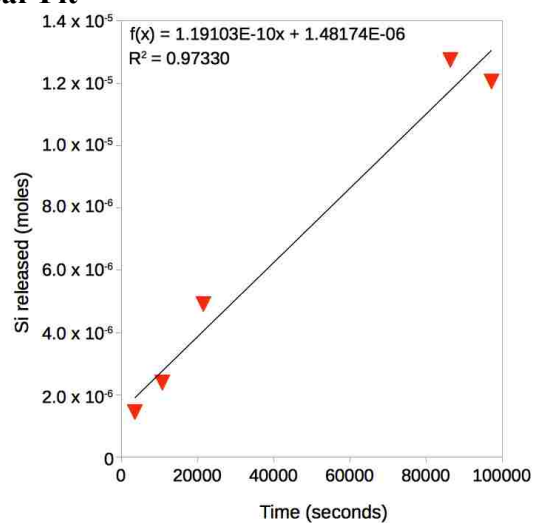
Material: Hisingerite **Initial pH:** 10.36 **Solution:** 0.01M NaCl **Specific Surface Area (BET):** 507.266 m²/g
Batch ID: 50:50-p10.3-1 **Material mass:** 0.1497 g **Total Surface Area (BET):** 75.9377 m²
N/A = no analysis.

Time (sec)	pH	Volume (mL)	Concentration Si (ppm)	Moles Si released
0	10.36	180		0
3600	10.04	170	0.20526	1.4484 x 10 ⁻⁶
10800	9.73	160	0.37307	2.3910 x 10 ⁻⁶
21600	9.43	150	0.71901	4.9177 x 10 ⁻⁶
86400	7.25	140	1.98938	1.2750 x 10 ⁻⁵
97200	6.99	130	1.88120	1.2057 x 10 ⁻⁵
108000	7.08	120	1.95460	1.2527 x 10 ⁻⁵
183600	6.82	110	2.46158	1.5776 x 10 ⁻⁵
356400	6.72	100	4.52585	2.9006 x 10 ⁻⁵
957300	6.58	90	5.22729	3.3502 x 10 ⁻⁵
1562100	6.56	80	5.16958	3.3132 x 10 ⁻⁵

Si Release



Linear Fit



Analytical uncertainty is 10%.

Regression analysis		Std. Error
<i>R Squared</i>	0.97330	N/A
<i>Si release rate</i>	1.19 x 10 ⁻¹⁰	1.14 x 10 ⁻¹¹

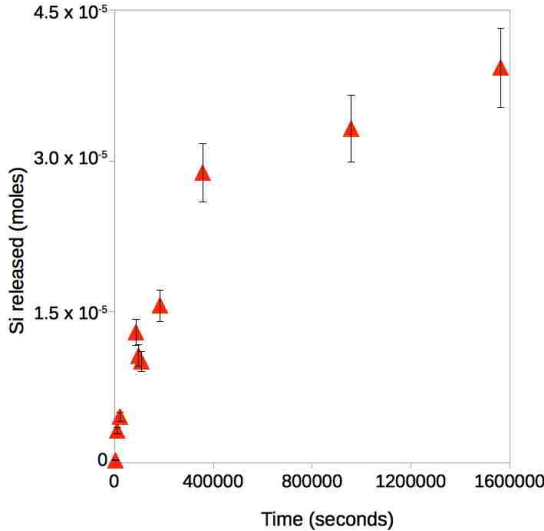
Diss. Rate Mineral (R_{diss}) 1.57 x 10⁻¹² mol m⁻² s⁻¹
Uncertainty of fit 1.50 x 10⁻¹³ mol m⁻² s⁻¹

Table S28. Dissolved silica analysis for experiment 50:50-p10.3-2

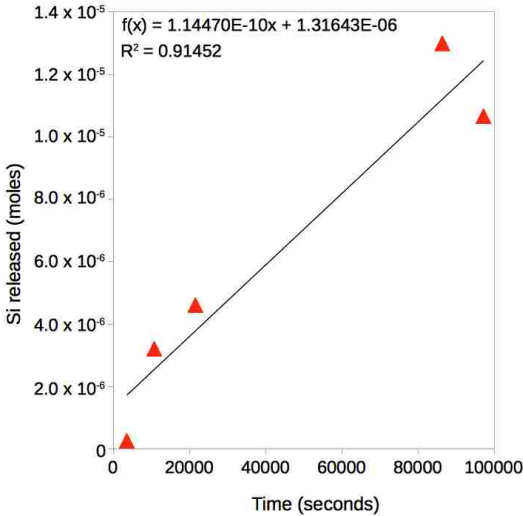
Material: Hisingerite **Initial pH:** 10.36 **Solution:** 0.01M NaCl **Specific Surface Area (BET):** 507.266 m²/g
Batch ID: 50:50-p10.3-2 **Material mass:** 0.1503 g **Total Surface Area (BET):** 76.2421 m²
N/A = no analysis.

Time (sec)	pH	Volume (mL)	Concentration Si (ppm)	Moles Si released
0	10.36	180		0
3600	10.03	170	0.22600	2.6071 x 10 ⁻⁷
10800	9.78	160	0.49974	3.2028 x 10 ⁻⁶
21600	9.42	150	0.12207	4.6082 x 10 ⁻⁶
86400	7.34	140	2.02721	1.2992 x 10 ⁻⁵
97200	6.85	130	1.66260	1.0656 x 10 ⁻⁵
108000	6.99	120	1.57180	1.0074 x 10 ⁻⁵
183600	6.75	110	2.43908	1.5632 x 10 ⁻⁵
356400	6.66	100	4.49912	2.8835 x 10 ⁻⁵
957300	6.55	90	5.18363	3.3222 x 10 ⁻⁵
1562100	6.51	80	6.12844	3.9277 x 10 ⁻⁵

Si Release



Linear Fit



Analytical uncertainty is 10%.

Regression analysis		Std. Error
R Squared	0.91452	N/A
Si release rate	1.14 x 10 ⁻¹⁰	2.02 x 10 ⁻¹¹

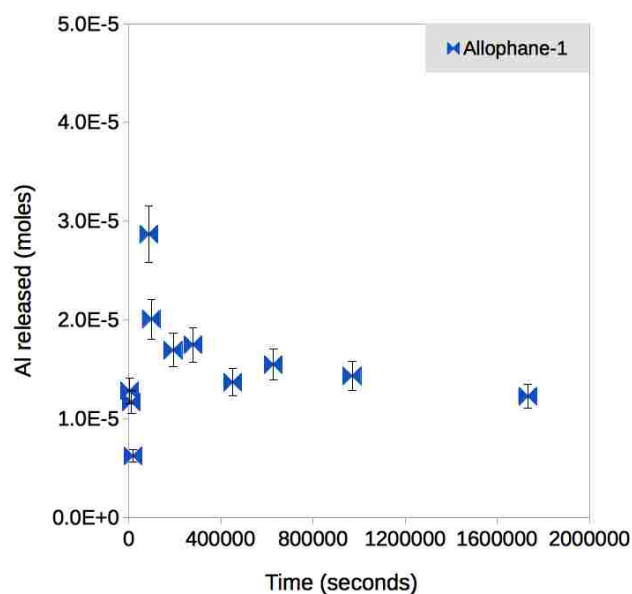
Diss. Rate Mineral (R_{diss}) 1.50 x 10⁻¹² mol m⁻² s⁻¹
Uncertainty of fit 2.65 x 10⁻¹³ mol m⁻² s⁻¹

Table S29. Dissolved Al analysis for experiment Al+Si-p3-1

Material: Allophane **Initial pH:** 3.01 **Solution:** 0.01M NaCl **Specific Surface Area (BET):** 385.6192 m²/g
Batch ID: Al+Si-p3-1 **Material mass:** 0.1501 g **Total Surface Area (BET):** 57.8814 m²
*N/A = no analysis. *Below practical quantitation limit (<1.0 ppm)*

Time (sec)	pH	Volume (mL)	Concentration Al (ppm)	Moles Al released
0	3.01	180		0
3600	3.25	170	1.92255	1.28258 x 10 ⁻⁵
10800	3.38	160	1.75224	1.16896 x 10 ⁻⁵
18000	3.48	150	0.88649*	6.23482 x 10 ⁻⁶ *
86400	4.08	140	4.67470	2.86989 x 10 ⁻⁵
97200	4.10	130	3.12696	2.00944 x 10 ⁻⁵
192000	4.28	120	2.51791	1.69342 x 10 ⁻⁵
278400	4.31	110	2.63445	1.74957 x 10 ⁻⁵
451200	4.31	100	1.78043	1.36975 x 10 ⁻⁵
627600	4.34	90	2.21760	1.54798 x 10 ⁻⁵
969600	4.34	80	1.90785	1.43318 x 10 ⁻⁵
1732800	4.42	70	1.29105	1.22744 x 10 ⁻⁵

Al Release



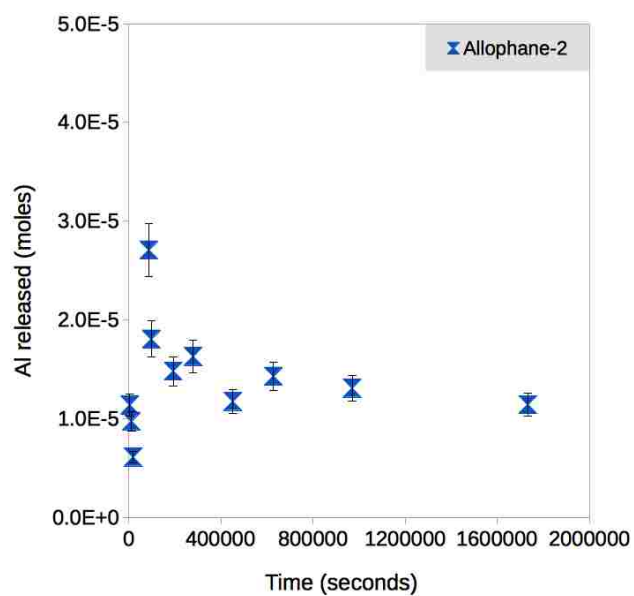
Analytical uncertainty is 10%.

Table S30. Dissolved Al analysis for experiment Al+Si-p3-2**Material:** Allophane **Initial pH:** 3.01 **Solution:** 0.01M NaCl **Specific Surface Area (BET):** 385.6192 m²/g**Batch ID:** Al+Si-p3-2 **Material mass:** 0.1499 g **Total Surface Area (BET):** 57.8043 m²

N/A = no analysis. *Below practical quantitation limit (<1.0 ppm)

Time (sec)	pH	Volume (mL)	Concentration Al (ppm)	Moles Al released
0	3.01	180		0
3600	3.25	170	1.70567	1.13789 x 10 ⁻⁵
10800	3.38	160	1.46358	9.76391 x 10 ⁻⁶
18000	3.48	150	0.88296*	6.10559 x 10 ⁻⁵ *
86400	4.08	140	4.42170	2.70903 x 10 ⁻⁵
97200	4.10	130	2.79917	1.80700 x 10 ⁻⁵
192000	4.28	120	2.16845	1.47974 x 10 ⁻⁵
278400	4.31	110	2.47821	1.62899 x 10 ⁻⁵
451200	4.31	100	1.45728	1.17493 x 10 ⁻⁵
627600	4.34	90	2.08310	1.43007 x 10 ⁻⁵
969600	4.34	80	1.75398	1.30809 x 10 ⁻⁵
1732800	4.42	70	1.25180	1.14058 x 10 ⁻⁵

Al Release



Analytical uncertainty is 10%.

Table S31. Dissolved Al analysis for experiment 1:99-p3-1

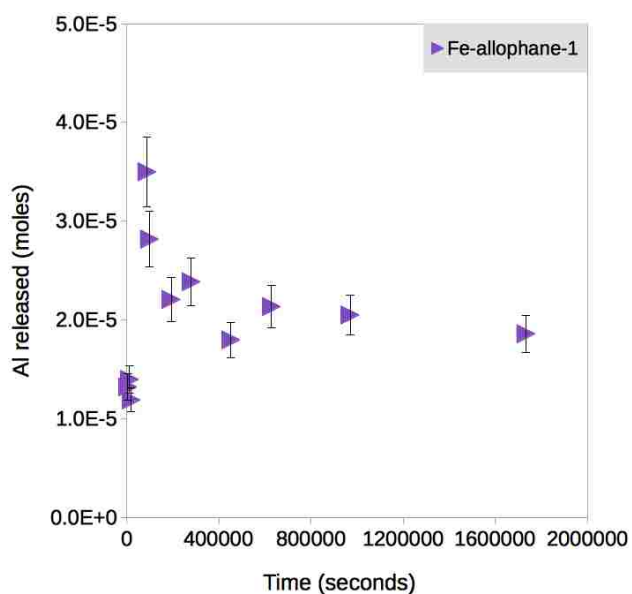
Material: Fe-allophane **Initial pH:** 3.01 **Solution:** 0.01M NaCl **Specific Surface Area (BET):** 350.2424 m²/g

Batch ID: 1:99-p3-1 **Material mass:** 0.1503 g **Total Surface Area (BET):** 52.6414 m²

*N/A = no analysis. *Below practical quantitation limit (<1.0 ppm)*

Time (sec)	pH	Volume (mL)	Concentration Al (ppm)	Moles Al released
0	3.01	180		0
3600	3.21	170	1.98146	1.32187 x 10 ⁻⁵
10800	3.34	160	2.09513	1.39771 x 10 ⁻⁵
18000	3.43	150	1.76427	1.18925 x 10 ⁻⁵
86400	4.04	140	5.66020	3.49953 x 10 ⁻⁵
97200	4.04	130	4.43361	2.81762 x 10 ⁻⁵
192000	4.27	120	3.25739	2.20731 x 10 ⁻⁵
278400	4.29	110	3.62953	2.38661 x 10 ⁻⁵
451200	4.35	100	2.30624	1.79808 x 10 ⁻⁵
627600	4.33	90	3.13407	2.13558 x 10 ⁻⁵
969600	4.36	80	2.90467	2.05056 x 10 ⁻⁵
1732800	4.35	70	2.33121	1.85927 x 10 ⁻⁵

Al Release



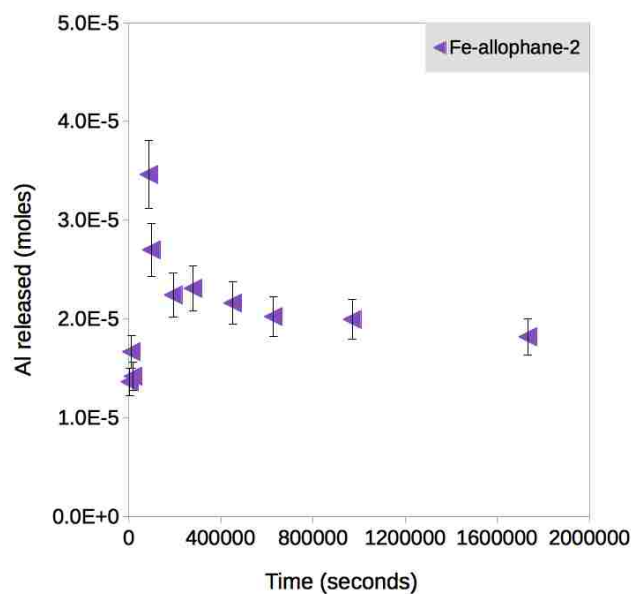
Analytical uncertainty is 10%.

Table S32. Dissolved Al analysis for experiment 1:99-p3-2**Material:** Fe-allophane **Initial pH:** 3.01 **Solution:** 0.01M NaCl **Specific Surface Area (BET):** 350.2424 m²/g**Batch ID:** 1:99-p3-2 **Material mass:** 0.1502 g **Total Surface Area (BET):** 52.6064 m²

N/A = no analysis. *Below practical quantitation limit (<1.0 ppm)

Time (sec)	pH	Volume (mL)	Concentration Al (ppm)	Moles Al released
0	3.01	180		0
3600	3.24	170	2.04277	1.36278 x 10 ⁻⁵
10800	3.38	160	2.50000	1.66781 x 10 ⁻⁵
18000	3.48	150	2.10593	1.41952 x 10 ⁻⁵
86400	4.13	140	5.55018	3.46195 x 10 ⁻⁵
97200	4.14	130	4.17811	2.69917 x 10 ⁻⁵
192000	4.31	120	3.29745	2.24222 x 10 ⁻⁵
278400	4.32	110	3.43744	2.30967 x 10 ⁻⁵
451200	4.35	100	3.10266	2.16077 x 10 ⁻⁵
627600	4.35	90	2.76524	2.02321 x 10 ⁻⁵
969600	4.38	80	2.68842	1.99474 x 10 ⁻⁵
1732800	4.37	70	2.15872	1.81806 x 10 ⁻⁵

Al Release



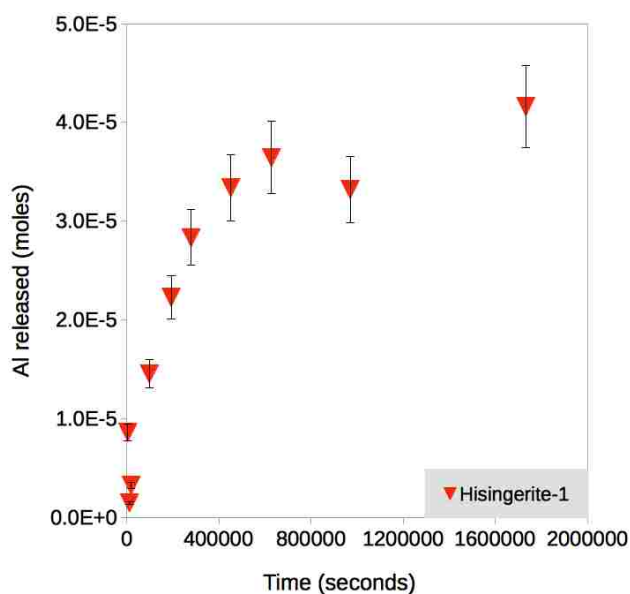
Analytical uncertainty is 10%.

Table S33. Dissolved Al analysis for experiment 50:50-p3-1**Material:** Hisingerite **Initial pH:** 3.01 **Solution:** 0.01M NaCl **Specific Surface Area (BET):** 507.2660 m²/g**Batch ID:** 50:50-p3-1 **Material mass:** 0.1496 g **Total Surface Area (BET):** 75.8870 m²

N/A = no analysis. *Below practical quantitation limit (<1.0 ppm)

Time (sec)	pH	Volume (mL)	Concentration Al (ppm)	Moles Al released
0	3.01	180		0
3600	3.07	170	1.29015	8.60689 x 10 ⁻⁶
10800	3.08	160	0.22201*	1.48106 x 10 ⁻⁶ *
18000	3.07	150	0.50716*	3.27770 x 10 ⁻⁶ *
86400	3.25	140	N/A	N/A
97200	3.23	130	2.61974	1.45641 x 10 ⁻⁵
192000	3.38	120	4.10983	2.22957 x 10 ⁻⁵
278400	3.46	110	5.36622	2.83492 x 10 ⁻⁵
451200	3.63	100	6.49740	3.33801 x 10 ⁻⁵
627600	3.73	90	7.25085	3.64518 x 10 ⁻⁵
969600	3.89	80	6.37419	3.32027 x 10 ⁻⁵
1732800	3.97	70	8.89289	4.16041 x 10 ⁻⁵

Al Release

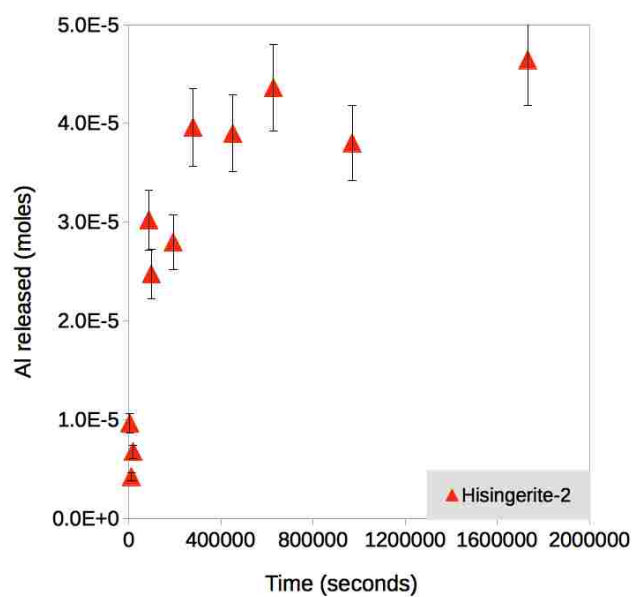


Analytical uncertainty is 10%.

Table S34. Dissolved Al analysis for experiment 50:50-p3-2**Material:** Hisingerite **Initial pH:** 3.01 **Solution:** 0.01M NaCl **Specific Surface Area (BET):** 507.2660 m²/g**Batch ID:** 50:50-p3-2 **Material mass:** 0.1503 g **Total Surface Area (BET):** 76.2421 m²

N/A = no analysis. *Below practical quantitation limit (<1.0 ppm)

Time (sec)	pH	Volume (mL)	Concentration Al (ppm)	Moles Al released
0	3.01	180		0
3600	3.07	170	1.44570	9.64462 x 10 ⁻⁶
10800	3.12	160	0.63351*	4.22629 x 10 ⁻⁶ *
18000	3.12	150	1.03564	6.75997 x 10 ⁻⁶
86400	3.35	140	4.99046	3.02120 x 10 ⁻⁵
97200	3.35	130	4.00653	2.47419 x 10 ⁻⁵
192000	3.54	120	4.62576	2.79550 x 10 ⁻⁵
278400	3.64	110	7.04278	3.96005 x 10 ⁻⁵
451200	3.81	100	6.90269	3.89774 x 10 ⁻⁵
627600	3.88	90	8.03478	4.35928 x 10 ⁻⁵
969600	3.96	80	6.52934	3.80132 x 10 ⁻⁵
1732800	4.00	70	9.05375	4.64337 x 10 ⁻⁵

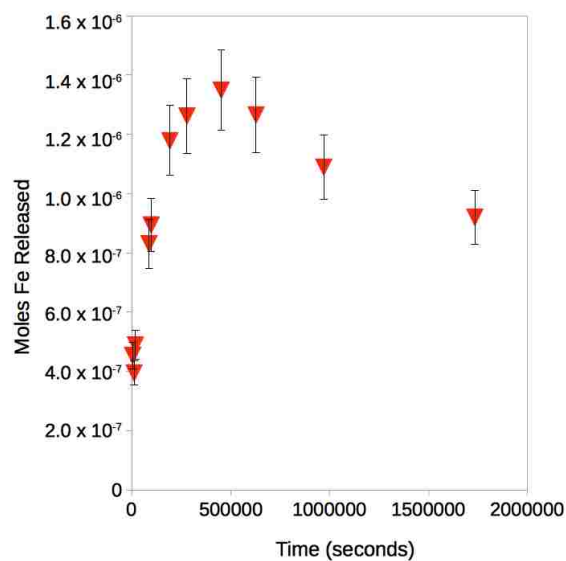
Al Release

Analytical uncertainty is 10%.

Table S35. Dissolved Fe analysis for experiment 50:50-p3-1**Material:** Hisingerite **Initial pH:** 3.01 **Solution:** 0.01M NaCl **Specific Surface Area (BET):** 507.2660 m²/g**Batch ID:** 50:50-p3-1 **Material mass:** 0.1496 g **Total Surface Area (BET):** 75.8879 m²

N/A = no analysis. *Below practical quantitation limit (0.2 ppm Fe)

Time (sec)	pH	Volume (mL)	Concentration Fe (ppm)	Moles Fe released
0	3.01	180		0
3600	3.07	170	0.140817598*	4.53884 x 10 ⁻⁷ *
10800	3.08	160	0.122647323*	3.95318 x 10 ⁻⁷ *
18000	3.07	150	0.153659716*	4.89724 x 10 ⁻⁷ *
86400	3.25	140	0.2727395	8.30896 x 10 ⁻⁷
97200	3.23	130	0.296661764	8.95151 x 10 ⁻⁷
192000	3.38	120	0.409877568	1.17898 x 10 ⁻⁶
278400	3.46	110	0.44567439	1.26231 x 10 ⁻⁶
451200	3.63	100	0.48634088	1.34969 x 10 ⁻⁶
627600	3.73	90	0.443861187	1.26602 x 10 ⁻⁶
969600	3.89	80	0.3453857	1.08968 x 10 ⁻⁶
1732800	3.97	70	0.240194559	9.20154 x 10 ⁻⁷

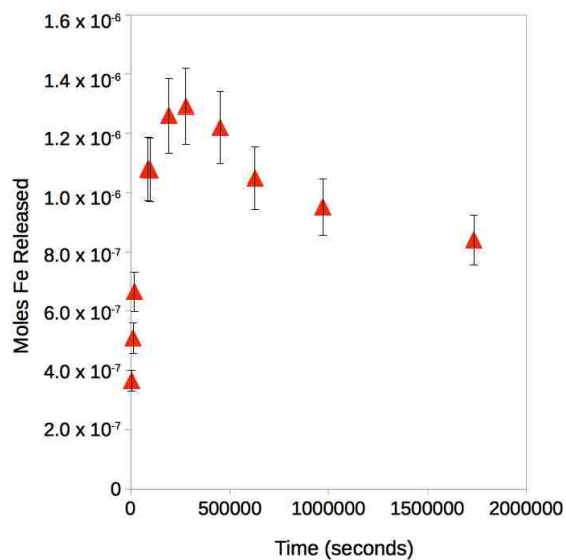
Fe Release

Analytical uncertainty is 10%.

Table S36. Dissolved Fe analysis for experiment 50:50-p3-2**Material:** Hisingerite **Initial pH:** 3.01 **Solution:** 0.01M NaCl **Specific Surface Area (BET):** 507.2660 m²/g**Batch ID:** 50:50-p3-2 **Material mass:** 0.1503 g **Total Surface Area (BET):** 76.2421 m²

N/A = no analysis. *Below practical quantitation limit (0.2 ppm Fe)

Time (sec)	pH	Volume (mL)	Concentration Fe (ppm)	Moles Fe released
0	3.01	180		0
3600	3.07	170	0.113315754*	3.65240 x 10 ⁻⁷ *
10800	3.12	160	0.15801996*	5.09331 x 10 ⁻⁷ *
18000	3.12	150	0.209302962	6.65444 x 10 ⁻⁷
86400	3.35	140	0.353962302	1.07990 x 10 ⁻⁶
97200	3.35	130	0.353024065	1.07738 x 10 ⁻⁶
192000	3.54	120	0.425870329	1.26000 x 10 ⁻⁶
278400	3.64	110	0.43948409	1.29170 x 10 ⁻⁶
451200	3.81	100	0.405464619	1.21859 x 10 ⁻⁶
627600	3.88	90	0.319258809	1.04879 x 10 ⁻⁶
969600	3.96	80	0.264877349	9.51412 x 10 ⁻⁷
1732800	4.00	70	0.195920333*	8.40281 x 10 ⁻⁷ *

Fe Release

Analytical uncertainty is 10%.

REFERENCES

- Abidin, Z., Matsue, N., Henmi, T., 2004. Dissolution mechanism of nano-ball allophane with dilute alkali solution. *Clay Science* 12, 213-222.
- Achilles, C. N., Downs, R. T., Ming, D. W., Rampe, E. B., Morris, R. V., Treiman, A. H., Morrison, S. M., Blake, D. F., Vaniman, D. T., Ewing, R. C., Chipera, S. J., Yen, A. S., Bristow, T. F., Ehlmann, B. L., Gellert, R., Hazen, R. M., Fendrich, K. V., Craig, P. I., Grotzinger, J. P., Des Marais, D. J., Farmer, J. D., Sarrazin, P. C., Morookian, J. M., 2017. Mineralogy of an active eolian sediment from the Namib dune, Gale crater, Mars. *Journal of Geophysical Research Planets* 122, 2344-2361.
- Baker, L.L., Strawn, D.G., 2012. Fe K-edge XAFS spectra of phyllosilicates of varying crystallinity. *Physics and Chemistry of Minerals* 39, 675-684.
- Baker, L.L., Strawn, D.G., McDaniel, P.A., Nickerson, R.D., Bishop, J.L., Ming, D.W., Morris, R.V., 2011. Poorly Crystalline Iron-Bearing Aluminosilicates and Their Importance on Mars, 42nd Lunar and Planetary Science Conference. LPI, The Woodlands, Texas, p. 1939.
- Bibring, J.P., Langevin, Y., Mustard, J.F., Poulet, F., Arvidson, R., Gendrin, A., Gondet, B., Mangold, N., Pinet, P., Forget, F., Berthe, M., Bibring, J.P., Gendrin, A., Gomez, C., Gondet, B., Jouglet, D., Poulet, F., Soufflot, A., Vincendon, M., Combes, M., Drossart, P., Encrenaz, T., Fouchet, T., Merchiorri, R., Belluci, G., Altieri, F., Formisano, V., Capaccioni, F., Cerroni, P., Coradini, A., Fonti, S., Korablev, O., Kottsov, V., Ignatiev, N., Moroz, V., Titov, D., Zasova, L., Loiseau, D., Mangold, N., Pinet, P., Doute, S., Schmitt, B., Sotin, C., Hauber, E., Hoffmann, H., Jaumann, R., Keller, U., Arvidson, R., Mustard, J.F., Duxbury, T., Forget, F., Neukum, G., 2006. Global mineralogical and aqueous mars history derived from OMEGA/Mars Express data. *Science* 312, 400-404.

- Bish, D.L., Blake, D.F., Vaniman, D.T., Chipera, S.J., Morris, R.V., Ming, D.W., Treiman, A.H., Sarrazin, P., Morrison, S.M., Downs, R.T., Achilles, C.N., Yen, A.S., Bristow, T.F., Crisp, J.A., Mrookian, J.M., Farmer, J.D., Rampe, E.B., Stolper, E.M., Spanovich, N., MSL Science Team, 2013. X-ray diffraction results from Mars Science Laboratory: mineralogy of Rocknest at Gale crater. *Science* 341, 1238932.
- Bish, D.L., Duffy, C.J. in *Thermal Analysis in Clay Science*, J. W. Stucki, D. L. Bish, Eds. (Clay Minerals Society, Boulder, CO, 1990), vol. 3, pp. 95–189.
- Bishop, J.L., Rampe, E.B., Bish, D.L., Abidin, Z., Baker, L.L., Matsue, N., Henmi, T., 2013. Spectral and Hydration Properties of Allophane and Imogolite. *Clays and Clay Minerals* 61, 57-74.
- Bishop, J.L., Rampe, E.B., 2016. Evidence for a changing Martian climate from the mineralogy at Mawrth Vallis. *Earth and Planetary Science Letters* 448, 42-48.
- Blake, D.F., Morris, R.V., Kocurek, G., Morrison, S.M., Downs, R.T., Bish, D., Ming, D.W., Edgett, K.S., Rubin, D., Goetz, W., Madsen, M.B., Sullivan, R., Gellert, R., Campbell, I., Treiman, A.H., McLennan, S.M., Yen, A.S., Grotzinger, J., Vaniman, D.T., Chipera, S.J., Achilles, C.N., Rampe, E.B., Sumner, D., Meslin, P.Y., Maurice, S., Forni, O., Gasnault, O., Fisk, M., Schmidt, M., Mahaffy, P., Leshin, L.A., Glavin, D., Steele, A., Freissinet, C., Navarro-Gonzalez, R., Yingst, R.A., Kah, L.C., Bridges, N., Lewis, K.W., Bristow, T.F., Farmer, J.D., Crisp, J.A., Stolper, E.M., Marais, D.J.D., Sarrazin, P., MSL Science Team, 2013. Curiosity at Gale Crater, Mars: Characterization and Analysis of the Rocknest Sand Shadow. *Science* 341, 1239505.
- Bleeker, P., Parfitt, R.L., 1974. Volcanic ash and its clay mineralogy at Cape Hoskins, New Britain, Papua New Guinea. *Geoderma* 11, 123-135.
- Cama, J., Metz, V., Ganor, J., 2002. The effect of pH and temperature on kaolinite dissolution rate under acidic conditions. *Geochimica et Cosmochimica Acta* 66, 3913-3926.

- Carr, M.H., 1996. Water erosion on Mars and its biologic implications. *Endeavour* 20, 56-60.
- Dehouck, E., McLennan, S.M., Meslin, P.Y., Cousin, A., 2014. Constraints on abundance, composition, and nature of X-ray amorphous components of soils and rocks at Gale crater, Mars. *Journal of Geophysical Research-Planets* 119, 2640-2657.
- Denaix, L., 1993. Synthèse et propriétés d'aluminosilicates non lamellaires : l'imogolite et les allophanes, Sciences de la Terre. Université Pierre et Marie Curie (Paris 6), Paris, FRA, p. 223.
- Eaton, A.D., Clesceri, L.S., Rice, E.W., Greenberg, A.E., Franson M.A.H., 2005. Standard Methods for the Examination of Water and Wastewater, Centennial ed. American Public Health Association, Washington, DC.
- Eggleton, R.A., Tilley, D.B., 1998. Hisingerite: a ferric kaolin mineral with curved morphology. *Clays and Clay Minerals* 46, 400-413.
- Gainey, S.R., Hausrath, E.M., Hurowitz, J.A., Milliken, R.E., 2014. Nontronite dissolution rates and implications for Mars. *Geochimica Et Cosmochimica Acta* 126, 192-211.
- Grotzinger, J.P., Gupta, S., Malin, M.C., Rubin, D.M., Schieber, J., Siebach, K., Sumner, D.Y., Stack, K.M., Vasavada, A.R., Arvidson, R.E., Calef, F., 3rd, Edgar, L., Fischer, W.F., Grant, J.A., Griffes, J., Kah, L.C., Lamb, M.P., Lewis, K.W., Mangold, N., Minitti, M.E., Palucis, M., Rice, M., Williams, R.M., Yingst, R.A., Blake, D., Blaney, D., Conrad, P., Crisp, J., Dietrich, W.E., Dromart, G., Edgett, K.S., Ewing, R.C., Gellert, R., Hurowitz, J.A., Kocurek, G., Mahaffy, P., McBride, M.J., McLennan, S.M., Mischna, M., Ming, D., Milliken, R., Newsom, H., Oehler, D., Parker, T.J., Vaniman, D., Wiens, R.C., Wilson, S.A., 2015. Deposition, exhumation, and paleoclimate of an ancient lake deposit, Gale crater, Mars. *Science* 350, aac7575.
- Gustafsson, J.P., Karlton, E., Bhattacharya, P., 1998. Allophane and imogolite in Swedish soils. Royal Institute of Technology (KTH), Stockholm.

- Henmi, T., Wells, N., Childs, C.W., Parfitt, R.L., 1980. Poorly-ordered iron-rich precipitates from springs and streams on andesitic volcanoes. *Geochimica et Cosmochimica Acta* 44, 365-372.
- Huertas, F.J., Chou, L., Wollast, R., 1999. Mechanism of kaolinite dissolution at room temperature and pressure Part II: kinetic study. *Geochimica et Cosmochimica Acta* 63, 3261-3275.
- Huffman, E.O., 1960. Rates and mechanisms of dissolution of some ferric phosphates. *Soil Science*, 1-8.
- Ingles, O.G., Willoughby, D.R., 1967. An Occurrence of Hisingerite with Evidence of Its Genesis. *Soil Science* 104, 383-385.
- Iyoda, F., Hayashi, S., Arakawa, S., John, B., Okamoto, M., Hayashi, H., Yuan, G.D., 2012. Synthesis and adsorption characteristics of hollow spherical allophane nano-particles. *Applied Clay Science* 56, 77-83.
- Leshin, L.A., Mahaffy, P.R., Webster, C.R., Cabane, M., Coll, P., Conrad, P.G., Archer, P.D., Jr., Atreya, S.K., Brunner, A.E., Buch, A., Eigenbrode, J.L., Flesch, G.J., Franz, H.B., Freissinet, C., Glavin, D.P., McAdam, A.C., Miller, K.E., Ming, D.W., Morris, R.V., Navarro-Gonzalez, R., Niles, P.B., Owen, T., Pepin, R.O., Squyres, S., Steele, A., Stern, J.C., Summons, R.E., Sumner, D.Y., Sutter, B., Szopa, C., Teinturier, S., Trainer, M.G., Wray, J.J., Grotzinger, J.P., MSL Science Team, 2013. Volatile, isotope, and organic analysis of martian fines with the Mars Curiosity rover. *Science* 341, 1238937.
- Liang, D.-T., Readey, D.W., 1987. Dissolution Kinetics of Crystalline and Amorphous Silica in Hydrofluoric-Hydrochloric Acid Mixtures. *Journal of the American Ceramic Society* 70, 570-577.
- Meslin, P.Y., Gasnault, O., Forni, O., Schroder, S., Cousin, A., Berger, G., Clegg, S.M., Lasue, J., Maurice, S., Sautter, V., Le Mouelic, S., Wiens, R.C., Fabre, C., Goetz, W., Bish, D., Mangold, N., Ehlmann, B., Lanza, N., Harri, A.M., Anderson, R., Rampe, E., McConnochie, T.H., Pinet, P.,

Blaney, D., Leveille, R., Archer, D., Barraclough, B., Bender, S., Blake, D., Blank, J.G., Bridges, N., Clark, B.C., DeFlores, L., Delapp, D., Dromart, G., Dyar, M.D., Fisk, M., Gondet, B., Grotzinger, J., Herkenhoff, K., Johnson, J., Lacour, J.L., Langevin, Y., Leshin, L., Lewin, E., Madsen, M.B., Melikechi, N., Mezzacappa, A., Mischna, M.A., Moores, J.E., Newsom, H., Ollila, A., Perez, R., Renno, N., Sirven, J.B., Tokar, R., de la Torre, M., d'Uston, L., Vaniman, D., Yingst, A., MSL Science Team, 2013. Soil Diversity and Hydration as Observed by ChemCam at Gale Crater, Mars. *Science* 341.

Milliken, R.E., Bish, D.L., 2014. Distinguishing hisingerite from other clays and its importance for Mars, 45th Lunar and Planetary Science Conference. LPI, Houston, TX.

Milliken, R.E., Swayze, G.A., Arvidson, R.E., Bishop, J.L., Clark, R.N., Ehlmann, B.L., Green, R.O., Grotzinger, J.P., Morris, R.V., Murchie, S.L., Mustard, J.F., Weitz, C., 2008. Opaline silica in young deposits on Mars. *Geology* 36, 847.

Montarges-Pelletier, E., Bogenez, S., Pelletier, M., Razafitianamaharavo, A., Ghanbaja, J., Lartiges, B., Michot, L., 2005. Synthetic allophane-like particles: textural properties. *Colloids and Surfaces a-Physicochemical and Engineering Aspects* 255, 1-10.

Morris, R.V., Vaniman, D.T., Blake, D.F., Gellert, R., Chipera, S.J., Rampe, E.B., Ming, D.W., Morrison, S.M., Downs, R.T., Treiman, A.H., Yen, A.S., Grotzinger, J.P., Achilles, C.N., Bristow, T.F., Crisp, J.A., Des Marais, D.J., Farmer, J.D., Fendrich, K.V., Frydenvang, J., Graff, T.G., Morookian, J.M., Stolper, E.M., Schwenzer, S.P., 2016. Silicic volcanism on Mars evidenced by tridymite in high-SiO₂ sedimentary rock at Gale crater. *Proc Natl Acad Sci USA* 113, 7071-7076.

Morris, R.V., Golden, D.C., Bell, J.F., Shelfer, T.D., Scheinost, A.C., Hinman, N.W., Furniss, G., Mertzman, S.A., Bishop, J.L., Ming, D.W., Allen, C.C., Britt, D.T., 2000. Mineralogy, composition, and alteration of Mars Pathfinder rocks and soils: Evidence from multispectral, elemental, and

magnetic data on terrestrial analogue, SNC meteorite, and Pathfinder samples. *Journal of Geophysical Research: Planets* 105, 1757-1817.

Mustoe, G.E., 1996. Hisingerite - A Rare Iron Mineral from Walker Valley, Skagit County, Washington. *Washington Geology* 24, 14-19.

Nagasawa, K., 1978. Weathering of volcanic ash and other pyroclastic materials, in: Sudo, T., Shimoda, S. (Eds.), *Clay and clay minerals of Japan*. Elsevier Science Publishing Company, Amsterdam, pp. 105-125.

Ohashi, F., Wada, S.I., Suzuki, M., Maeda, M., Tomura, S., 2002. Synthetic allophane from high-concentration solutions: nanoengineering of the porous solid. *Clay Minerals* 37, 451-456.

Parfitt, R.L., 1990. Allophane in New Zealand - a review. *Australian Journal of Soil Research* 28, 343.

Rampe, E.B., Ming, D.W., Blake, D.F., Bristow, T.F., Chipera, S.J., Grotzinger, J.P., Morris, R.V., Morrison, S.M., Vaniman, D.T., Yen, A.S., Achilles, C.N., Craig, P.I., Des Marais, D.J., Downs, R.T., Farmer, J.D., Fendrich, K.V., Gellert, R., Hazen, R.M., Kah, L.C., Morookian, J.M., Peretyazhko, T.S., Sarrazin, P., Treiman, A.H., Berger, J.A., Eigenbrode, J., Fairén, A.G., Forni, O., Gupta, S., Hurowitz, J.A., Lanza, N.L., Schmidt, M.E., Siebach, K., Sutter, B., Thompson, L.M., 2017. Mineralogy of an ancient lacustrine mudstone succession from the Murray formation, Gale crater, Mars. *Earth and Planetary Science Letters* 471, 172-185.

Rampe, E.B., Morris, R.V., Archer, P.D., Agresti, D.G., Ming, D.W., 2016. Recognizing sulfate and phosphate complexes chemisorbed onto nanophase weathering products on Mars using in-situ and remote observations. *American Mineralogist* 101, 678-689.

Rampe, E.B., Morris, R.V., Ruff, S.W., Horgan, B., Dehouck, E., Achilles, C.N., Ming, D.W., Bish, D.L., Chipera, S.J., 2014. Amorphous Phases on the Surface of Mars, 8th International Conference on Mars, Pasadena, CA, United States.

- Rampe, E.B., Kraft, M.D., Sharp, T.G., Golden, D.C., Ming, D.W., Christensen, P.R., 2012. Allophane detection on Mars with Thermal Emission Spectrometer data and implications for regional-scale chemical weathering processes. *Geology* 40, 995-998.
- Rampe, E.B., Kraft, M.D., Sharp, T.G., Golden, D.C., Ming, D.W., Christensen, P.R., Ruff, S.W., 2011. Detection of allophane on Mars through orbital and in-situ thermal infrared spectroscopy, 42nd Lunar and Planetary Science Conference, The Woodlands, TX.
- Schwertmann, U., Cornell, R.M., 2000. *Iron Oxides in the Laboratory: Preparation and Characterization*. Wiley-VCH, Weinheim, Germany.
- Shayan, A., 1984. Hisingerite Material from a Basalt Quarry near Geelong, Victoria, Australia. *Clays and Clay Minerals* 32, 272-278.
- Singer, R.B., 1985. Spectroscopic observation of Mars. *Advances in Space Research* 5, 59-68.
- Smith, D.K., 1998. Opal, cristobalite, and tridymite: Noncrystallinity versus crystallinity, nomenclature of the silica minerals and bibliography. *Powder Diffraction* 13, 2-19.
- Squyres, S.W., Arvidson, R.E., Ruff, S., Gellert, R., Morris, R.V., Ming, D.W., Crumpler, L., Farmer, J.D., Marais, D.J., Yen, A., McLennan, S.M., Calvin, W., Bell, J.F., 3rd, Clark, B.C., Wang, A., McCoy, T.J., Schmidt, M.E., de Souza, P.A., Jr., 2008. Detection of silica-rich deposits on Mars. *Science* 320, 1063-1067.
- Steiner, M.H., Hausrath, E.M., Elwood Madden, M.E., Tschauner, O., Ehlmann, B.L., Olsen, A.A., Gainey, S.R., Smith, J.S., 2016. Dissolution of nontronite in chloride brines and implications for the aqueous history of Mars. *Geochimica et Cosmochimica Acta* 195, 259-276.
- Sutter, B., McAdam, A.C., Mahaffy, P.R., Ming, D.W., Edgett, K.S., Rampe, E.B., Eigenbrode, J.L., Franz, H.B., Freissinet, C., Grotzinger, J.P., Steele, A., House, C.H., Archer, P.D., Malespin, C.A.,

- Navarro-González, R., Stern, J.C., Bell, J.F., Calef, F.J., Gellert, R., Glavin, D.P., Thompson, L.M., Yen, A.S., 2017. Evolved gas analyses of sedimentary rocks and eolian sediment in Gale Crater, Mars: Results of the Curiosity rover's sample analysis at Mars instrument from Yellowknife Bay to the Namib Dune. *Journal of Geophysical Research: Planets* 122, 2574-2609.
- Tu, V.M., Hausrath, E.M., Tschauner, O., Iota, V., Egeland, G.W., 2014. Dissolution rates of amorphous Al- and Fe-phosphates and their relevance to phosphate mobility on Mars. *American Mineralogist* 99, 1206-1215.
- Van der Gaast, S.J., Vaars, A.J., 1981. A Method to Eliminate the Background in X-Ray-Diffraction Patterns of Oriented Clay Mineral Samples. *Clay Minerals* 16, 383-393.
- Vaniman, D.T., Bish, D.L., Ming, D.W., Bristow, T.F., Morris, R.V., Blake, D.F., Chipera, S.J., Morrison, S.M., Treiman, A.H., Rampe, E.B., Rice, M., Achilles, C.N., Grotzinger, J.P., McLennan, S.M., Williams, J., Bell, J.F., 3rd, Newsom, H.E., Downs, R.T., Maurice, S., Sarrazin, P., Yen, A.S., Morookian, J.M., Farmer, J.D., Stack, K., Milliken, R.E., Ehlmann, B.L., Sumner, D.Y., Berger, G., Crisp, J.A., Hurowitz, J.A., Anderson, R., Des Marais, D.J., Stolper, E.M., Edgett, K.S., Gupta, S., Spanovich, N., MSL Science Team, 2014. Mineralogy of a mudstone at Yellowknife Bay, Gale crater, Mars. *Science* 343, 1243480.
- Wada, K., 1989. Allophane and Imogolite, in: Dixon, J.B., Weed, S.B. (Eds.), *Minerals in Soil Environments*. Soil Science Society of America, Madison, Wisconsin, USA, pp. 1051-1087.
- Wada, K., Yoshinaga, N., 1969. The structure of imogolite. *American Mineralogist* 54, 50-71.
- Weitz, C.M., Bishop, J.L., Baker, L.L., Berman, D.C., 2014. Fresh exposures of hydrous Fe-bearing amorphous silicates on Mars. *Geophysical Research Letters* 41, 8744-8751.

- Welch, S.A., Ullman, W.J., 2000. The temperature dependence of bytownite feldspar dissolution in neutral aqueous solutions of inorganic and organic ligands at low temperature (5–35°C). *Chemical Geology* 167, 337-354.
- Yen, A.S., Ming, D.W., Vaniman, D.T., Gellert, R., Blake, D.F., Morris, R.V., Morrison, S.M., Bristow, T.F., Chipera, S.J., Edgett, K.S., Treiman, A.H., Clark, B.C., Downs, R.T., Farmer, J.D., Grotzinger, J.P., Rampe, E.B., Schmidt, M.E., Sutter, B., Thompson, L.M., 2017. Multiple stages of aqueous alteration along fractures in mudstone and sandstone strata in Gale Crater, Mars. *Earth and Planetary Science Letters* 471, 186-198.
- Yoshinaga, N., Aomine, S., 1962. Allophane in Some Ando Soils. *Soil Science and Plant Nutrition* 8, 6-13.

CURRICULUM VITAE

S. J. Ralston

Graduate Research Assistant

E-mail: ralsts1@unlv.nevada.edu

Education and Qualification

Master's in Geoscience, University of Nevada, Las Vegas (2016-Present)

- Concentration in Planetary Science
- Research project: "Dissolution rates of allophane, Fe-allophane, and hisingerite: implications for aqueous alteration on Mars and the analysis of returned martian samples."

BS in Earth and Atmospheric Sciences, Georgia Institute of Technology (2010-2014)

- Graduated with High Honors
- Modules included: planetary science; earth-systems modeling; remote sensing

Work Experience

Mars Research Intern, Jacobs Technology (Jan. 2018-Present)

- Conducted multiple experiments for ongoing research projects at NASA Johnson Space Center under Mars Research staff
- Gained proficiency in multiple analytical techniques and instruments

Graduate Research Assistant, UNLV Geoscience (Jan. 2016-Jan. 2018)

- Synthesized allophane and hisingerite for use in dissolution experiments
- Gained proficiency in multiple analytical techniques and instruments
- Drafted, revised, and submitted research proposals based on experiments and literature review

Undergraduate Teaching Assistant, Georgia Institute of Technology (Aug. 2013-Dec. 2013)

- Supervised in-class activities and proctored tests for undergraduate Earth Sciences class
- Instructed and graded laboratory activities throughout the semester

Undergraduate Researcher, Georgia Institute of Technology (May 2012-July 2013)

- Examined Martian surface composition and texture using CRISM and HiRISE data
- Learned and effectively utilized ENVI software for image processing
- Presented results at AGU Fall Meeting 2013

Prior Research and Funding

Southwest Travel Award, 2018

- Granted by Southwest Airlines for travel to NASA Johnson Space Center
- Project: "Dissolution of allophane, Fe-allophane, and hisingerite and implications for Gale Crater, Mars"

GSA Graduate Student Research Grant, 2017

- Granted by the Geological Society of America in the amount of \$1,525
- Project: "Constraining and elucidating the aqueous history of Gale Crater, Mars by examining the dissolution properties of the amorphous soil component"

UNLV GPSA Research Sponsorship, Summer 2016

- Granted by the UNLV Graduate and Professional Student Association
- Project: "Mars-Analogous Allophane Synthesis and Characterization"

President's Undergraduate Research Award, Summer 2012

- Granted by the Georgia Institute of Technology
- Project: "Concentrations of hydrated sulfates in equatorial Martian sediments"

Achievements

UNLV Geosymposium 2016, 2017

- Awarded "Best Graduate Poster" in both 2016 and 2017 for posters of graduate research, including initial work and progress accomplished

Academic Honors

- Georgia Tech Dean's List, Fall 2012, Spring 2013
- Georgia Tech Faculty Honors, Spring 2012
- National Merit Scholarship, 2010, 2011, 2012, 2013
- HOPE Scholarship, 2010, 2012, 2013

Publications

Ralston, S. J., Hausrath, E. M., Tschauner, O., Rampe, E. B., Christoffersen, R. (2018), Dissolution rates of allophane, Fe-containing allophane, and hisingerite and implications for Gale Crater, Mars, Abstract 2823, XLIV Lunar and Planetary Science Conference, The Woodlands, TX, 19-23 March.

Beaty, D. W., V. J. Hipkin, C.M. Caudill, R. Hansen, E. M. Hausrath, C. Maggiori, R. McCoubrey, J. Parrish, and S. J. Ralston, in review, Geological Evaluation of the MSRAD Field Site by a Human Field Party: Implications for Rover-based Exploration Operations and for the Future Human Exploration of Mars, in the Special Issue "Preparing for Mars Sample Return through the CanMars Mars Sample Return Analogue Deployment (MSRAD)", Planetary and Space Science, submitted Jan. 2018.

Ralston, S. J., Hausrath, E. M., Tschauner, O., Rampe, E. B., (Clark)-Hogancamp, J. V., Christoffersen, R. (2017), Fe-containing allophane and hisingerite dissolution and implications for Gale Crater, Mars, Abstract 2868, XLVIII Lunar and Planetary Science Conference, The Woodlands, TX, 20-24 March.

Ralston, S. J., Wray, J. J. (2013), Correlations between textures and infrared spectra of the martian surface in Valles Marineris, Abstract P23F-1847 presented at 2013 Fall Meeting, AGU, San Francisco, Calif., 9-13 Dec.